THE OHIO STATE UNIVERSITY

IMPLEMENTATION OF A DIGITAL OPTICAL MATRIX-VECTOR MULTIPLIER USING A HOLOGRAPHIC LOOK-UP TABLE AND RESIDUE ARITHMETIC

by

Sarry F. Habiby

The Ohio State University

ElectroScience Laboratory

Department of Electrical Engineering
Columbus, Ohio 43212

Technical Report No. 712257-6
Grant No. NSG 3302
August 1987

National Aeronautics and Space Administration
Lewis Research Center
21000 Brookpark Road
Cleveland, Ohio 44135

NOTICES

When Government drawings, specifications, or other data are used for any purpose other than in connection with a definitely related Government procurement operation, the United States Government thereby incurs no responsibility nor any obligation whatsoever, and the fact that the Government may have formulated, furnished, or in any way supplied the said drawings, specifications, or other data, is not to be regarded by implication or otherwise as in any manner licensing the holder or any other person or corporation, or conveying any rights or permission to manufacture, use, or sell any patented invention that may in any way be related thereto.

50272-101

REPORT DOCUMENTATION PAGE	1. REPORT NO.	2.	3. Recipient's Accession No.

4. Title and Subtitle

IMPLEMENTATION OF A DIG[redacted]TICAL MATRIX-VECTOR MULTIPLIER USING A HOLOGRAPHIC LOOK-UP TABLE AND RESIDUE ARITHMETIC

5. Report Date
August 1987

6.

7. Author(s)
Sarry F. Habiby

8. Performing Organization Rept. No.
712257-6

9. Performing Organization Name and Address
The Ohio State University
ElectroScience Laboratory
1320 Kinnear Road
Columbus, Ohio 43212

10. Project/Task/Work Unit No.

11. Contract(C) or Grant(G) No
(C)
(G) NSG 3302

12. Sponsoring Organization Name and Address
National Aeronautics and Space Administration
Lewis Research Center
21000 Brookpark Road
Cleveland, Ohio 44135

13. Type of Report & Period Covered
Technical Report

14.

15. Supplementary Notes

16. Abstract (Limit: 200 words)

The design and implementation of a digital (numerical) optical matrix-vector multiplier are presented in this report. The objective is to deomonstrate the operation of an optical processor designed to minimize computation time in performing a practical computing application. This is done by using the large array of processing elements in a Hughes liquid crystal light valve, and relying on the residue arithmetic representation, a holographic optical memory, and position coded optical look up tables. In the design, all operations are performed in effectively one light valve response time regardless of matrix size.

The features of the design that allow fast computation include the residue arithmetic representation, the mapping approach to computation, and the holographic memory. In addition, other features of the work presented include a practical light valve configuration for efficient polarization control, a model for recording multiple exposures in silver halides with equal reconstruction efficiency, and using light from an optical fiber for a reference beam source in constructing the hologram.

The basic components of the designed system were constructed and used to demonstrate the operation of the device. Results of the implemented operations are presented in photographs of the system outputs. The design can be extended to implement larger matrix arrays without any increased computation time.

17. Document Analysis a. Descriptors

b. Identifiers/Open-Ended Terms

c. COSATI Field/Group

18. Availability Statement	19. Security Class (This Report) Unclassified	21. No. of Pages 155
	20. Security Class (This Page) Unclassified	22. Price

(See ANSI-Z39.18) See Instructions on Reverse

OPTIONAL FORM 272 (4-77)
(Formerly NTIS-35)
Department of Commerce

TABLE OF CONTENTS

LIST OF TABLES

LIST OF FIGURES

FIGURES PAGE

CHAPTER I

INTRODUCTION

The design and implementation of a digital (numerical) optical matrix-vector multiplier are presented in this report. A Hughes liquid crystal light valve, (LCLV) [1], the residue arithmetic representation [2], and a holographic optical memory are used to construct position coded optical look up tables [3]. All operations are performed in effectively one light valve response time with a high information density.

The purpose of this work is to present the design, and demonstration of a matrix-vector multiplier designed for minimum computation time. Many operations are processed simultaneously by efficiently utilizing the large number of image elements accessible in a spatial light modulator. The look up table approach, a holographic memory, and position coding using the residue arithmetic representation reduce the effective computation time to one device response time regardless of the matrix size. This provides a practical computing mechanism with a high throughput. As a typical end product of this design, 220 simultaneous 2x2 matrix-vector products could be performed, each with a dynamic range of 1155.

The interest in matrix multiplication is twofold. Matrix multiplication is a fundamental mathematical tool employed in computer solutions of many real-world systems with applications in a variety of disciplines. On the other hand, matrix multiplication presents an opportunity to study the advantages of using parallel optical processing in computers (in both hardware and software) as opposed to using sequential computing machines in cases where parallel arithmetic operations are inherently more appropriate, such as in matrix multiplication.

Background

Optical computing has been investigated for several decades. It has taken both analog and digital forms and has been considered for a range of applications as a means of performing high speed, parallel computations. A review of the pertinent features of optical data processing is presented in Appendix A. Analog optical techniques based on the theory of Fourier optics and used to perform optical correlation, pattern recognition, and image processing have been well established in the literature [4,5,6].

More recently, digital optical computing has been studied [7,8] and demonstrated [9,10,11]. In optical digital computing the fundamental advantages are the high information density associated with the parallel processing of optical signals in a two dimensional array format, as opposed to serial (high speed) processing in digital electronic circuits, and also the ability to propagate optical signals in a small

volume without being limited by interference between signals or channels. Digital optical computer designs range from dedicated processors with specific applications such as the work presented in this report for implementing an optical matrix vector multiplier [12], to the general all purpose optical computer designs [13,14].

In order to perform real time computing it is necessary to have a nonlinear optical transducer, typically in the form of a spatial light modulator (SLM). In this design the SLM is the Hughes liquid crystal light valve (LCLV); it has been used in previous work in a range of optical computation applications [15,16,17,18]. Other optical light modulators [19] and transducers being tested and used include the MSLM [20], the TI deformable mirror device [21], (OTO-DMD), and semiconductor based etalon devices [14,22,23,24].

One approach to optical computing relies on systolic array processors employing the principle of sequential shifting of the input and output matrix elements [25] designed to implement the repeated multiplication and addition operations used in matrix multiplication. Several such designs have been reported using acousto-optic transducers [26] and RUBIC cube processors [27,28].

A different approach is presented here [29]. Specific aspects of this approach for matrix multiplication to be considered include the Hughes LCLV just mentioned, residue arithmetic, position coding, and holographic memory.

Optical matrix multiplier designs generally have inputs in an array in one plane imaged individually, by rows or columns, or in parallel via lenses onto a 'processing' plane. In this plane the input information

is 'operated' upon to generate the desired arithmetic manipulations to perform multiplication or addition. The results of this 'processing' are in turn imaged back via further anamorphic optics onto an output plane where an output array represents the product vector or matrix.

The ground work for optical matrix-vector algebra was initially presented by Cutrona [5] and later developed and improved by Heinz et al. [30]. However, such techniques were not designed with efficiency as a goal; energy in the form of irrelevant light outputs had to be sacrificed, especially as the matrix order increased. Intensity coding of inputs and outputs was used in various digital designs; typical of such systems are the works reported by Tamura and Wyant [25], and Goodman, et al. [31].

Position coding of inputs and outputs for matrix vector multiplication has been used by Huang, and Guest and Gaylord, [3,32,33] as a means of establishing a high signal to noise ratio. Position coding has also been used by Psaltis and Casasent [34] in optical signal processing.

Residue arithmetic (described in more detail in a subsequent section) has been used in various designs [3,33,34,35,36,37,38,39,40,41] and is used for representing numbers in this design as well.

Designs using holographic optical storage have also been studied [3,42,43,44,45] involving superimposed recordings based on carrier or spatial multiplexing techniques. Analysis of holographic recordings is extensive [46,47,48,49,50,51,52,53,54,55] and empirical results on holographic multiplexing have been reported [56,57,58,59,60]. In this

design, the holographic storage plays a role in implementing residue arithmetic table look up operations.

Problem Statement

The purpose of this work is to present the design, and demonstration a matrix-vector multiplier designed for minimum computation time regardless of matrix size. It combines the concepts used in previous works, including residue arithmetic [3], position coding of numbers [33], a mapping approach to arithmetic operations, and a holographic table look up [3,32], using a Hughes LCLV.

Contents of Report

In the following chapters various aspects of the design and demonstration are discussed in more detail. The design description and theory are presented in Chapter II. The residue arithmetic operations based on position coded optical mappings and using a holographic table look up are further defined, and the theory of the light valve operation in a new configuration, as well as the hologram superimposed exposure theory are presented. The experiments performed and the results demonstrating the device operation are given in Chapter III. Photographs of patterns stored in the holographic memory and of the matrix-vector outputs in one modulus are presented. Chapter IV contains a summary of the presented work and suggestions for future research.

The appendices include material on background for optical data processing, (A), analysis of polarization decomposition in liquid crystals, (B), hologram coupled wave theory (C), the matrix vector multiplier apparatus, (D and E), the hologram construction apparatus, (F), the optical fiber coupler, (G), and response time (H).

CHAPTER II

DESIGN DESCRIPTION AND THEORY

In this Chapter a general design description and the theory for the optical matrix-vector multiplier are presented. This design uses the Hughes liquid crystal light valve [1], position coding [32,33,34], holographic storage [3], and the residue arithmetic representation [2]. These components and principles are combined in a new approach, using optical mappings to perform arithmetic operations. The theory behind the light valve operation and the hologram construction is presented. System energy considerations pertaining to operating power limits are then discussed. Finally an expression for the theoretical number of parallel matrix-vector multipliers constructed using one LCLV is derived.

Objective

The objective of this design is to gain speed, using a relatively slow spatial light modulator, by taking advantage of the large number of image elements in a typical optical system, and by using look up tables to perform arithmetic operations in implementing a matrix-vector multiplier. The total number of operations in this case is limited only by the information content of the Hughes liquid crystal light valve, and the arithmetic representation of numbers, residue arithmetic. By efficiently allocating the large number of spatial light modulator image

elements and storing two dimensional arrays of light beam patterns needed in position coded optical look up tables, the effective computation time for a matrix-vector multiplication is reduced to one device response time. This provides a practical computing mechanism with a high throughput.

The design system diagram is shown in Figure 1. Succinctly depicted in the diagram are the basic operations of a matrix vector product as identified in Equation (1);

$$c_i = \sum_j a_{ij} \cdot b_j \qquad (1)$$

where the product of matrix A elements a_{ij}, and vector B elements b_j, produces vector C with elements c_i, where i=1,2,...,n, and j=1,2,...n. The arithmetic operations are a set of products performed in the

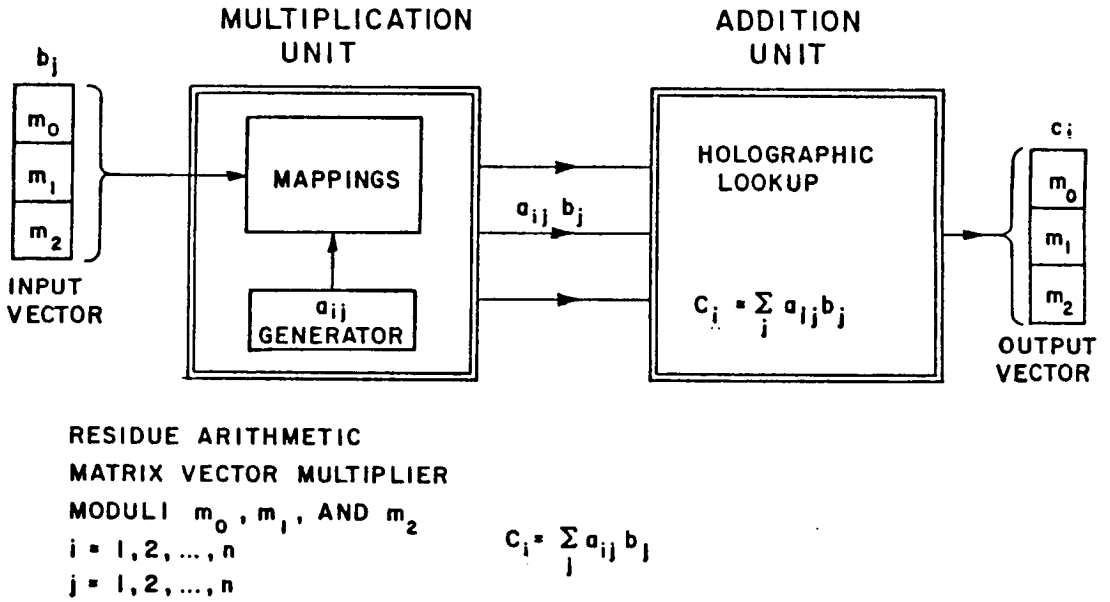

Figure 1. System diagram.

multiplication unit followed by a set of sums performed in the addition unit. The multiplication unit is shown to the left of center with input vector elements b_j shown to its left, and the addition unit is shown to the right of center with output vector elements, c_i shown to its right. Note that the elements of the a_{ij} matrix represent a particular state of a system and are internally generated in the multiplication unit. It is assumed that the system matrix state, a_{ij}, remains fairly constant such that the system matrix elements change infrequently. The system interaction with its environment takes the form of a matrix vector product whereby the vector b_j represents a state of the environment. The residue arithmetic notation is depicted in the figure by the moduli m_0, m_1, and m_2 used in representing the input and output vector element values.

Although not shown in Figure 1, the inputs and outputs are position coded, whereby the position of a light source or image in a linear array represents the magnitude of a number in the residue arithmetic notation used. These sources are either on or off resulting in a high signal to noise ratio in distinguishing between states of different inputs and outputs. This provides a consistent input and output coding such that the output of a particular unit can be directly used as the input to another unit without the need for any opto-electronic conversions.

Mappings are used to connect these postion coded inputs and outputs. The mappings are optically implemented to provide interconnection paths using arrays of light beam patterns; each operation or algorithm performed is associated with a specific pattern. To perform an operation, all that is required is a pattern imaged onto

the light valve write beam side, and a position coded input source on the read beam side. The pattern is recalled from memory and its form is a function of the number represented and the operation performed. The particular configuration of the spatial light modulator is such that once the spatial light modulator responds to the pattern, in one device response time, the light beam from a position coded input is directly mapped to a position coded output at the speed of light (propagation delay only).

Both multiplication and addition operations are implemented using look up tables based on such optical interconnection mappings. Two storage mechanisms are used to accomplish the mappings, a holographic storage unit and a microprocessor controlled CRT [11], providing the large memory required to store the look up table patterns. The multiplication pattern coordinates are stored in the microprocessor memory driving the CRT. The addition patterns are stored in the holographic memory. Referring back to Figure 1, it is noted that the multiplier stored patterns represent the matrix element input to the product. The position coded input sources represent the vector element inputs. Once a product is performed, the position coded output product is used as an input to the multiplexed holographic storage. The pattern generated from the holographic memory is then used as a mapping for the addition unit to provide an output sum.

There are two main factors that allow implementing the matrix vector product in one response time, independent of matrix size. These are the residue arithmetic representation and the holographic memory. Residue arithmetic, permits the efficient use of the memory available.

In this type of representation, it is easy to implement arithmetic operations using mappings with a minimum number of inputs and outputs and thus a minimum number of stored patterns. Furthermore, arithmetic operations on residues can be performed in parallel, without carry.

The role of the holgraphic memory is evident in that the patterns generated from the holographic storage, due to the multiplier output product, instantaneously provide the adder write beam input so that an addition operation can be performed. Assuming that the a_{ij} matrix elements rarely change and the patterns corresponding to those matrix elements have already been impressed onto the spatial light modulator for the multiplication look up table, then the only response time, other than the propagation delay of the light beams to perform a parallel set of products and sums, is the device response time needed for the addition mapping unit.

Comparing this design to those listed in a report by Athale [61], where algorithms for performing matrix-matrix products are organized in three main categories, N-parallel, N^2-parallel, and N^3-parallel, it is seen that this design falls into the N^3-parallel category which is the most efficient. (As the order of N increases, the larger the degree of parallelism in the computation). This is associated with the computation time required to perform the product. The number of clock cycles necessary to perform nxn matrix-matrix products ranges from a maximum of n^3 operations for the N-parallel case to a minimum of 1 cycle for the N^3-parallel case. That is to say that all the elements of the C matrix are generated in one operation or one device response time using N^3-parallel algorithms. The design presented

here can be extended for matrix-matrix products with no additional response time where all the columns of the C matrix can be generated simultaneously.

Design Description

In this section, the principal components and coding techniques of the particular matrix vector multiplier are presented. This includes a description of residue arithmetic, input and output coding, look up table mapping units, the Hughes liquid crystal light valve (LCLV), and holographic storage. Combining the described components, the overall system is discussed, introducing a new approach to using the light valve in which the effect of the slow device switching time is minimized.

The residue arithmetic representation will be introduced first as the implementation of any operation or algorithm is dependent on the arithmetic representation. This will be significant in forming the patterns used in the position coded optical look up tables.

Residue Arithmetic

A short review of residue arithmetic is presented for completeness. In residue arithmetic, a number is represented by a set of residues with respect to a set of moduli [2]. The residue of a number in a particular modulus is the remainder after dividing the number by the modulus. Thus, for example, consider the number seven and moduli two, three and five. Seven has residue of one with respect to modulus two, (one modulo two), and similarly is represented by one modulo three and two modulo five. Thus, the number seven would be represented by the triplet (1,1,2) with respect to moduli 2, 3, and 5. This representation

requires a limited set of numbers, those forming the equivalence partitions of the residues, 0 to m-1 for each modulo m, and it has a range unique up to the product of the relatively prime moduli used [29]. The operations of addition, subtraction and multiplication are performed quite simply using residue arithmetic. The residues with respect to a given modulus are combined using the desired operation and the modulus is cast out if necessary. Consider the residue representations of nine and three modulo 2, 3, and 5; they are (1,0,4) and (1,0,3), respectively. Starting with modulus two, adding one to one gives two which gives zero after modulus two is cast out. (Thus one plus one is zero modulo two.) Similarly, with respect to modulus three, zero plus zero gives zero, and in modulus five, four, the residue of nine, plus three, the residue of three, give seven which after five is cast out gives a remainder of two; hence, four plus three gives two modulo five. The triplet (0,0,2) corresponds to decimal twelve as expected. (See Appendix A). Similarly, subtraction and multiplication operations can be performed.

An important feature to note is that all the operations can be performed in parallel (simultaneously), as there is no interaction between the residues of different moduli; for example, there is no carry involved in arithmetic operations. It is then practical to perform arithmetic operations on the smaller set of numbers, the residues resulting from the equivalence partitions, using look up tables. The representation requires a number of moduli, each with its own look up table; nevertheless, they can all be used simultaneously since operations are performed independently in each modulus.

Mappings

It has been indicated that an array or pattern of write beams is used in defining a mapping. The maps or interconnection patterns, each representing a different operation, can now be established.

A typical set of mappings is shown in Figure 2. In Figure 2a two mappings are shown, for multiplication by one and by four modulo five. On the left hand side of the figure the interconnections are defined with input on the left and output on the right. Multiplication by one is evident, since every number on the input side is mapped into itself on the output side. The mapping for times-four modulo five is easily verified. For example four times three is twelve, which, after dividing by five, gives a residue of two. Thus the input of three in the times-four table is connected to the output of two.

An alternative form for the patterns representing multiplication by one and four modulo five are also shown, on the right side of Figure 2a. The input is represented along the vertical axis and the output is represented on the horizontal axis shown at the top. The dark spot in each row and column indicates a connection between a position coded input and a position coded output. In the pattern for multiplication by 4, the dark area in the fourth row is in the third column, indicating that an input of three multiplied by four modulo five gives an output of two. Note that there is one and only one spot in each row indicating that the mapping is one-to-one. These patterns are the exact write beam patterns to be used in implementing the required look up tables.

A complete set of mapping patterns for multiplication modulo 5 is shown at the left in Figure 2b. The patterns for addition shown on the

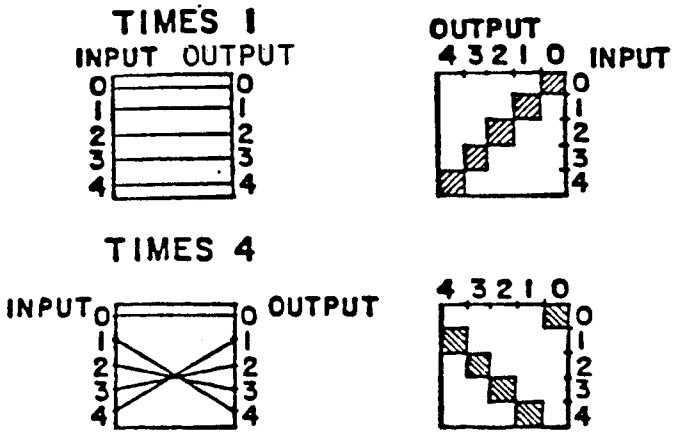

a. Interconnections.

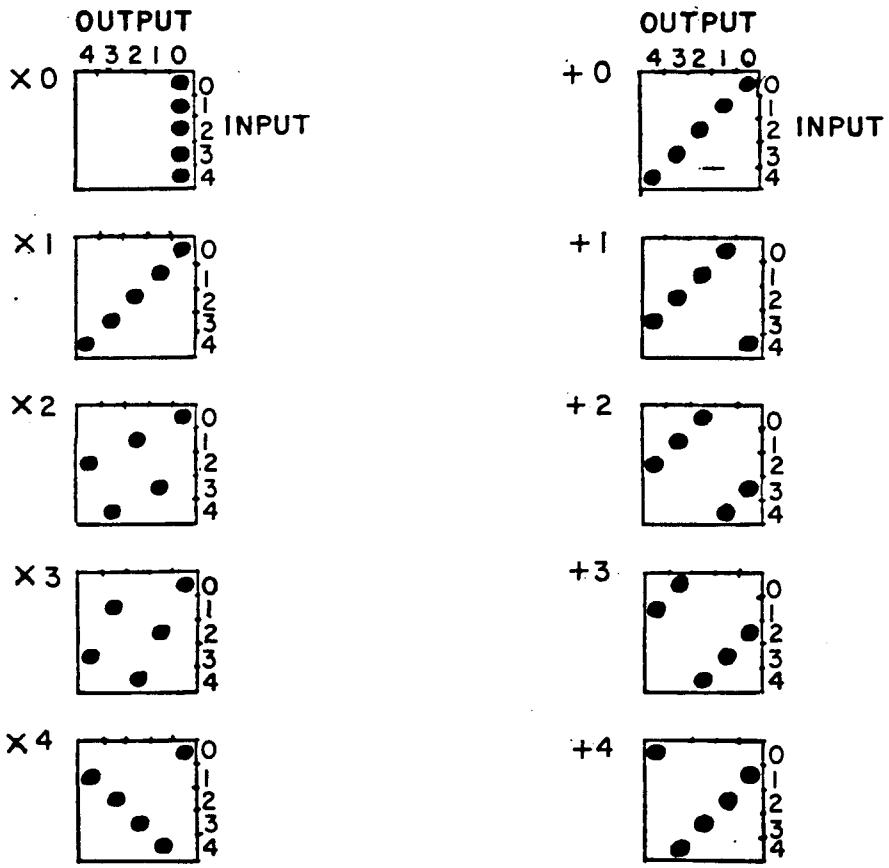

b. Multiplication and addition patterns

Figure 2. Modulo 5 mappings.

right are even simpler, consisting of sets of slant lines. These patterns will be referred to in describing the implementation of the look up tables.

Hughes Liquid Crystal Light Valve: 'Birefringent Gate'

The central component in this design is the Hughes liquid crystal light valve (LCLV) [1,62]. This device characteristically performs like an optically controlled birefringent mirror with an array of 600x600 image elements in one square inch. Each element is independently controlled such that the intensity of an input light beam incident on the back of the device, the write beam side, at a given image element position controls the polarization of a second beam reflected off the other side, the read beam side, at that image element position. With input light on the write beam side, the light valve acts like a half-wave plate, rotating the reflected beam polarization by 90°; without a write beam input, the read beam polarization is unchanged.

The light valve is used to create an array of 'birefringent gates' to implement the mappings of Figure 2. The basic birefringent gate configuration is shown in Figure 3. A cross-section of the gate is shown in the figure with a write beam on the left, and a read beam on the right. The 'polarizing' mirror to the right of the LCLV, represented by a line, reflects light of one polarization and transmits the orthogonal component. It is, in fact, a system of optical components composed of polarizing prisms, mirrors, and lenses yet to be described.

As shown in Figure 3, the initial read beam is polarized such that it is transmitted by the polarizing mirror. Its polarization is then rotated by 90° upon the first reflection off the light valve and it is

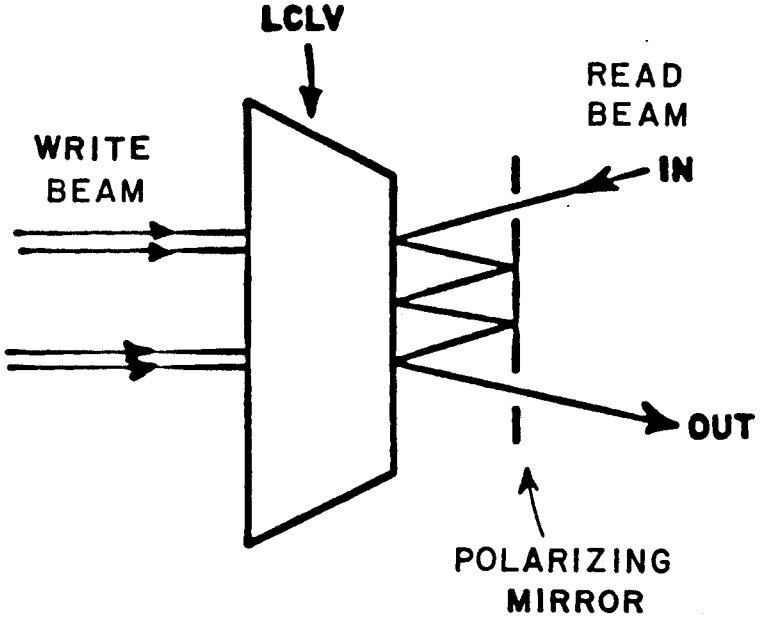

Figure 3. Birefringent gate.

subsequently reflected back and forth and shifted sideways between the polarizing mirror and the light valve. Finally, after a predetermined number of reflections, the polarization is again rotated by 90° upon reflection by the LCLV and that reflected beam passes through the polarizing mirror at the desired output position.

Optical look up tables for performing multiplication and addition are constructed using the birefringent gate principle described above. The operation shown in Figure 3 involves one row on the array of input read beams and the corresponding row of the write beam pattern. The operation is duplicated in other planes parallel to the plane of the figure with a different number of predetermined reflections in each row to implement the complete table.

Look up Table Implementation

An implementation of a look up table is shown in Figure 4. The light valve is shown in the center of the figure with a 'polarizing mirror' to it's right. In the mapping unit light comes in through any one of a vertical column of input positions shown to the right of the mirror, the vertical position indicating the numerical value. The mapping is represented by the pattern of beams provided at the left side of the light valve; the grid is shown in the sketch to indicate the pattern orientation.

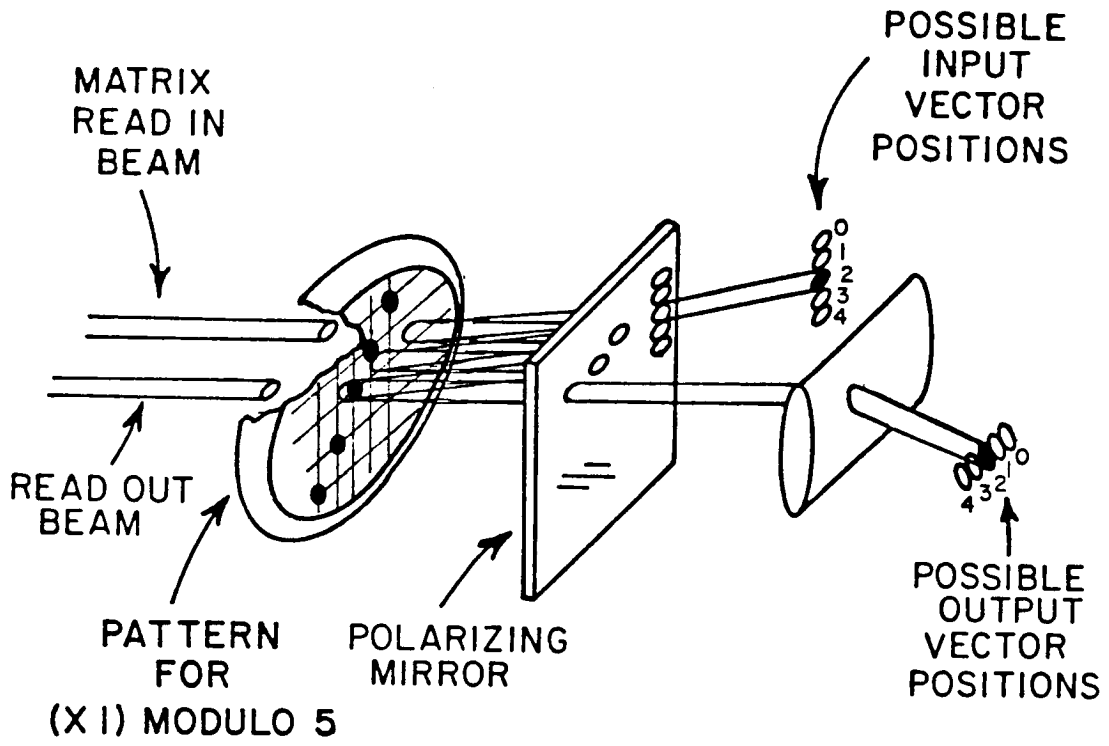

Figure 4. Look up table implementation.

In the example shown in Figure 4, an input of 2 and the pattern for times 1 modulo 5, shown in Figure 2b, are used. An output is obtained after three reflections off the light valve. After the light is transmitted through the polarizing mirror it is directed towards the horizontal axis by the cylindrical lens. The output value is then indicated by the position along the horizontal output axis, 2 in this case. The use of the cylindrical lens in all applications may not be practical so alternative methods for achieving the final position coded output have been considered [63]. This type of mapping unit look up table is used for addition and multiplication in the matrix multiplier.

The patterns used for the write beam arrays must be stored and recalled. The two mechanisms used in this design to accomplish this task were described briefly earlier in this chapter. For the implementation of multiplication look up tables the maps are electronically generated using a microprocessor controlled CRT where the desired pattern coordinates are stored in the microprocessor memory. The second mechanism is a holographic memory composed of a set of carrier and space-multiplexed multi-exposure bleached holograms.

Holographic Memory

The holographic memory used in this design consists of a set of carrier and spatially multiplexed [64] phase volume transmission holograms recorded in a silver halide emulsion. It is used to store a number of patterns in the same small emulsion area. Further, the film plate contains many such spatially separated areas. The recordings are made with plane wave object and reference beams, as described later.

The recorded patterns are reconstructed from the holographic memory by supplying a pattern address associated with a set of input spots in the focal plane of a lens. The reconstruction configuration is shown in Figure 5 with the hologram shown in the center, an array of five point sources at the left, and an output plane on the right. The lens collimates the spherical beams into plane waves, each travelling in a different direction towards the same hologram area. The hologram reconstructs a different diffracted beam for each point source, i.e., each reconstruction beam direction.

The generated diffracted beams produce real images (patterns) that superimpose in the same output plane. A real image is obtained by using collimated reference and reconstruction beams, reversing the emulsion orientation by rotating 180° about the y axis with respect to the construction orientation [65], and using the conjugate image. Since a planar object (masks) was used in the same plane for each of the hologram exposures, then all images will be in the same plane.

In Figure 5, only one of the point sources is on at any one time. Input zero is used in Figure 5(a) to generate the pattern associated with zero, input 2 is used in Figure 5(b) and a different pattern associated with two is generated in the same output plane.

Thus using this type of holographic recording a set of stored patterns are reconstructed using a set of position coded inputs. Each source position and associated reconstructed pattern represent a number.

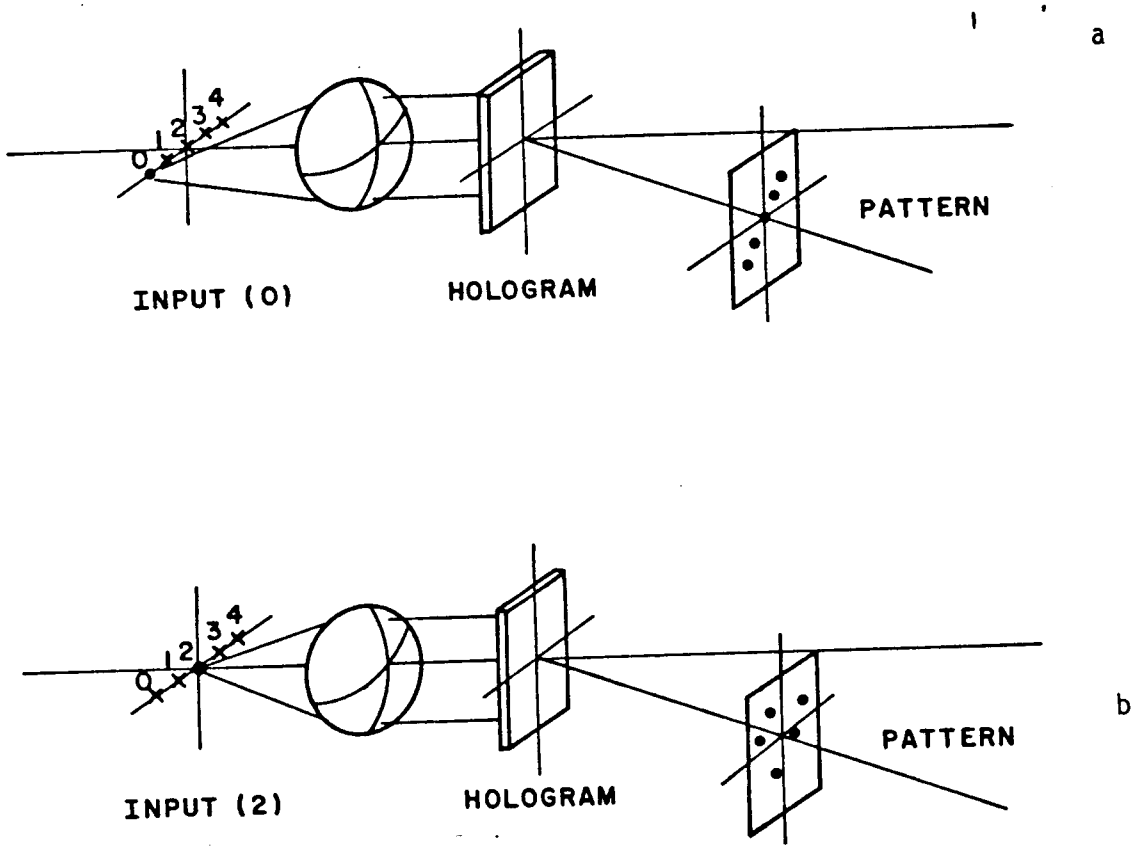

Figure 5. Hologram reconstruction configuration.

Overall System.

The matrix-vector multiplier is a combination of all the principles and devices of the previous discussions. The basic matrix-vector product operations, multiplication and addition using residue artithmetic, physically implemented using a set of parallel mapping units [29], are shown schematically in Figure 6. Two light valves are shown, one at the left and one at the right. Actually different portions of the same light valve can be used. The multiplication input patterns representing matrix elements a_{ij} are generated by a CRT shown at the left. The position coded input vector elements b_j shown at the top center are directed to the appropriate mapping units implemented on the light valve at the left. The resulting position coded output products, $a_{ij}b_j$, now act as position coded inputs to a holographic storage unit. The reconstructed patterns are used as input maps for the addition operation implemented on the light valve at the right. A position coded source representing zero shown at the top right is an input to the first addition mapping unit. The resultant position coded output serves as the input of the next mapping unit, and so on; in this way the summation over j of the $a_{ij}b_j$ products is performed giving the output c_i. The whole process is to be duplicated in different areas for different values of 'i' so that a complete matrix vector product can be implemented by multiplying and adding matrix and vector elements in parallel.

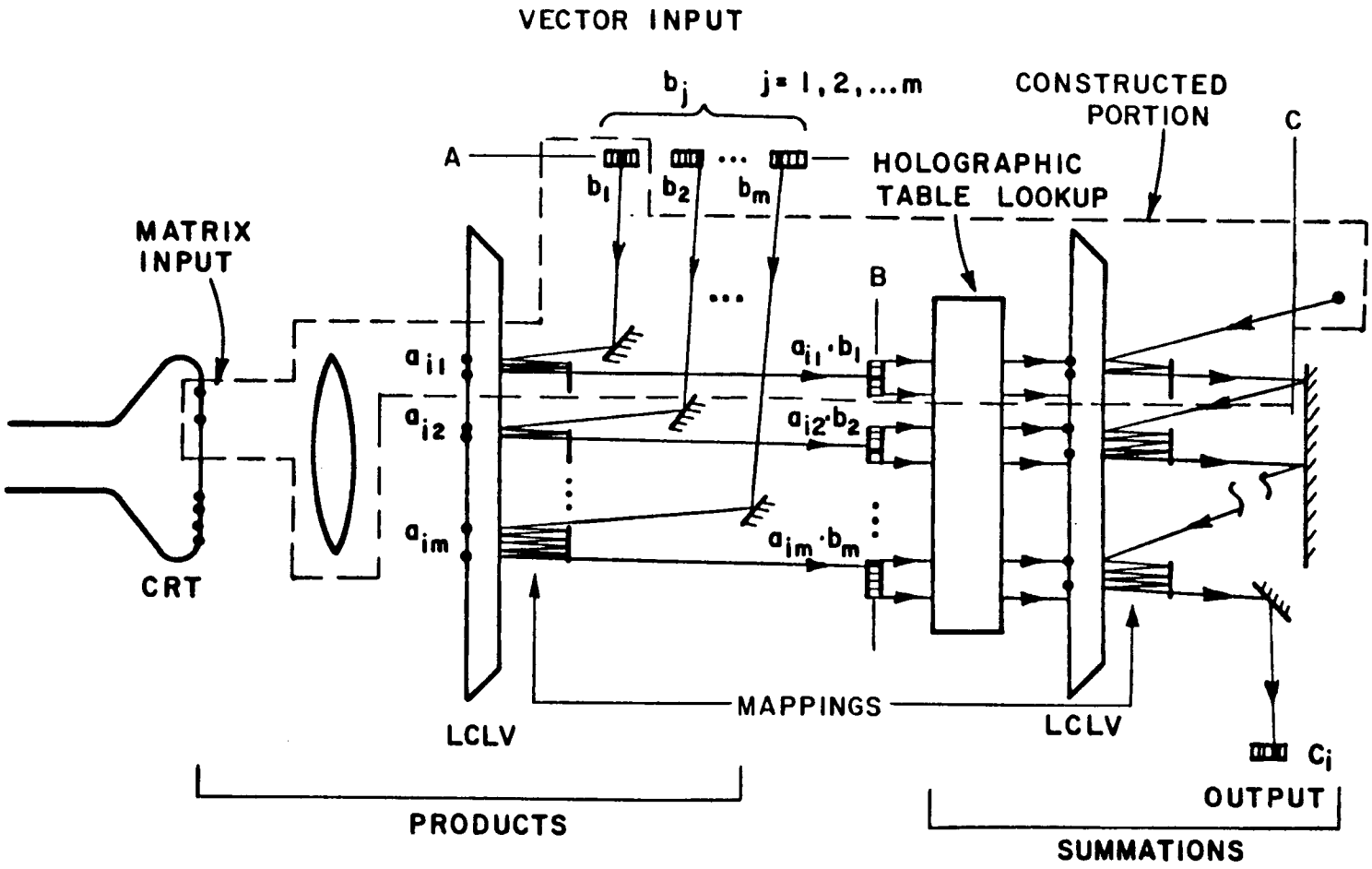

Figure 6. Overall system: matrix vector multiplier.

The output vector is attained after one light valve response time and the negligibly small propagation delay needed to reflect and shift the light through successive addition mapping units. Indeed the response time is independent of the matrix size and dependence on the relatively slow light valve response is minimized by requiring only one light valve response time, that which the light valve requires to respond to the patterns generated from the holographic memory. It is assumed that initially the light valve had already responded to the matrix element patterns generated by the CRT and that these patterns change infrequently.

In this way it is possible to perform the matrix vector products with high speed and efficiency which is the ultimate goal in the design described in this report. As noted, this involves a tradeoff, primarily with respect to SLM space allocation in optically implementing the mappings. Furthermore, extending the proposed method to perform matrix-matrix products requires no additional response times, only additional SLM space allocation and holographic storage area. The various matrix row or column vectors can be operated upon in parallel.

Based on the approach shown in Figure 6, an experiment demonstrating the basic components of a matrix vector multiplier is reported. CRT generated patterns are used to implement a multiplication mapping unit. Its output is used to generate an addition mapping pattern from a holographic memory. The generated pattern is imaged onto an addition mapping unit and an output sum is produced. The experiments performed including the construction of the holographic memory are described in the following chapter.

Theoretical Aspects.

In this section various theoretical aspects of the matrix-vector multiplier will be considered. The theory of operation of the Hughes liquid crystal light valve in the desired configuration is discussed first, followed by the theory used in determining the hologram requirements for optimum reconstruction from superimposed exposures. The system energy limits and requirements are then considered, and finally an expression for the number of parallel matrix vector multipliers of the type described in this design implemented on one LCLV will be derived.

Hughes Liquid Crystal Light Valve

To perform the multiple reflect and shift operations on the light valve it was necessary to input light beams at non normal incidence on the output side. An optimum optical configuration was chosen to properly exhibit the birefringence with the type of LCLV and input used.

The situation is depicted in Figure 7 with a portion of the liquid crystal layer of the LCLV where the liquid crystal molecules have been rotated due to an induced internal electric field. The birefringent liquid crystal molecules were initially aligned with a director orientation, $\hat{n}$, in the y direction. The incidence plane for the light is horizontal with incident and reflected beams at angle γ from the normal. The incident beam is linearly polarized at 45° to the horizontal and vertical axes of a plane orthogonal to the incidence direction. Note particularly that the plane of tip of the liquid crystal molecules is coincident with the incidence plane of the light; the director orientation makes an angle θ with the y axis in that plane.

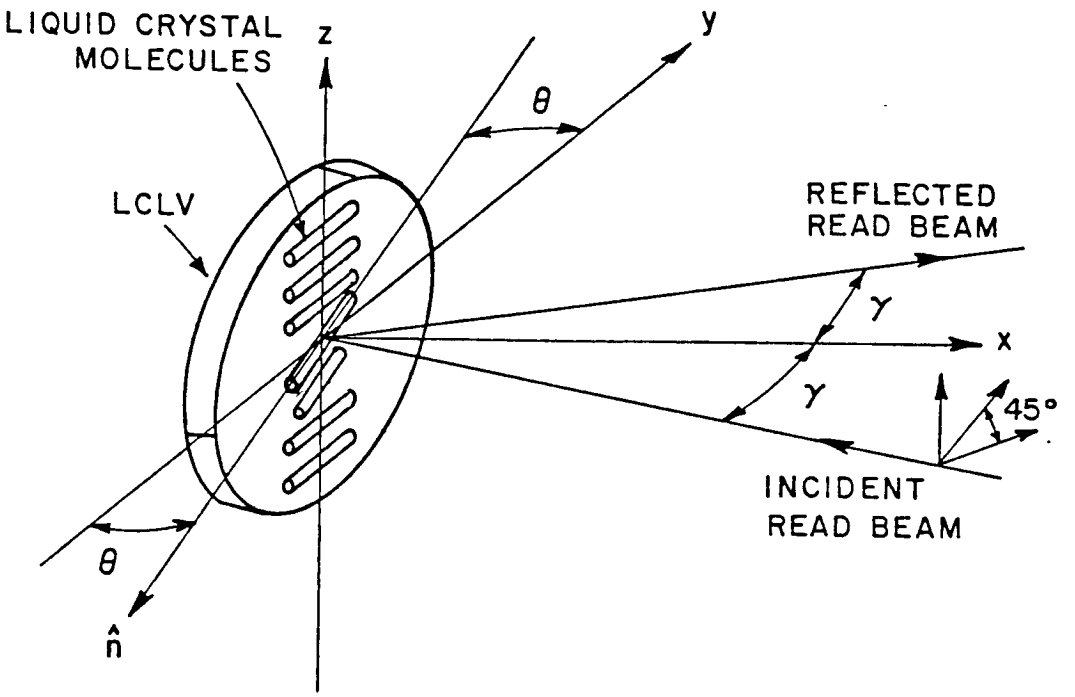

Figure 7. LCLV Orientation.

The birefringence of the liquid crystal molecules is dependent on the incidence angle γ and the tip angle θ. For the normal incidence (γ=0) case the input beam polarized at 45° can be decomposed into two orthogonal components of equal magnitude along the fast and slow axes directions, (the z and y axes respectively in Figure 7). An applied field causes the liquid crystal molecules to tip by an angle θ from their unbiased state. There are specific values of θ at which an integer multiple of 180° phase delay is incurred between the orthogonal compoments, giving an effective 0° or 90° rotation in polarization [15,62].

At non normal incidence, ($\gamma \neq 0$), it is necesary that the incidence plane and the liquid crystal molecules tip plane be coincident as shown in Figure 7. In this case, the fast axis will always be vertical and

the slow axis will be directed in the horizontal plane such that the input polarization is decomposed into equal components. The effective induced phase delay is a function of $\theta \pm \gamma$. A detailed mathematical analysis of this case is given in Appendix B. The impact of this requirement will be seen in the new light valve configuration described in the experimental section of this report, where the plane of incidence is tipped at 45° and the input polarization will either be vertical or in the horizontal plane.

Analytical Description of Holographic Memory

An analytical discussion of the holographic memory is presented in this section. This is done in two parts. In part (a), two equations relating angular width or sensitivity to the hologram emulsion thickness and the number of superimposed exposures are presented showing the conditions for optimum reconstruction efficiency. These equations are derived using coupled wave theory [46,47]. Part (b) contains a discussion of the conditions for equal reconstruction efficiency from successive exposures. An explanation is presented for the exposure adjustment needed to maintain equal reconstruction efficiency for successive recordings in making a multiple exposure holographic memory.

a. Relationships for hologram angular sensitivity and number of superimposed exposures

Two figures of merit are considered in analyzing the desired holograms, the angular sensitivity and the number of superimposed exposures with maximum reconstruction efficiency. Relationships between

the angular half-width, δ, the number of superimposed exposures, N, and reconstruction efficiency, η, in terms of the physical parameters of a holographic recording medium and geometry are derived in this sub-section. Graphs obtained from plotting two derived expressions are presented relating both N and the emulsion thickness, T, to angular half-width. From these equations and graphs, the theoretical angular sensitivity and reconstruction efficiency are presented for the emulsion used in the experiments of the next chapter (Kodak 649-F).

A transmission hologram was chosen for this application because it has better angular sensitivity than a reflection hologram [51] Furthermore, phase transmission holograms produced by bleaching the emulsion will be used to achieve optimum reconstruction efficiency.

Consider the simple hologram construction geometry shown in Figure 8 where a cross section view is given with plane wave object and reference beams incident on a photographic emulsion from the same side. Looking at an x-z plane in the emulsion, let the emulsion normals be in the z direction. The recorded pattern shown is in the form of a parallel grating with fringes parallel to the z axis and a grating period Λ. The associated grating vector $\underline{\kappa}_g$, (vector quantities are underlined), has a magnitude $\kappa_g = 2\pi/\Lambda$.

The pattern is recorded using plane wave construction beams incident with wavefront normals at an angle θ_a in air or Bragg angle θ_o in the emulsion, on opposite sides of the emulsion normal. The angular

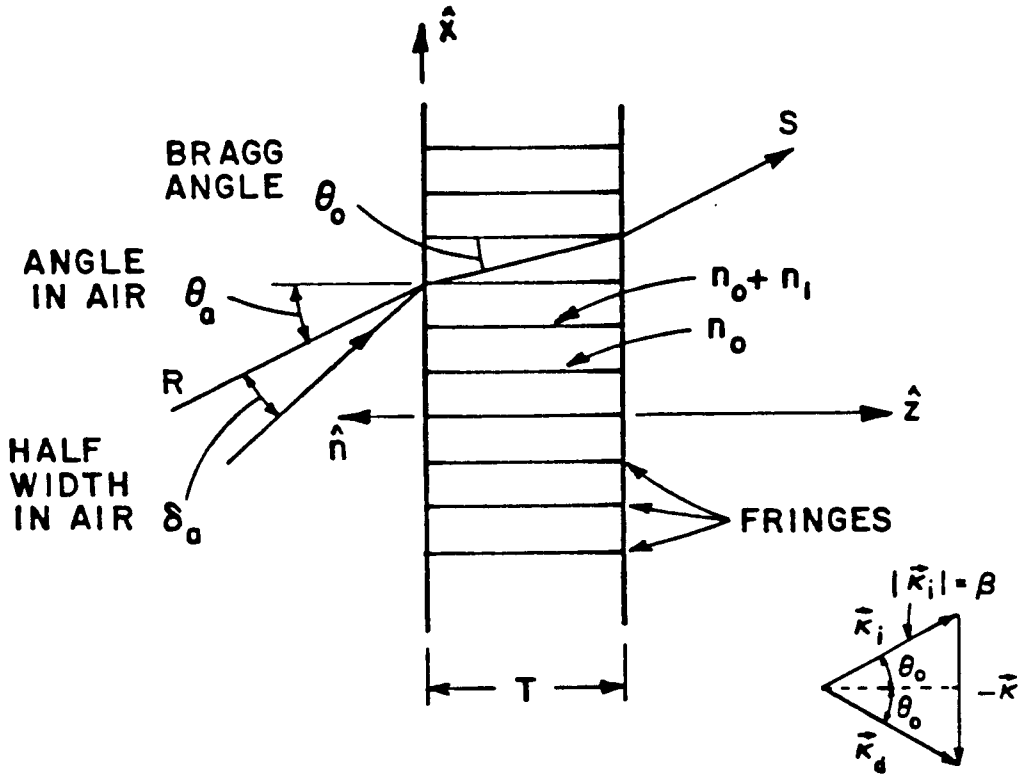

Figure 8. Hologram geometry.

sensitivity of the emulsion and therefore its angle multiplexing potential is related to the deviation angle δ_a from Bragg incidence. This is the small angle δ_a in the x-z plane between the original reference or carrier beam direction and a second reoriented reference beam. A second reference beam direction at an angle $\theta_a \mp \delta_a$ relative to the z direction is used for a second exposure onto the same area of the emulsion. The second exposure can now be recorded using a different object beam but at the same object beam angle.

To obtain N superimposed exposures the procedure given above is repeated N times, each time changing the reference beam direction by an angle δ_a from the prior exposure. This results in a set of N gratings corresponding to a set of reference beams whose incidence angles are centered about θ_a and range from $\theta_a-(N/2)\delta_a$ to $\theta_a+(N/2)\delta_a$, in increments of δ_a. However, the number N is dependent on δ_a, the half power angle, and is a function of the emulsion properties previously listed.

The results of Kogelnik's coupled wave theory [47] for a phase transmission hologram are used to derive the desired relationships. The derivation which follows is based on one of six cases presented by Kogelnik and later Collier, Burkhardt and Lin [50] to study reconstruction efficiency of holographic recordings.

Denoting the field or intensity associated with the reference beam with a subscript 'r' and the object beam with a subscript 'o', the two plane waves propagating towards the emulsion on either side of the emulsion normal produce an intensity interference pattern of the form:

$$(I_{inc})_{SE} = \frac{1}{2\bar{Z}_o}\left((E_{r0})^2 + (E_{00})^2 + 2E_{r0}E_{00}\cos[(\underline{\kappa}_r-\underline{\kappa}_o).\underline{r}] \right) \qquad (2)$$

or

$$(I_{inc})_{SE} = I_o + I_1 \cos(\underline{\kappa}.\underline{r}) \qquad (3)$$

where $\underline{\kappa} = \underline{\kappa}_r - \underline{\kappa}_o$.

The resultant sinusoidal variation in absorption is converted into a sinusoidal variation in refractive index after the chemical processing. Assuming an average refractive index (associated with the index change due to the bias exposure), n_o, and a peak change in index due to exposure, n_1, then the effective index variation can be expressed as:

$$n = n_0 + n_1 \cos(\underline{\kappa}\cdot\underline{r}) \qquad (4)$$

The intensity distribution given in Equation (3) determines the amplitude transmission of the emulsion on which the hologram is recorded. Upon bleaching the emulsion, a phase transmission hologram is obtained. This bleached emulsion is modelled by a dielectric medium where the index variation produced by $(I_{inc})_{SE}$ is of the form given in Equation (4).

Collier, Burkhardt and Lin's notation [50] is used in studying the coupling between the reconstructing wave, E_R, and a reconstructed (diffracted) wave satisfying the Bragg condition E_S. Specifically, the coupling is characterized in terms of a diffraction efficiency η, defined as the ratio SS^*/RR^* where S and R are the complex amplitudes of the diffracted wave and reconstruction wave respectively. The forms for S and R are obtained by a solution of the wave equations governing the propagation of the reconstructing and resultant diffracted waves. These forms are derived in Appendix C.

The analysis is conveniently performed in terms of the parameters ξ and ν relating the coupling coefficients and intrinsic properties of the recording medium. For the lossless phase transmission hologram case

$$\xi = \delta\beta T\sin\theta_0 = \delta(2\pi n_0/\lambda_a)T\sin\theta_0 \qquad (5)$$

$$\nu = \pi n_1 T/\lambda_a \cos\theta_0 \qquad (6)$$

where $\beta = 2\pi n_0/\lambda_a$, λ_a is the free space wavelength, and n_1 is the variation in index due to the single exposure. Note that ξ is proportional to δ, the deviation angle from Bragg incidence, and is a normalized angle; ν is proportional to n_1 and is a normalized coupling constant.

Solving the wave equation with the appropriate boundary conditions for this case gives [10,31]:

$$S(T(\xi,\nu)) = -j \exp(-j\xi) \frac{\sin[(\xi^2+\nu^2)^{1/2}]}{(1+\xi^2/\nu^2)^{1/2}} \tag{7}$$

Applying the definition of η, and the geometry of Figure 8,

$$\eta = SS^*/RR^* = |S(T)|^2/|R(0)|^2 \tag{8}$$

and assuming that the reconstructing wave has unity amplitude, then the efficiency can be directly expressed in terms of the diffracted wave amplitude:

$$\eta = |S(T(\xi,\nu))|^2 = \frac{\sin^2[(\xi^2+\nu^2)^{1/2}]}{(1+\xi^2/\nu^2)} = \nu^2 \frac{\sin^2[(\xi^2+\nu^2)^{1/2}]}{(\xi^2+\nu^2)} \tag{9}$$

By studying the argument of the sine function, conditions for maximum reconstruction efficiency and minimum coupling into diffracted beams from other gratings recorded in the same emulsion can be obtained.

Consider the case where $\delta = 0$. This implies that $\xi=0$, and Equation (9) reduces to:

$$\eta = \sin^2(\nu) \tag{10}$$

In this case the Bragg condition is satisfied and reconstruction at the Bragg angle results in 100% reconstruction or coupling ($\eta=1$) between incident and diffracted beams for a medium with the correct interaction length or thickness. Setting $\nu = \pi/2$ gives the following relationship from which the proper thickness, T, for the desired energy interchange is obtained:

$$\nu = \pi n_1 T/\lambda_a \cos\theta_o = \pi/2 \tag{11}$$

Solving for T from Equation (11) gives:

$$T = \lambda_a \cos\theta_o \,/\, 2\, n_1 \tag{12}$$

When Equation (12) is satisfied, 100% diffraction efficiency is obtained; for other values of ν, η will be smaller.

The half angle or deviation angle that gives $\eta = 0$ will be denoted by δ_{co} inside the medium (δ_{ca} in air). The efficiency goes to zero when the sine function argument in Equation (9) goes to π. Given ν, then Equation (9) is used to relate δ_{co} to the emulsion parameters, and the following condition results:

$$(\xi^2+\nu^2)^{1/2}\Big|_{\nu=\pi/2} = \pi \tag{13}$$

Combining Equations (5), (12), and (13), and solving for δ_{co} gives:

$$\delta_{co} = (3)^{1/2}\lambda_a/4\ T\ n_o \sin\theta_o \tag{14}$$

Equation (14) gives the half angle for 100% diffraction efficiency and the relationship to the emulsion thickness T. It is one of the desired equations which will be plotted.

Now consider the maximum number of holograms that can be superimposed in this emulsion for specific values of ν. Equations (3) and (4) dealing with the index variation are first extended for a carrier multiplexed hologram of N exposures. Assuming the same refractive index variation for each exposure, then the total incident intensity for multiple exposures is expressed by extending the form of Equation (3) to a summation:

$$(I_{inc})_{ME} = (N|E_{r0i}|^2 + \sum_i |E_{00i}|^2 + 2 \sum_i E_{r0i}E_{00i}\cos[(\underline{\kappa}_{ri}-\underline{\kappa}_o).\underline{r}]) \; / \; 2Z_o \tag{15}$$

where i = 1, 2, ..., N. Similarly, Equation (4) is rewritten to give:

$$n = n_o + \sum_i n_i \cos(\underline{\kappa}_i \cdot \underline{r}) \tag{16}$$

It is assumed that the index variations of the individual exposures, n_i, are all the same, $n_i = n_1$ for i = 1, 2,..., N. The conditions under which this assumption holds are presented in the next section. In addition, the recording medium has a maximum index variation, Δn, specific to the individual material used. This sets an upper limit on N, the number of superimposed exposures, such that:

$$2 N n_1 \leq \Delta n \tag{17}$$

(The factor of two comes from the cosine term in Equation (16) as it varies from -1 to +1.) The value of n_1 is obtained from Equation (12) and substituting in the above expression gives:

$$N \leq \Delta n \; T/\lambda_a \cos\theta_o \tag{18}$$

Taking the upper bound and substituting for T from Equation (14) gives:

$$N_{max} = (3)^{1/2} \Delta n \; / \; 4 \; \delta_{co} \; n_o \sin\theta_o \cos\theta_o \tag{19}$$

This is the second desired equation.

The equations for N and T can be expressed in terms of the angles in air, denoted by subscript 'a' for more practical applications. Snell's law is used to relate the angles in air and the angles inside the emulsion (subscript 'o'):

$$n_o \sin \theta_o = \sin \theta_a \tag{20}$$

$$n_o \sin (\theta_o + \delta_{co}) = \sin (\theta_a + \delta_{ca}) \tag{21}$$

For a small angle δ_{ca}, Equation (21) reduces to:

$$n_o \delta_{co} \cos\theta_o = \delta_{ca} \cos\theta_a \tag{22}$$

With the substitution,

$$n_o \cos\theta_o = n_o [1-\sin^2(\theta_o)]^{1/2} = (n_o^2 - \sin^2\theta_a)^{1/2}, \tag{23}$$

Equations (14) and (19) can be written in their final form giving the two desired Equations, (24) and (25):

$$T = (3)^{1/2} \lambda_a [(n_o^2 - \sin^2\theta_a)^{1/2}]/4\delta_{ca} \sin\theta_a \cos\theta_a \tag{24}$$

and

$$N_{max} = (3)^{1/2} \Delta n \, n_o / 4 \, \delta_{ca} \sin\theta_a \cos\theta_a \tag{25}$$

If less than the 100% reconstruction efficiency assumed in Equation (11) is acceptable, then combining Equations (6), (10), (17) and (23) gives an expression for η, the efficiency for a desired number of exposures, N_d:

$$\eta = \sin^2(\Delta n \, n_o \, \pi T/2 \, N \, \lambda_a \sqrt{n_o^2 - \sin^2\theta_a}) \tag{26}$$

This also allows for more exposures at the same emulsion thickness.

Equations (24) and (25) are plotted in Figure 9 showing a family of curves for N, the number of allowed exposures, as a function of angular half width, δ_{ca}, for different Δn on the upper portion of the figure, and thickness , T, as a function of δ_{ca} in the lower portion of the figure. The set of curves shown are for different values of Δn with 100% reconstruction efficiency. Changing the desired reconstruction efficiency to a smaller value shifts the N versus δ_{ca} curves upward, giving a larger N for the same value of δ_{ca}. By choosing a recording material, the thickness and range Δn are determined and δ_{ca} and N can be

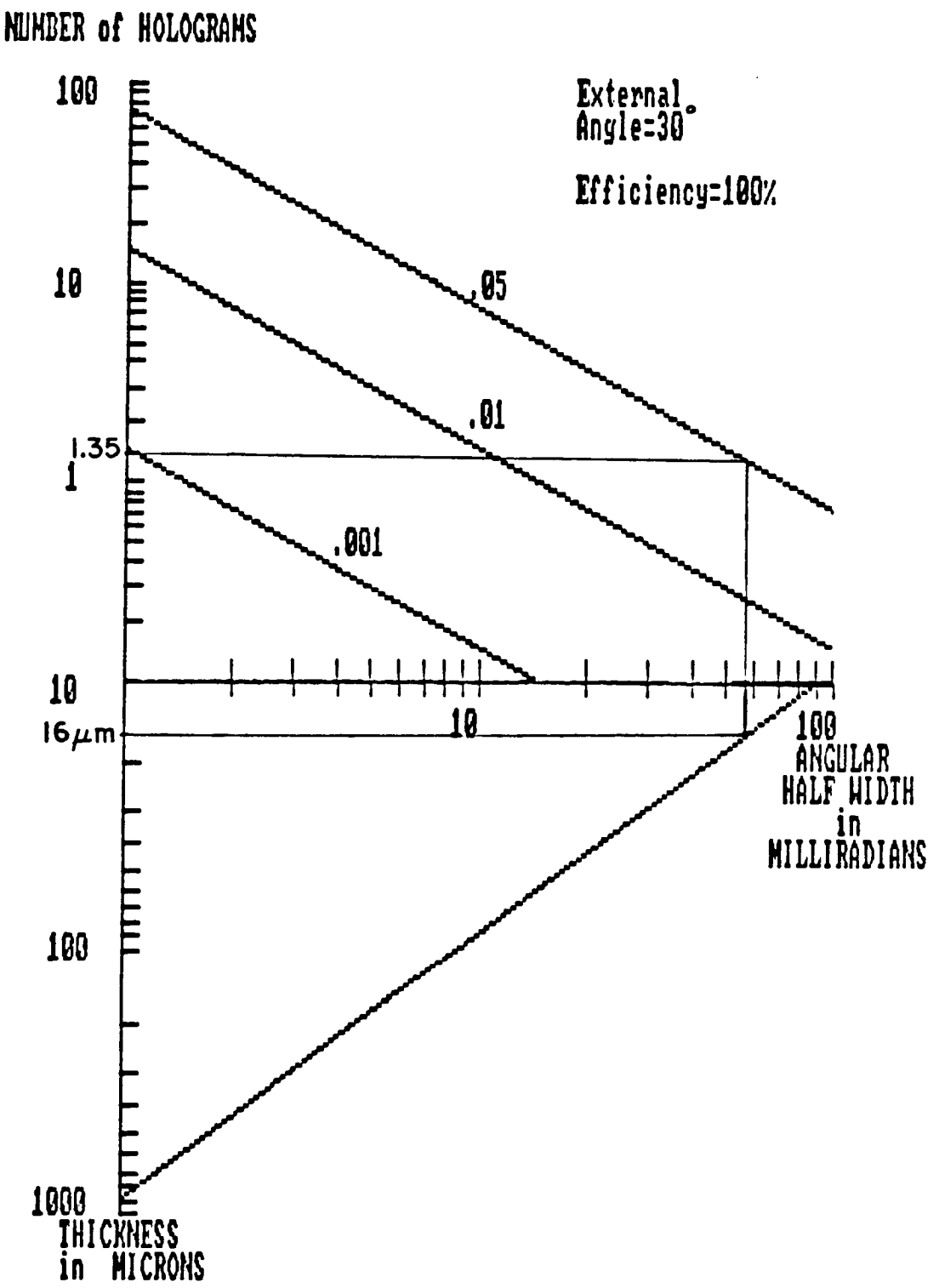

Figure 9. N and T as a function of δ.

found from the graphs. Typical values for Δn range from .001 or smaller for photochromic materials [50] to about 0.05 for silver halide emulsions [60].

For example, consider the silver halide emulsion used to make the holographic memory described in the experiment of the following chapter. The Kodak 649F plates used have a 16μm thick emulsion and a refractive index of about 1.5. From Equation (24) assuming incidence angles of 30° and a wavelength of 632.8nm, an angular deviation angle of about 56 mrad (about 3°), is obtained. Referring to Figure 9, and using the thickness as an entry to the lower vertical axis of the graph also gives an angular half width of about 56 mrad. At this value of δ_{ca} it is seen that for a silver halide emulsion with Δn of 0.05 then at most one 100% efficient hologram can be achieved (N=1.34).

Increasing the emulsion thickness in Figure 9, it is seen that the half angle decreases while the number of possible high efficiency exposures increases. However, Kodak 649F film is among the thickest commercially available photographic emulsions. Other materials such as photochromics have smaller Δn ranges so that for a given thickness and efficiency, fewer superimposed exposures are possible. The materials with the lower Δn values (.001) have to be much thicker, on the order of .1cm to 1cm in order to achieve a significant number of superimposed exposures (20-30) with 100% reconstruction efficiency. The thicker the emulsion the smaller δ_{ca} allowed.

Removing the 100% reconstruction efficiency restriction and using Equation (26) for the same 649F emulsion used in the example above, then

for five superimposed exposures, $N_d = 5$, the expected reconstruction efficiency is given by:

$$\eta = \sin^2(.05 \times 1.5 \times \pi \times 16 / 2 \times 5 \times .6328 \times \sqrt{1.5^2 - \sin^2 30°})$$

$$= .167$$

or about 16.7% efficiency.

The analysis presented here assumes equal reconstruction efficiency from the successive exposures. However, certain conditions must be met in order to achieve this. These conditions are discussed in the following section.

b. Equal efficiency for multiple exposures

In this sub-section the conditions for equal reconstruction efficiency from successive exposures in making a multiple exposure holographic memory are discussed. It has been shown in the literature [56,57,58,59] that reconstruction efficiency drops for successive equivalent exposures, i.e., reciprocity law failure of a silver halide emulsion. An explanation of this phenomena and a solution are presented.

The purpose of requiring equal reconstruction efficiency from successive exposures is that the reconstructed patterns are going to function as write beam patterns for the light valve mapping units and must operate at a uniform intensity level. The procedure involves adjusting all exposure levels to achieve the same index change from each recording in the set of superimposed exposures.

The change in the transmission of a processed film as a function of the initial exposure for a silver halide emulsion is physically due to the photosensitive emulsion. A latent image is formed after exposure

creating sensitivity centers at impurity sites or dislocations where clusters of silver atoms gather [66,67]. Later, during the process of development, these atom clusters attract the remaining silver in the crystal which converts to a silver grain. The number of sensitized crystals ultimately determines the density of silver grains in the processed emulsion.

Once a single sensitivity center is formed in a crystal it has a high probability of conversion to a silver grain during development. Any subsequent exposures creating more sites in that crystal does not further enhance its developability.

Now consider a series of exposures and note that a smaller population of unexposed crystals is available for each successive exposure. To match the density of silver grains from the first exposure, in the processed emulsion, a larger exposure is needed for each successive exposure. This is necessary to compensate for the number of sensitized grains no longer available. This implies that for multiple exposures in the same photographic emulsion area, due to the stochastic nature of the exposure model, a slightly different transmission versus exposure curve must be used to characterize the emulsion after each exposure, each with a larger slope than for prior exposures.

For example, let a power transmission level of 90% in the processed emulsion roughly corresponds to a density associated with a conversion of 10% of the initial silver grains. Starting out with this intensity level it is clear that no more than ten equivalent exposures can be recorded in this emulsion at that exposure level, as the silver grains

would be all used up (saturation). After the first exposure in which 10% of the silver grains were converted, a second exposure that converts the same number of grains requires an exposure level 11.1% stronger than the first, (10/(100-10) = 10/90 = .11).

Mathematically, one expresses the necessary increase in exposure level as a function of the desired percentage of the silver halide grains converted from each exposure as follows;

$$I_n/I_1 = 1/[1-(n-1)p] \qquad (27)$$

where I_1 is the intensity of the first exposure, p is the percentage of silver halide grains in the unexposed emulsion to be converted in each exposure ($0<p<1$), and n denotes the n^{th} exposure, ($1<n<N$). The percentage p is restricted by the number of exposures desired, $p \leq 1/N$.

A comparison of theoretical exposure levels obtained using Equation (27) and empirical results published [56,59] is presented in Table 1. Sets of sample theoretical exposures are tabluated in the first three columns showing relative exposure versus the number of the exposure in the series, for conversions of 5%, 8% and 10% of the grains in each exposure. Results from Johnsons' paper [59] are shown in the last column. Assuming 10% conversion it is clear that the tabluated values for exposure levels in that article and shown here are very closely matched.

Table 1

Exposure Level Adjustment for Uniform Reconstruction Efficiency

p_n	$(Exposure)_n / (Exposure)_1$			
	5%	8%	10%	Literature
1	1.00	1.00	1.00	1.00
2	1.05	1.09	1.11	1.11
3	1.11	1.19	1.25	1.24
4	1.18	1.32	1.43	1.45
5	1.25	1.47	1.67	

Now consider the results shown by Nishida and Sakaguci [56]. Using an exponential fit, data taken from a plot in that reference is shown in Figure 10. Data predicted by Equation (27), assuming a conversion percentage of 8%, is also plotted in Figure 10, and closely matches the empirical data.

The model presented in Equation (27) has proved accurate when applied to a small number of superimposed exposures, $n \leq 12$. It is not expected to work in this form to explain the required exposures involved in 100 superimposed exposures for example, where a bias intensity is used.

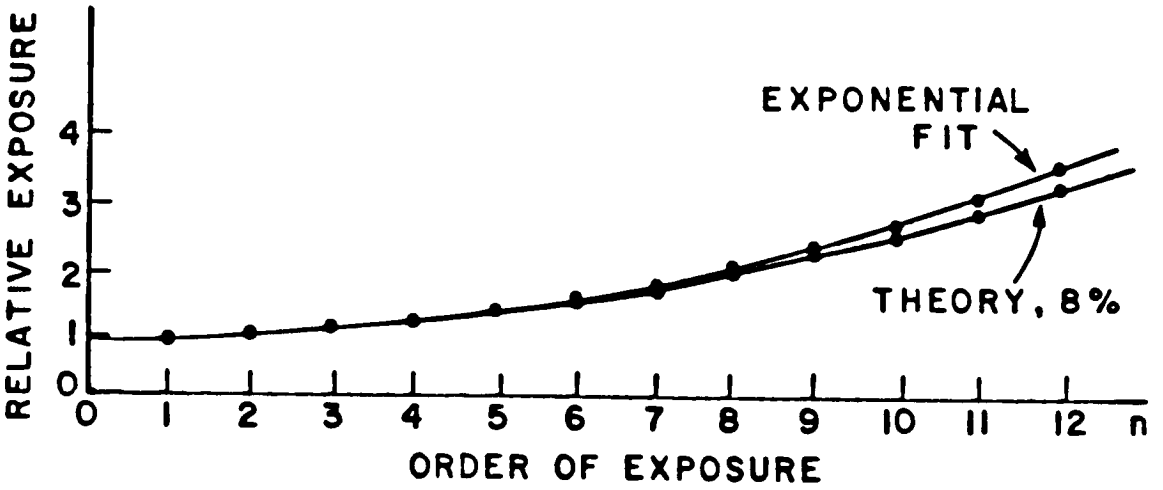

Figure 10. Reciprocity law failure plots.

In summary, in the first part of this section expressions relating angular half-width to the hologram emulsion thickness and to the number of superimposed exposures were derived showing the conditions for maximum reconstruction efficiency. These expressions were plotted in Figure 9. In the second part, the conditions for equal reconstruction efficiency from the successive superimposed exposures were discussed. A model was presented for the necessary exposure adjustments, (Equation (27)), to maintain equal reconstruction efficiency from successive recordings.

System Energy Considerations

The design has several features essential in considering the energy requirments for system operation. These energy requirements and features are briefly outlined in this section.

Recalling Figure 6, it is seen that the transfer of energy and information starting from the multiplication mapping unit read beam side to the holographic memory and then to the addition mapping unit write beam side defines the 'critical path' for energy considerations. The energy limits are summarized in the following 4 categories.

1) There is an upper limit in the power per unit area for the focussed read beam in the liquid crystal; beyond this limit thermal effects in the liquid crystal layer may be detrimental to the beam polarization control. The input read beam intensity entering the liquid crystal layer, I_{LC} must be below a maximum value, I_{MAX}.

$$I_{LC} \leq I_{MAX} \tag{28}$$

2) There will be losses after traversing the various lenses, mirrors, and prisms used in the multiple reflections off the 'polarizing mirror'. In general for a system requiring L lenses, M mirrors, and P prisms using an arithmetic representation that requires 'p' passes through the 'polarizing mirror' optics, the transmission per pass, TR, is a function of the transmission of the i^{th} lens, LT_i, the reflectivity of the j^{th} mirror, MR_j, and the transmission of the k^{th} prism, PT_k. This gives the following expression:

$$TR = \prod_i (LT_i) \prod_j (MR_j) \prod_k (PT_k) \tag{29}$$

where i = 1,2,...,L; j = 1,2,...,M ; and k = 1,2,...,P. Furthermore, if

there are p passes through the combination of components, then the system transmission, TS, is given by:

$$TS_p = (TR)^p \tag{30}$$

This expression directly relates the initial read beam intensity I_{LC} to the output intensity after p passes, $(I_{out})_p$, in other words, the look up table output:

$$(I_{out})_p = (TR)^p \cdot I_{LC} \tag{31}$$

3) There will also be a loss in the hologram reconstruction process expressed by the hologram efficiency, η_{hol}. The reconstructed beam intensity, I_{rec} is given by:

$$(I_{rec})_p = \eta_{hol} \cdot (I_{out})_p \tag{32}$$

4) There is a lower limit on the power per unit area for the LCLV write beam input. This is determined by the light valve input requirements, limited by the CdS sensitivity. The LCLV write beam intensity must be larger than this minimum limit, I_{min} or I_{CdS}, hence:

$$(I_{rec})_p \geq I_{CdS} = I_{MIN}. \tag{33}$$

for all p.

Combining Equations (28) through (33) gives the following relationships:

$$I_{CdS} < (I_{rec})_p = \eta_{hol} \cdot (I_{out})_p = \eta_{hol} \cdot (TR)^p \cdot I_{LC} \tag{34}$$

and

$$I_{LC} \leq I_{MAX} \tag{35}$$

Portions of the derivation presented in these four categories will be used later.

To satisfy all the energy requirements it is desirable to minimize all the possible energy losses in the system by using lenses with quality AR coatings, mirrors with high reflectivity coatings, polarizing elements with high extinction ratios and phase holograms with high efficiency reconstruction. The arithmetic representation used in the design determines the desired number of passes required through the system; ultimately, the system energy requirements will set a practical limit.

System capacity

In this section, the number of parallel matrix-vector multipliers that can be implemented using one light valve will be derived. The light valve is assumed to have a resolution of 600 lines/inch [2].

The number of matrix-vector multipliers is a function of the pattern sizes on the write side of the light valve. The same pattern sizes are used for multiplication and addition and the same number of patterns is required for each operation. The pattern size is a function of the moduli used in the residue arithmetic representation, requiring m_i^2 elements for each of the m_i moduli. The number of patterns is determined by the size of the matrices; for an nxn matrix, n^2 patterns are needed for multiplication and another n^2 for addition, $2n^2$ in total.

Mathematically this can be represented as follows: the number of parallel matrix vector multipliers (N_{MVM}) implemented in 1 in^2 is:

$$N_{MVM} = I[(600)^2(1)/\ 2n^2\Sigma_i(m_i)^2] \qquad (36)$$

where I[ ] denotes the integer part of the argument.

Some examples are given using Equation (36). Using moduli (19,20,21) and 2x2 matrices gives a dynamic range of about 8000, with 37 parallel matrix vector multipliers. For 5x5 matrices and moduli (9,10,11) the dynamic range is 990, with 23 parallel matrix vector multipliers. Consider the following example where (roughly) the same dynamic range is obtained first using 3 moduli and then 4 moduli [68], and 2x2 matrices. Moduli (9,10,11) give 149 parallel matrix vector multipliers; for moduli (3,5,7,11) the range is 1155 with 220 parallel. matrix vector multipliers

Chapter Summary

The design description and theory for the optical matrix-vector multiplier was presented in this chapter. The design objectives were outlined first. They include a mapping approach to residue arithmetic and speed with a single LCLV response time because of the holographic memory. The principal components and coding techniques of the particular matrix vector multiplier design were then presented. This included a description of residue arithmetic, input and output coding, look up table mapping units, the Hughes liquid crystal light valve, and holographic storage. Combining the described components, the overall system was discussed, introducing a new approach to using the light valve in which the effect of the slow device switching time is minimized. Then the theory of the light valve operation in the desired configuration where high contrast was maintained and theoretical aspects of the holographic memory construction were presented. The system energy limits and requirements were then considered, and finally an expression for the theoretical number of parallel matrix-vector multipliers constructed using one light valve was derived.

CHAPTER III

EXPERIMENTS AND RESULTS

Introduction

The construction of the optical digital matrix vector multiplier demonstration apparatus is now presented. There are two main points of emphasis, the apparatus for the optical matrix vector multiplier and its operation, and the apparatus for the holographic memory construction.

The hardware for both the matrix-vector multiplier and the hologram construction is described showing diagrams and photograph based drawings of the matrix vector multiplier and hologram construction apparatus and discussing the pertinent features of each. The demonstration of operation of the matrix vector multiplier and the system performance is then presented. Photographs of simultaneous multiplier and adder outputs will be used to show that a given multiplier output results in the expected value in the adder output.

Apparatus Description

The optical matrix vector multiplier demonstration apparatus and the hologram construction apparatus are now described. The matrix vector multiplier apparatus is described first and then its pertinent features are discussed. Following that, the holographic memory construction apparatus is described and the pertinent procedures for its operation are given.

Matrix-Vector Multiplier Apparatus

The constructed matrix-vector multiplication apparatus is used to demonstrate the essential features of the matrix vector multiplier through the implementation of the basic system design shown in Figure 6. The constructed segments are outlined by the dashed line in Figure 6 showing the components for one modulus of the residue arithmetic representation. Matrix elements represented by multiplication patterns for one modulus are generated by a CRT. The input vector is represented by one set of position coded input spots for one residue. A multiplication operation is performed as shown at the left in Figure 6. The output product goes to the holographic memory where all the addition patterns for the residue modulus, one for each multiplier output, can be reconstructed. The generated pattern is the input to the addition operation. This addition mapping unit is shown at the right in Figure 6.

Now consider the apparatus itself shown in Figure 11. The system is designed with one light valve but emulates the operations in Figure 6. The light valve is shown in the center with the CRT providing matrix element inputs shown at the top. The multiple reflection operation is performed not by a single mirror but by an optical loop configuration. This is shown in the center of Figure 11. There are two beams in the loop, one for multiplication, and the other, reflecting off a different portion of the light valve area, for addition. The hologram, reconstructed by the multiplication loop output and generating the input for the addition loop pattern, is shown at the right. The input vector locations would be at the lower left and the output vector at the right.

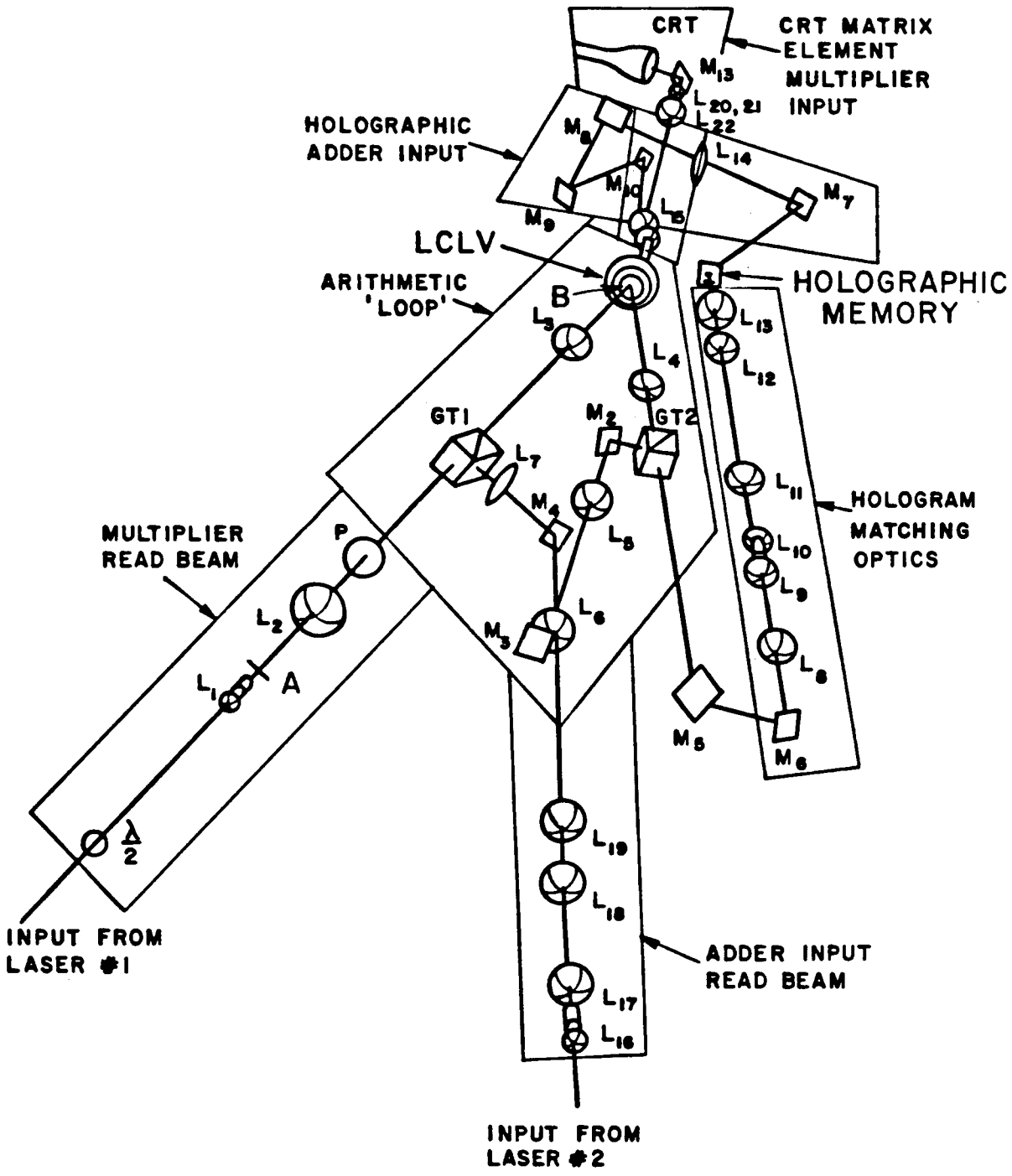

Figure 11. Optical matrix vector multiplier experimental apparatus.

The optical components for the matrix vector multiplier are shown in Figure 11 and also listed in Appendix D. The design uses two laser sources, and appropriate lenses and mirrors and prisms. There are six groups of components, each with a specific task. The fundamental themes of the design are featured in two of the groups. The first group is used to implement the multiple reflections and sidesteps between the light valve and the 'polarizing mirror' described in Figures 3 and 4. This is shown in the center of Figure 11. A loop configuration rather than a multiple bounce configuration is used to most simply provide multiple reflections at adjacent spots on the light valve. There are two beams in the loop one for multiplication and the other for addition. The second group of components is used to implement the theme of a holographic memory with position coded inputs and pattern outputs, the generated patterns forming the write beam input for the addition look up table. The hologram is on the right in Figure 11.

Of the four remaining groups, the multiplication write beam input is provided by the group of components shown at the top of Figure 11, including a microprocessor controlled CRT. The next group which provides the multiplier input read beam is shown at the bottom. The last two groups provide the adder input read beam at the bottom of the figure, and matching optics between the multiplication loop output and the holographic memory input, shown at the right.

In the following sections a-f, the operation of each group of components is briefly outlined. The order will follow that of light flow: read beam input to the multiplication loop, output to the holographic memory, hologram generated input to the light valve for the

adder, the adder loop input, and finally the multiplier CRT input to the light valve.

a. Multiplication input read beam component description

The components providing a polarized input read beam for the multiplier look up table, are shown at the lower left in Figure 11. They are: LASER 1, not shown, $\lambda/2$ plate, M1, L1, and L2, and their object is to provide a collimated input with the desired horizontal polarization to enter the loop.

Referring to Figure 11 it is seen that microscope objective L1 and lens L2 provide the collimated beam in which a Glan Thompson polarizing prism, GT1 is placed. This type of prism transmits a horizontal polarization and reflects a vertical polarization when placed in collimated space. The half wave plate placed immediately following the laser rotates the laser's vertical polarization by 90° to give a horizontally polarized read beam transmitted by GT1. (The beam is focussed onto the light valve by lens L3.)

b. Loop component description

The loop duplicates the sideways shift and multiple bounces required for implementing the polarizing mirror described in Figures 3 and 4. The same set of loop components is used in implementing both the multiplication and addition operations. The loop components are shown in the center of Figure 11. The LCLV is shown at the top, prism GT1 at the left, and prism GT2 at the right. The remaining loop components include L3, L4, M2, L5, L6, M3, M4, and L7. The purpose of the loop is to generate the desired set of sidestepped spots in the

light valve plane. This is done in two stages. First the spot on the light valve is imaged onto auxiliary mirror M3 using collimating lens L4 and focussing lens L5, and then imaged back onto the light valve using collimating lens that of L7 and focussing lens L3. Lens L6 is a field lens imaging the aperture of L5 onto L7. The sidestep on the light valve is controlled by tilting mirrors M2 and M4 causing the beam to shift sideways as it reflects and proceeds successively to different light valve spots.

The two Glan Thompson prisms provide a means of input to the system, (GT1), and output from the system, (GT2), by responding to light valve polarization control. They must operate in collimated space which is provided between the pair of lenses used to image from light valve to auxiliary mirror (between L4 and L5) and back (between L7 and L3). The light valve operating condition is set so that if the write beam intensity provided by a pattern of light beams is bright then the read beam polarization is changed by 90°, and if the write beam intensity is dark the read beam polarization is unchanged. In this way the 'polarizing mirror' of Figures 3 and 4 is realized.

The polarizations of the light beams in the loop are significant. To remain within the loop and be reflected by the Glan Thompson prisms the light must be vertically polarized. The read beam input to the multiplication loop is horizontally polarized and is transmitted by GT1. After bouncing off the light valve the reflected beam polarization must be changed to a vertical orientation if it is to stay in the loop. The read beam input to the addition look up table comes in past the edge of mirror M3 and is already vertically polarized. The beam remains in this

loop until its polarization is changed on one of the successive reflections off the light valve in which case it is transmitted by prism GT2 and exits the loop.

c. Hologram and associated component description

The hologram and associated components used in matching the loop output to the hologram input are shown in at the right in Figure 11. They include lenses and mirrors M5, M6, L8, L9, L10, L11, L12 and L13 with the holographic plate shown at the top right. A horizontally polarized beam is transmitted by prism GT2 and is directed by mirrors M5 and M6 to the lens system composed of L8 through L12. These lenses effectively convert the collimated output beams so as to have the size and propagation direction required to address the hologram, as determined by the hologram construction. (Details of the hologram construction will be described later.)

Lens L8 focusses the light valve output beam in the focal plane of the microscope objective lens L10. In the focal plane the light goes to one of a position coded array of spots corresponding to the spots on the light valve. L9 is a field lens in that plane. Lenses L11 and L13 form a telescope to give the desired angular magnification to the beams from the microscope objective. L11 focusses the collimated beams, L12 is a field lens in that focal plane, and L13 recollimates the light in the desired direction.

d. Holographic memory output imaging components

The object of these components is to project patterns generated by the holographic memory imaged onto the write side of the light valve in

the area corresponding to the addition unit. The patterns are imaged using lenses L14, L15, and mirrors M7, M8, M9, and M10, onto an area on the light valve write side, adjacent to the area on which the CRT patterns are imaged. These components are outlined in Figure 11.

The incidence plane of the hologram is not the horizontal plane for reasons to be discused later. The mirrors M7, M8, M9, and M10 are used to properly direct the resultant reconstructed images onto the light valve write beam input side, with the desired orientation.

e. Adder input read beam components

The objective of these components is to provide the polarized input read beam for the addition loop. This is done by producing a focussed spot in the plane of mirror M3, just past the edge of that mirror.

The vertically polarized read beam from an argon laser source, LASER 2, not shown, is oriented by mirrors M11 and M12 and focussed by microscope objective lens L16 in the focal plane of lens L18. Lens L17, a field lens in that plane, is used to regulate the beam shape and size. The collimated beam provided past lens L18 is in turn focussed by L19 to a point in the plane of and just past the edge of mirror M3. It is oriented by mirrors M11 and M12 towards mirror M4 and lens L7 of the loop, as desired. Mirror M3 is in a plane conjugate to the light valve and the focussed spot is conjugate to the first reflection spot in the addition mapping unit in the area associated with the addition write beam pattern.

f. CRT imaging components

Finally, the components used in imaging the CRT generated patterns are identified. These are shown at the top in Figure 11 with the CRT at the top left and the LCLV in the center. Mirror M13 and lenses L20, L21, L22 and L15 image the CRT patterns with a magnification factor of 0.5, to match the spacing of the shifted read beams. Lens L20 images the CRT plane in the focal plane of lens L22. Lens L21 is a field lens in that plane. The combination of lenses L22 and L15 is then used to image that plane onto the light valve write side. The collimated space between lenses L22 and L15 is important in that it allows the placement of mirror M10 in part of the beam path, (M10 is used in imaging the hologram generated patterns as described earlier).

Matrix-vector Multiplier System Discussion

The pertinent features of the matrix-vector multiplier are discussed in this section, namely the light valve and incidence plane orientations and the extended system design and operation.

a. Light valve and incidence plane orientation

There are two features of interest pertaining to the light valve and incidence plane orientation. The first relates to the description presented earlier in Chapter II and also in Appendix B for a new light valve and read beam orientation. This orientation is shown in Figure 12, with successive reflected and shifted spots falling along a diagonal line in an incidence plane oriented at a 45° angle to the horizontal. This orientation will be referred to as the Diagonal Shift Orientation (DSO), as opposed to a horizontal or vertical spot shift. The light

valve orientation is such that the liquid crystal molecule tip plane is coincident with the incidence plane (see Chapter II). The relative orientation of these planes is the same as that depicted in Figure 7, but both are oriented at a 45° angle with respect to the horizontal.

The second feature relates to read beam polarization. The allowed planes of polarization are vertical and horizontal. These are oriented at 45° to the light valve fast and slow axes to ensure equal intensity decomposition along both components. This is consistent with the desired light valve orientation and also with the proper mounting and orientation of the Glan Thompson prisms which allow either a transmitted horizontal or a reflected vertical polarization state.

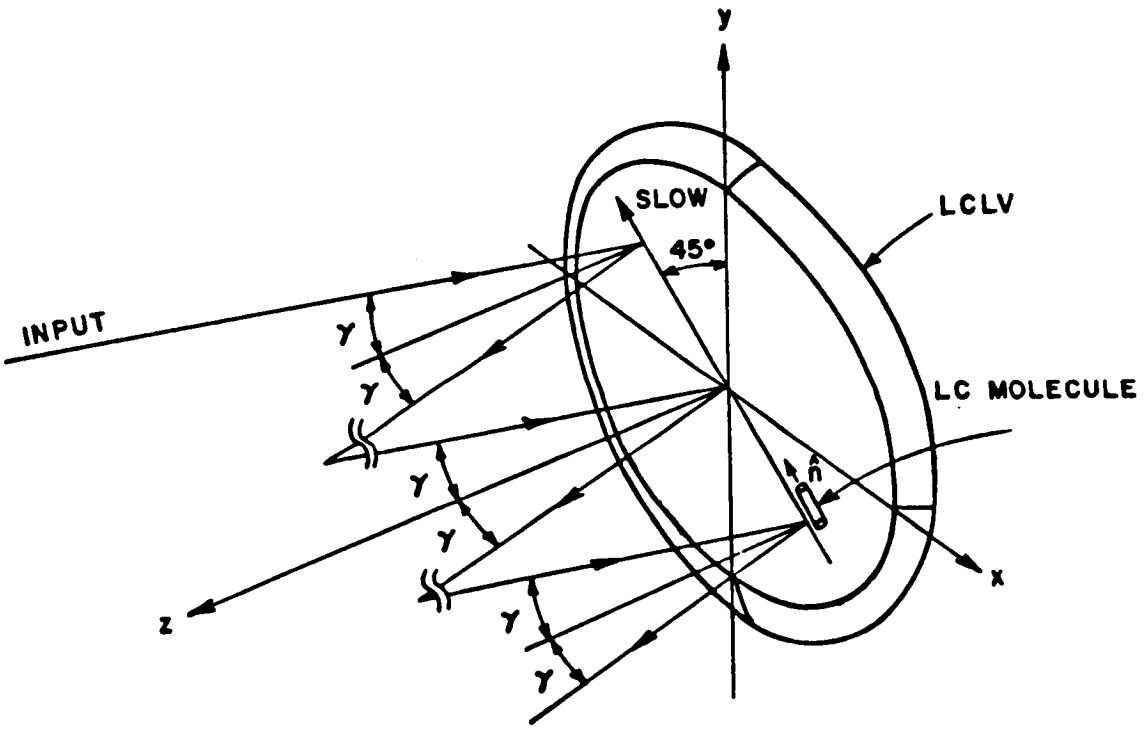

Figure 12. Diagonal Shift Orientation.

With this orientation the rows of reflected spots are all oriented at 45° angles and the allowed output positions are also in arrays of diagonal 45° lines. The write beam side patterns must also be rotated by 45°. The hologram plate is rotated as well since the position coded linear array of input spots is now arranged at a 45° angle. The 45° incidence plane is produced by mirrors M2 and M4 in the loop as they induce a shift direction with both horizontal and vertical components.

b. Extended system design and operation

The apparatus was designed in such a way that it could be extended to implement matrix-vector multipliers using the full LCLV resolution. Only a selected portion of the design, that necessary to demonstrate the principles of operation, was constructed, namely one multiplication operation activating one addition operation, and stored tables to implement all products and sums modulo 4 and 5. The light and beam pattern organization in several planes of the system is presented.

An indication of the coding in various planes is shown in Figure 13. These planes can be associated with the corresponding planes of Figures 6 and 11. In Figure 13a, the sources for two input vector components for two moduli, perhaps from an array of optical fibers, are positioned in a plane corresponding to the image plane of lens L1 in Figure 11, or plane 'A' in Figure 6. Note that the linear arrays are arranged in lines at 45° to the horizontal, corresponding to the Diagonal Shift Orientation.

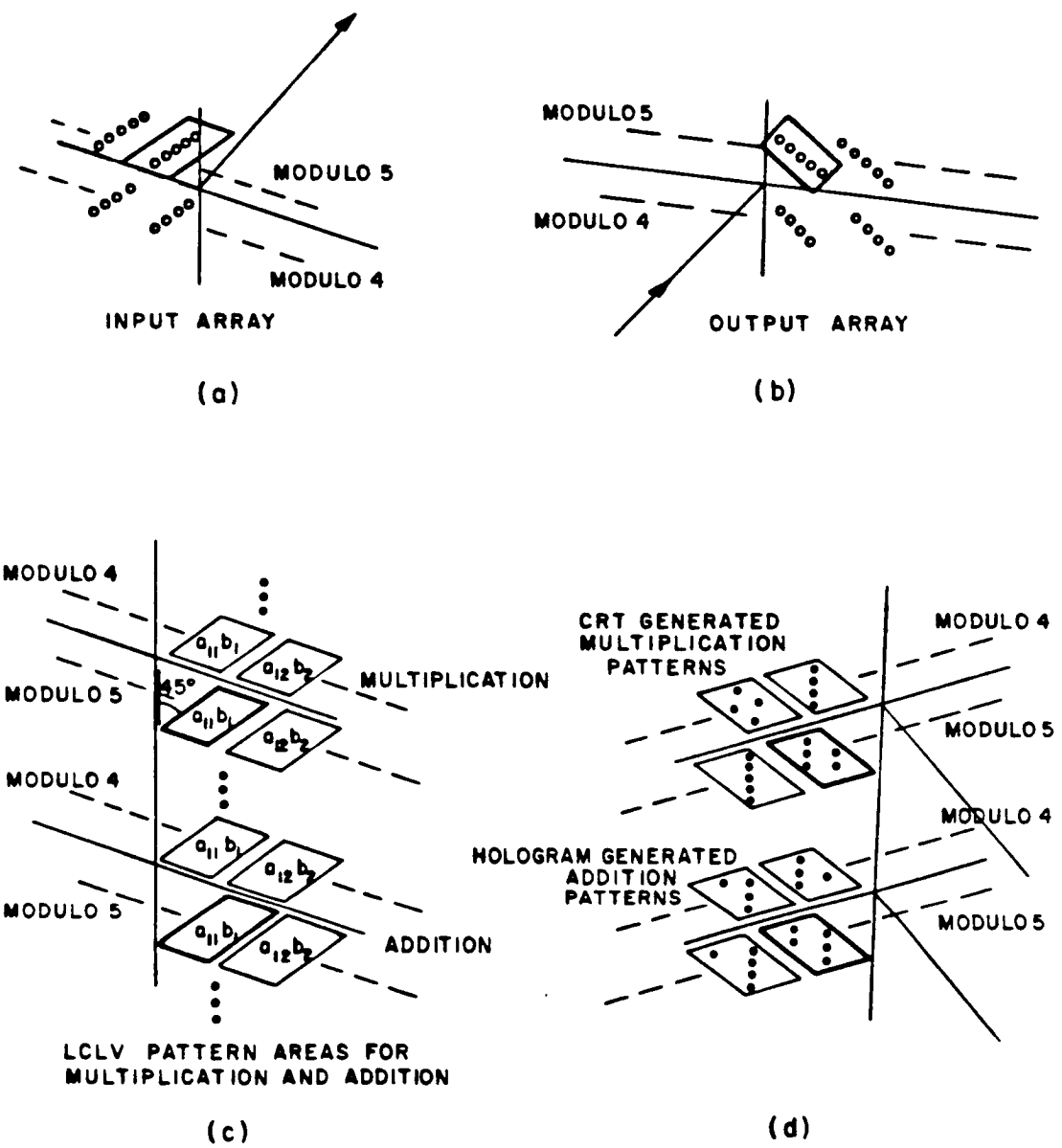

Figure 13. System beam and pattern organization.

In Figure 13b the light valve read side plane plane B in Figure 11, is shown with square areas corresponding to mapping unit patterns. There are two general portions, one for the multiplication patterns as shown on the light valve on the left side of Figure 6, and the other for addition patterns, corresponding to the light valve on the right side of Figure 6. Each portion has separate areas for the two moduli and the different matrix and vector elements in the product, with areas oriented at a 45° angle to the horizontal.

The multiplier output which also serves as the hologram input is shown at the top in Figure 13c. This is the focal plane of lens L8 in Figure 11, and corresponds to the array of position coded $a_{ij}b_j$ products to the left of the holographic table look up, plane B in Figure 6. The position coded arrays corresponding to the different product outputs are aligned at a 45° angle to the horizontal, as expected. Also shown at the bottom of Figure 13c is the adder output corresponding to plane C in Figure 6.

In Figure 13d, the light valve write beam input side is shown with the various CRT generated multiplication patterns on top and the hologram generated addition patterns on the bottom. These correspond to the pattern areas in Figure 13b viewed from the opposite side. Naturally these patterns are arranged with a 45° orientation to the horizontal to align with the associated read beam reflections in that orientation.

The portion of this design actually implemented includes one vector element input and one matrix element for one modulus. A multiplication and an addition operation are performed. These are highlighted in

Figure 13. The optics for redirecting the output from one adder to form an input to the successive adder locations were not implemented.

The multiplication loop operation was tested by moving the CRT pattern rather than the input vector position for convenience. Five possible multiplier outputs were demonstrated from all the possible modulo 5 position coded outputs. Each of these outputs reconstructed its own hologram pattern as input for one adder mapping location, the one highlighted in Figure 13d.

The holographic memory includes four separate recorded areas to test the feasiblity of using the holographic stored table. Two areas were for modulo 4 storage and the other two for modulo 5. Only one of the modulo 5 areas was used.

The components used in the demonstration of the apparatus were designed to allow light valve operation at its resolution limit of 600 line pairs per inch [1]. The lenses in the loop on the read side of the light valve were chosen to give focussed spots consistent with that limit.

However, the read beam spot size for this particular apparatus, designed to be on the order of $f\lambda/D$ for lens L3, is not limited by the CdS resolution. The best results were obtained when lens L3 was slightly defocussed giving a slightly larger spot size, to meet upper limits on power requirements. This is because of the power density limits of the liquid crystal which otherwise would be exceeded in the focused spot when the intensity was raised to overcome the efficiency limits of the particular hologram constructed. Using more efficient

holograms would allow the use of the designed resolution limits, with lower power from the laser source. (See Appendix E).

Hologram Construction Apparatus

The hologram construction apparatus is presented in this section. This includes a general description of the overall apparatus followed by a detailed description of the optical components for reference and object beam generation. It is characterized by a single mode optical fiber used as a position controlled reference beam source producing the different reference beam orientations and interchangable masks with the appropriate patterns for residue arithmetic modulo 4 and 5 addition. Four carrier multiplexed holograms were produced, two with five superimposed exposures for modulo 5 patterns and two others with four superimposed exposures for modulo 4 patterns.

A sketch of the hologram construction apparatus is shown in Figure 14. A detailed listing of all the components is given in Appendix F. A Spectra-Physics model 125 helium neon laser source is shown at the left. The hologram holder is shown at the bottom with the reference beam and associated optics on the left and the object beam and associated optics on the right. A shutter, and a semi-transparent mirror (STM 1) used as an attenuator, are placed in front of the variable beam splitter (STM 2). The reference beam is transmitted by STM 2 while the object beam is reflected onto mirror M4 and redirected through a beam expander toward the mask plane.

The key components forming the reference beam path are the optical fiber and its input and output coupling lenses. The beam transmitted by

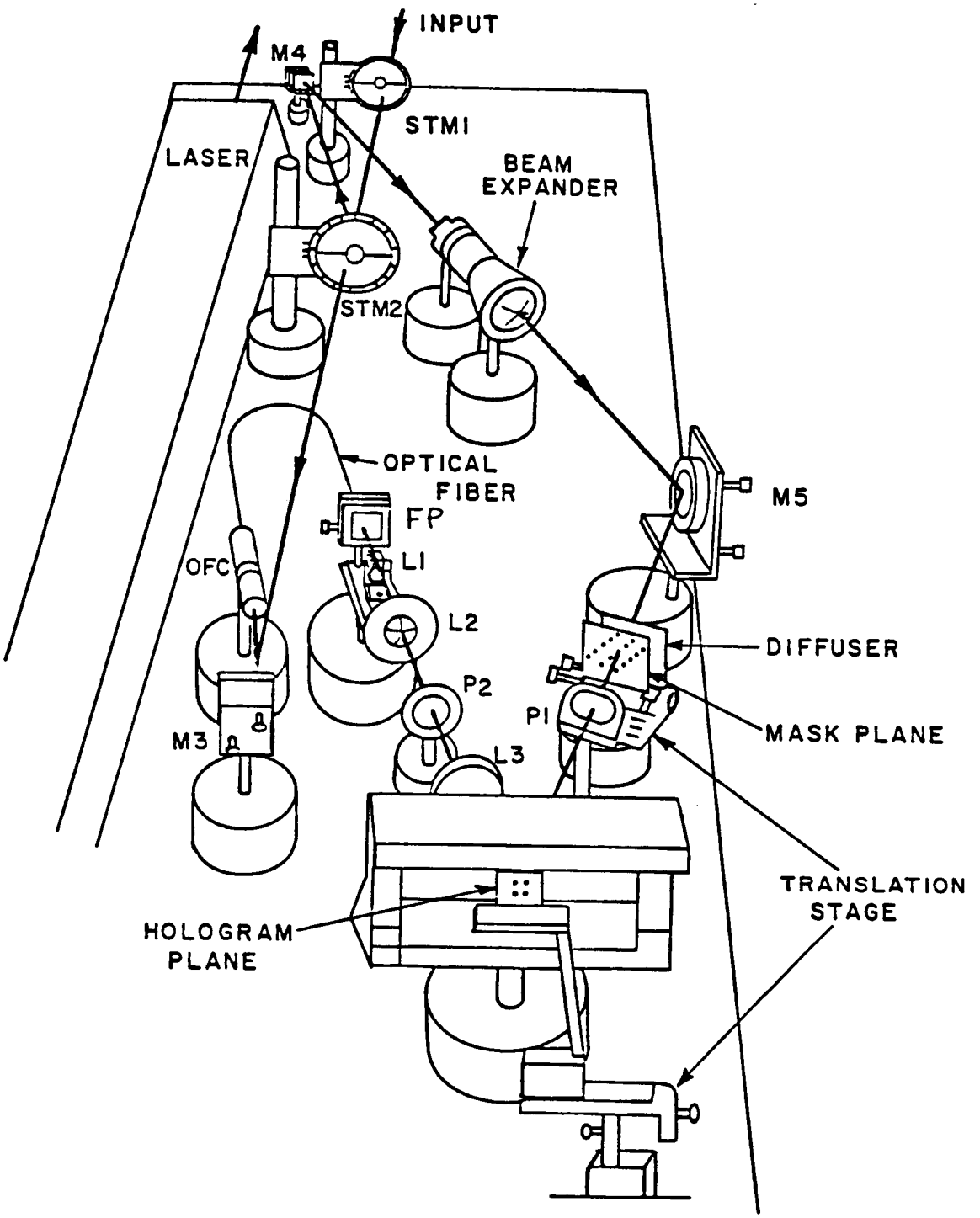

Figure 14. Sketch of hologram construction apparatus.

beamsplitter STM 2 is directed by mirrors M2 and M3 into a specially constructed optical fiber coupler, OFC in Figure 14, (see appendix G) containing a microscope lens and a spring loaded x-y translation mechanism that positions the fiber tip. The microscope objective can also be positioned in the axial direction to focus the input light beam onto the tip of a single mode optical fiber. At the output end, the fiber is placed in a Newport Research Corporation 5 axis fiber optic positioner, (FP), such that the fiber can be translated in the focal plane of a microscope objective lens, L1, which collimates the fiber output beam. Lenses L2 and L3 are separated by a distance equal to the sum of their focal lenghts, to provide the proper magnification and recollimation producing a plane wave reference at the hologram plane.

The fiber is translated only in the horizontal direction producing a set of collimated beams travelling in different directions centered around axes in a plane parallel to the optical bench. The collimated beams from microscope objective, L1, all pass through the same area in its exit pupil plane at different angles associated with the different optical fiber output positions. The hologram is located in a plane conjugate to this exit pupil, so that all collimated reference beams expose the same emulsion area, but travel at different incidence angles.

The allowed angles between the reference beams are determined from the recording emulsion properties discussed earlier in Chapter II. For this case the half power deviation angle is on the order of 3°. An angular magnification is necessary to match to the output of Lens L1. Lens L2 has a focal length of 250mm and lens L3 100mm, giving an angular magnification factor of about 2.5.

The object beam components are used to illuminate the hologram with the patterns to be stored. The object beam is reflected off beamsplitter STM2 and is directed onto a beam expander by mirror M4. A collimated beam of 1" diameter is produced from the beam expander and is directed by mirror M5 onto the mask plane as shown in Figure 14. A large screen, mounted on a translation stage, and composed of an array of holes provides the pattern masks. A diffuser positioned in front of the mask plane ensures that each hole in the masks contributes the same energy to the apertured exposure area. By translating the screen and appropriately covering the undesired hole, the desired pattern associated with a specific reference beam direction is positioned in the object beam path and is used to expose the hologram. The mask shapes correspond to the modulo four and five addition patterns which are quite simple and follow a consistent pattern. The modulo five patterns have the same form as the addition patterns shown in Figure 2b. The polarizers P1 and P2 assure that the object and reference beams used in the exposure have matching polarization. An aperture is placed in the hologram plane so that only one small area of the emulsion is exposed; this protects adjacent areas from being exposed to any stray diffuse light. Another translation stage is used to position the photosensitive emulsion behind the aperture.

For reconstruction, the hologram is reversed in orientation by rotating it by 180° about a vertical axis [65] and it is illuminated with plane wave reconstruction beams at the appropriate angles to form a set of real images in the same output plane. Kodak 649f-AH 2"x2" plates were used, and these were bleached for better efficiency. In order to

minimize possible thickness variations which invariably introduce spatial noise into the system, the emulsion was placed in a mineral oil liquid gate before using the hologram in the experimental matrix vector multiplier apparatus. Mineral oil has a refractive index of approximately 1.48 close to the emulsion refractive index of 1.5.

Hologram Exposures

It is desired to maintain a uniform reconstruction efficiency from the successive exposures. As described in this section, it is necessary to increase the exposure intensity for each successive exposure, in the manner established earlier in Chapter II. A table showing intensities of the reference and object beams and exposure times will be presented.

The superimposed exposures in four exposed areas, two with four superimposed exposures and two with five, were recorded using the construction apparatus of Figure 14. The fiber position and associated mask was changed after each of the angle multiplexed exposures. A detailed description of the recording procedure is given in Appendix F. The object and reference beam intensities used are given in Table 2. It is seen that the total intensity increases for each exposure while the ratio of reference to object beam intensity is maintained. The I_n/I_1 column in Table 2 shows the relative intensity levels used which closely match those determined from Equation (27) for 10% conversion per exposure. In the last column of Table 2, the reconstruction efficiency of one of the 5 carrier multiplexed exposure holograms is given in terms of the average intensity per reconstructed spot per pattern. It is seen that the reconstructed intensity, normalized to the first exposure intensity is uniform within a factor of .89 at worst.

Table 2

Exposure Table

	Intensity			Ratios		
Exposure # n	Reference beam	Object beam	Total	I_r/I_o	I_n/I_1	REC
1	.0960	.0357	.1350	2.69	1.0	1.0
2	.1053	.0395	.1490	2.66	1.1	0.97
3	.1210	.0455	.1700	2.66	1.25	0.89
4	.1287	.0510	.1850	2.52	1.37	0.95
5	.1395	.0539	.1972	2.59	1.46	0.9

After exposure, the 2"x2" Kodak 649F-AH plates used were processed using a popular processing and bleaching procedure found in the literature [69]. (See also Appendix F.)

Matrix-vector Multiplier System Performance

The performance of the optical matrix vector multiplier is documented in this section. This includes photographs of CRT and hologram generated patterns, a disussion of the signal levels in the 'loop' on the read beam side, and finally photographs of the actual multiplier and adder outputs.

Results are shown for the most significant operations, represented by the patterns highlighted in Figure 13. Modulo 5 is used. Instead of five multiplier input vector positions, one was used. All five output

products from the multiplication mapping were obtained, however, by moving the CRT pattern vertically. Each of these five output products then generates, from the holographic memory, the addition pattern associated with its numerical value. This addition pattern in turn is used to add the value it represents to a position coded value obtained in general from a previous addition, chosen at random to be 3 for demonstration purposes.

Look Up Table Patterns

The residue arithmetic multiplication mapping patterns for modulo 5 provided by the CRT are shown first, in Figure 15. These patterns are actual photograms (reverse images recorded on contact paper) in an image plane of the CRT, plane PL1 in Figure 11. The grids are included for convenience and were overlayed during photocopying. The successive rows in Figure 15 show the patterns for multiplication by 1, 2, 3, and 4 respectively, for the different input value shown at the top of each column. The patterns for multiplication by zero, not shown, are trivial as are the patterns for input zero. As before, the individual patterns have input rows labelled on the right side and output columns labelled on the top.

The patterns shown are comparable to the patterns in Figures 2 and 4, with two exceptions. First, the grids (and patterns) in Figure 15 are orientated at a 45° angle relative to the grid direction in Figure 4. This is due to the Diagonal Shift Operation (DSO), mentioned earlier. The second exception involves an additional spot placed in the zero column of each pattern due to polarization considerations in the

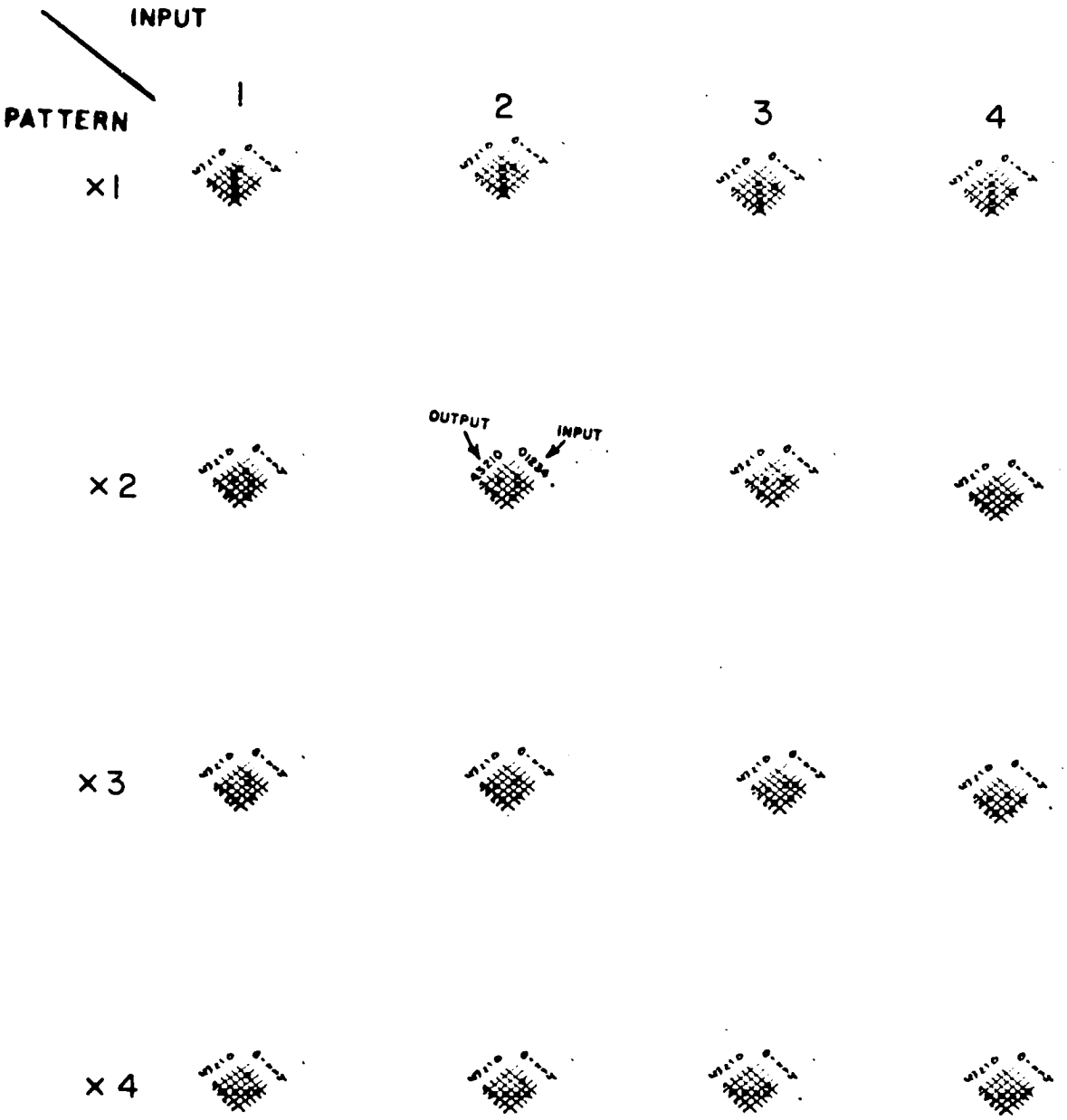

Figure 15. Photograms of modulo 5 multiplication patterns.

loop. This is the spot represented by the top input beam in Figure 3, the one that modifies the multiplication read beam polarization from its initial horizontal state to a vertical state so that it is successively reflected. For this apparatus, this spot appears only in the row used. For the more general case there would be a column of spots in the zero column, except in the zero row, as shown in the unrotated pattern in Figure 16 for multiplication by one modulo 5.

In the pattern for multiplication by 2 and input 3, the second row and third column of Figure 15, the product is 1 modulo 5 so that the pattern has spots in the zero and one output columns, in the input 3 row. The first spot changes the input read beam horizontal polarization to vertical. After one pass through the loop and another 90° rotation in polarization due to the second spot, the multiplier output in the '1' position is produced, as expected.

The residue arithmetic addition patterns generated from the holographic memory are shown in Figure 17. Five patterns, photograms of the actual patterns generated from one carrier multiplexed hologram are shown; in all eighteen patterns were recorded, two sets of four for modulo four arithmetic and two sets of five for modulo five. The other patterns are presented in Appendix F. Again the grids were overlayed during photocopying for ease of interpretation. These patterns match those of Figure 2 taking the Diagonal Shift Orientation into account, with one spot per row, since a vertically polarized read beam is used for the adder. The extra spot in the zero column that was needed for the multipler loop is not needed here because the beam enters the loop

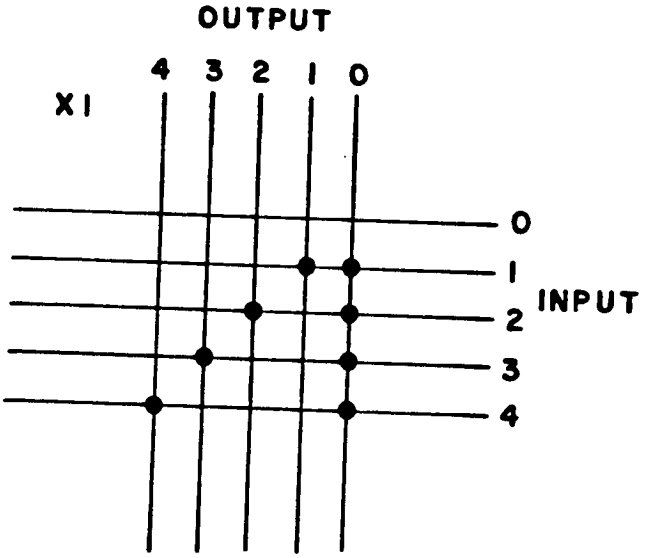

Figure 16. Multiplication pattern form.

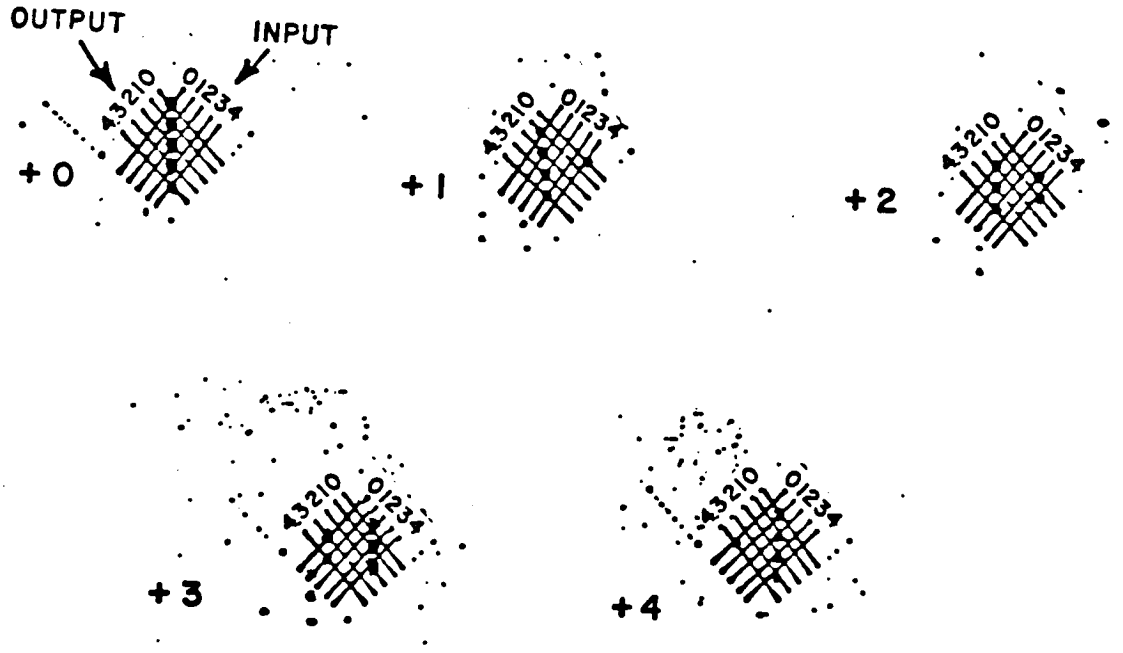

Figure 17. Photograms of modulo 5 addition patterns.

just past the edge of mirror M3 and not by being transmitted through Glan Thompson prism GT1. Note that there is data off to the side of the recorded patterns. These represent weaker reconstructed images.

Loop Signals

In this section the loop signal levels are discussed. Two tables of loop signal levels are shown, one for the multiplier loop and another for the adder loop signal levels. The signal is affected by transmission loss in system components, a disadvantage of multiple pass systems such as the one used here. Signal deterioration can occur due to polarization, reflection, and absorption losses. This system was designed to minimize this effect.

The light valve front surface Fresnel reflection losses are minimized by adding an anti-reflection coated optical flat in front of the light valve. The LCLV front window material is BK-7 glass with an index of refraction of about 1.52, and it is matched to an optical flat of the same material with a layer of mineral oil (index 1.491) in between the glass surfaces. With the placement of this optical flat the major light valve losses may be attributed to absorption loss in the liquid crystal layer. Measurements indicate that the light valve 'reflects' 90 $\mp$ 2 % of the incident read beam intensity.

Prisms GT1 and GT2 have anti-reflection coated exterior surfaces and a dielectric coating at the reflection interface. The measured prism throughput is about 95 % for both polarizations. Three dielectric mirrors are used; mirrors M3 and M4 have 97% reflectivity while M2 has 95% reflectivity. Lenses L3, L4, L5, L6, and L7 are anti-reflection coated with a Super AR coating [70] giving approximately 98%

transmission at the operating wavelength. The total loop transmission calculated by taking a product of measured individual component losses is 0.625.

Intensity measurements were taken in plane "A" past the hologram plane of Figure 11, where collimated light beams with intensities proportional to the beams from the analyzer prism GT2 are detected. In the multiplier output case, the relative intensities of the beam that comes straight through the hologram were recorded. The percentage of the energy diffracted by the hologram was taken to be the same for all beams. The addition loop outputs were recorded in the same plane although they do not go through an exposed area of the emulsion. In each case the data was normalized to the peak intensity measurement. A Quantrad Corporation 100-PV-BNC detector [71] and appropriate signal conversion and amplification circuitry was used.

The multiplication loop signal level data is shown in Table 3. The column headings indicate the position at which the recorded intensity was measured. The row number indicates the output position that would have all the light and thus the highest intensity, a normalized intensity of 1, in the ideal case. Non-zero values in other locations indicate leakage through the prisms due to improper polarization and non ideal prisms.

There are two items to note in the data presented. The first point is that there is a consistent drop in peak intensity level associated with a transmission per pass, TR, of about 0.60 for each pass through the loop, as predicted. This intensity reduction is comparable to the calculated .625 reduction factor per loop pass based on the measured

losses of the individual components given earlier. Using Equation (30) to determine the system transmission, which is associated with the drop in intensity after 4 loop passes, then with p = 4 and the transmission per pass, TR =.6, the system transmission is given by:

$$TS = I_p/I_o = I_4/I_o = (.6)^4 = .1296 \qquad (37)$$

From the data in Table 3, $I_o = 1$, $I_4 = .123$, and hence $I_4/I_o = .123$.

Table 3

Multiplication Loop Losses

spot on \ Output position	0	1	2	3	4
0	1.0	.0047	.0034	.0019	---
1	.022	.596	.004	.0028	---
2	.02	.012	.354	.0056	.0043
3	.022	.014	.012	.208	.0034
4	.021	.014	.022	.0078	.123

The second point is that the appearance of measurable signal levels at the 'off' positions in each column is also partly attributable to imperfect operation of polarizing prisms. The two Glan Thompson prisms are designed for 98% efficiency for the s-polarization and 95% efficiency for the p-polarization [72].

The main requirement for the system was that each multiplication output have sufficient intensity so as to reconstruct a single holographic image intense enough to drive the light valve. A requirement on the multiplication loop was that the secondary spots be sufficiently dim so as not to excite the light valve. Both these requirements were met.

Similar data will be shown for the addition loop. Recall that for the addition operation demonstrated the addition loop multiple reflections occur in the row corresponding to a position coded input of 3 and that each of the different patterns projected onto the light valve corresponds to a multiplier output product. The result of each addition after a number of reflections in the loop is a bright spot representing the sum in one of the position coded outputs. That spot intensity will be measured as well as the intensity of light leaking from the other reflections.

The addition loop signal level outputs are shown in Table 4. The data is arranged in a manner similar to that of Table 3. Each row represents intensities for light in the five adder multiple bounce positions, where in each row one spot is bright and the others dim. The column at the far left indicates the numerical value of the multiplier

output and the adder pattern used. The output sum expected is shown in the next column for the addition of three modulo 5 to the multiplier output. The data was normalized to the peak value in each row.

The data for the additon loop indicates that the intensity levels obtained from the multiplier outputs shown in Table 3 were sufficient for easy discrimination. In each case, the output intensity is stonger in the expected output position than the intensity in any other position by a ratio of 7:1 (8.45dB) or better.

The detector was also used to measure the system response time in the same plane. The result is shown in Appendix H.

Table 4

Addition Output Intensity (Plus 3 Modulo 5)

Output position / product	sum	0	1	2	3	4
0	3	.11	.087	.053	1.0	.0053
1	4	.116	.1	.052	.039	1.0
2	0	1.0	.094	.033	.028	.061
3	1	.142	1.0	.024	.011	.022
4	2	.103	.039	1.0	.008	.008

Multiplier and Adder Outputs

In this section photographs showing combined multiplier and adder output spots are presented. The light for these spots is transmitted undiffracted through the holographic plate and imaged onto a ground glass plate which is then photographed.

The photographs are shown in Figure 18. The grids were overlayed during the printing process. The top row shows the multiplier output and the bottom row the adder output which is always the output of the multiplier plus three modulo 5. For example, when the multiplier output is 4, (Figure 18 (e)), the adder output is 2, as $(4+3)_5 = 2$.

These pictures show vividly the operation, in principle, of the matrix-vector multiplier!

Chapter Summary

The optical digital matrix vector multiplier demonstration apparatus was presented in this chapter. The hardware for both the matrix-vector multiplier and the hologram construction was described using photograph based sketches and discussing the pertinent features of each. The system performance was presented using photographs of CRT patterns and hologram generated patterns, and a discussion of signal levels in the loop. Finally, photographs of the actual multiplier and adder outputs were presented showing that a given multiplier output produces the expected value in the adder output.

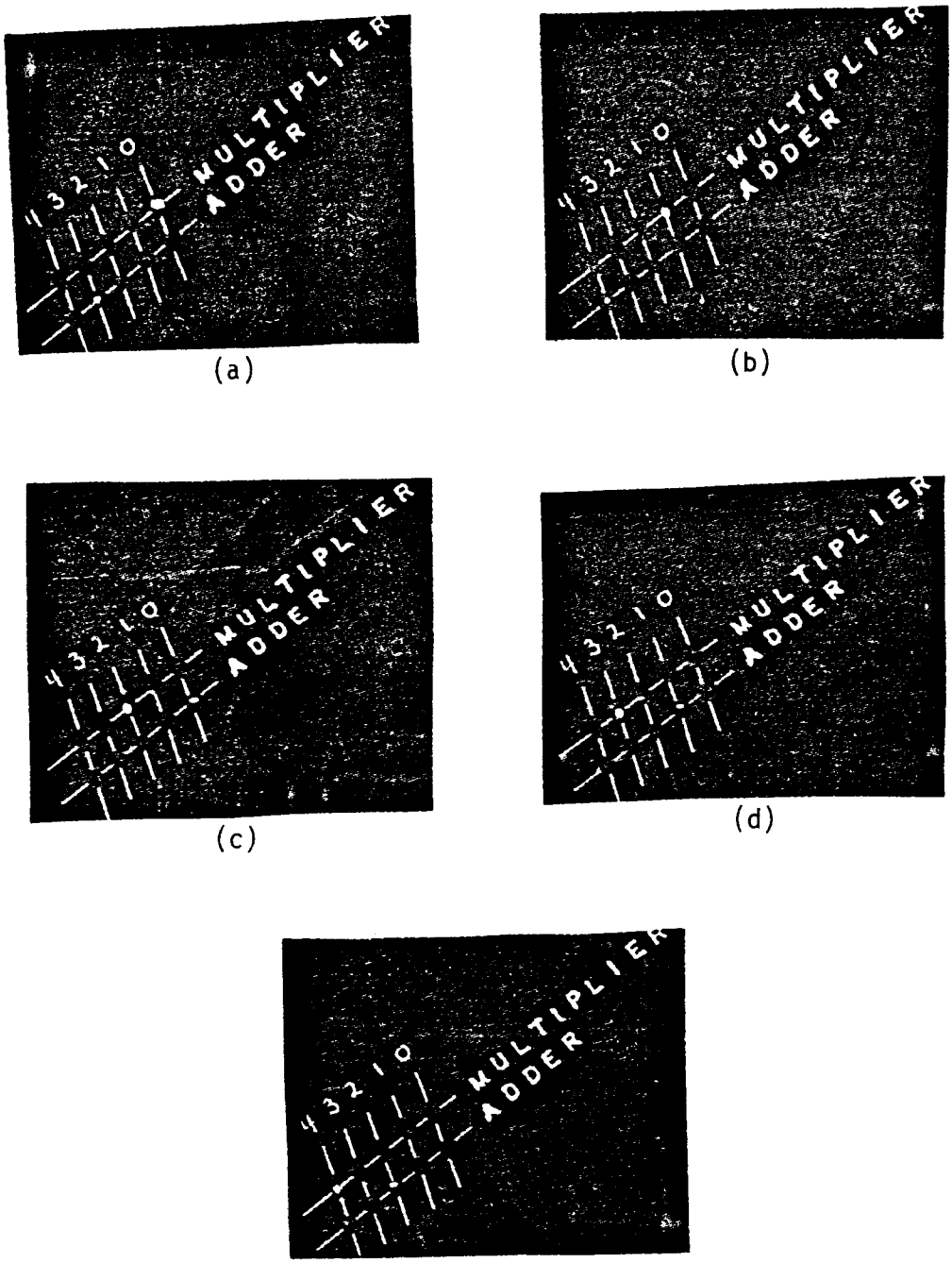

Figure 18. Photographs of multiplier and adder outputs.

CHAPTER IV

SUMMARY AND CONCLUSIONS

A summary of the work described in this report, and conclusions based on the results obtained are presented in this chapter. Suggestions for future work extending the work presented here are discussed.

Summary

The work presented here involves the design and demonstration of a digital (numerical) optical matrix-vector multiplier. The objective of the design was to gain computation speed by taking advantage of the large array of processing elements in a Hughes liquid crystal light valve, and relying on the residue arithmetic representation, a holographic optical memory, and position coded optical look up tables to perform arithmetic operations. In the design, all operations are performed in effectively one LCLV response time with a high information density.

In the first chapter, a brief review of the pertinent features of optical processing and matrix multiplication was presented. This was followed by a short description of the specific aspects of the approach considered in this matrix multiplier design namely the Hughes LCLV, residue arithmetic, position coding, look up table operations, and holographic memory.

Chapter II had two main points. The first was a general description for the optical matrix-vector multiplier, based on the components and principles presented in this design was given, leading to an overall view of the system. The second point involved theoretical aspects of the design including a description of the theory behind the light valve operation in a new optimum configuration, and the theory for the angular half width and number of superimposed exposures for the holographic memory. It also includes the system energy requirements and constraints and the expression for the theoretical number of parallel matrix-vector multipliers constructed using one light valve was derived.

The experimental aspects of this work were presented in Chapter III where the matrix vector multiplier apparatus and the hologram construction apparatus were described. The components for both the matrix-vector multiplier and the hologram construction, including an optical fiber reference beam source, were described showing diagrams and photograph-based drawings of the apparatus in each case. The demonstration of operation of the matrix vector multiplier and the system performance was then presented. Photographs of multiplier and adder output spots showed that a given multiplier output leads to the expected value in the adder output!

The report has several appendices, dealing with a range of topics. Background materials for the concepts and principles used are discussed in Appendix A. The liquid crystal performance at non-normal incidence is described in Appendix B, while hologram coupled wave theory is presented in Appendix C. The matrix vector multiplier apparatus is

described in Appendix D, and a design modification pertaining to resolution in Appendix E. The hologram construction apparatus and pertinent features of the exposure procedure, including a presentation of the stored patterns in the holographic memory, are given in Appendix F. A description of an optical fiber coupler used in the hologram construction is given in appendix G.

Conclusions

The objective of the work reported here was to demonstrate the optical matrix-vector multiplier designed for minimum computation time. A design for implementing the objective was presented relying on position coding, residue arithmetic, look up operations, a holographic memory and the resolution of spatial light modulators, to provide the high information density capability, and to allow computation in one LCLV response time.

We conclude that the device was constructed and demonstrated! The following attributes are noted.

- The implementation required a single device response time.
- The design used maximum light valve spatial capability.
- The operations using a simple mapping approach to residue arithmetic were successful.
- The holographic memory for multiplexing superimposed mapping patterns worked.
- An optimum LCLV configuration, relating liquid crystal tip plane, incidence plane, and incidence beam polarization, was used.

For future work, improvements in the system operation can be made in the following areas. First, system reflection and absorption losses can be minimized by using higher quality lenses, mirrors, and prisms, and high quality coatings. Losses in the spatial light modulators can be reduced by improving device extinction and contrast ratios. These must be taken into consideration in systems designed with many multiple reflections in the loop configuration, as these losses accumulate dramatically for each pass. Secondly, more efficient storage of the patterns will improve the system operation, by considering other coding forms such as a binary coded residue coding, or by improving the actual storage mechanism, investigating media for holograms that have thicker emulsions and a larger range of allowed refractive index change.

Other work involves developing a better match between hologram reference and reconstruction sources eliminating the needed matching optics used in this demonstration. Also, the sources for the loop read beams can be developed into arrays, perhaps optical fiber linear arrays for input vector elements, and the additional optics for the successive additons can be included in the design. The light valve resolution can also be fully exploited by having successive reflections from adjacent resolution element pixels along the reflection paths.

The principle of using the read side of the spatial light modulator and high resolution for multiple reflections, should not be limited to arithmetic operations of the type shown here but may be extended for optical signal processing in general. Many types of mappings, interconnections, optical switches and algoritms may be implemented using this principle.

APPENDIX A

Review of Pertinent Features of Optical Data Processing

The material presented in this appendix is a review of optical computing concepts relevant to matrix multiplier architectures and designs in general, concentrating mainly on those aspects pertaining to the design described in this report. It expands on the concepts presented in Chapter I.

Background

The concept of using optics and optical components for signal processing and computing has been well known for several decades. With the advent of the laser in the early 1960's [73], coherent Fourier based optical computing, spatial filtering, and holographic applications constituted a major effort in analog optical processing research. The Fourier transform properties of lens systems are well established and were popular in the 1960's in image processing, optical correlation, optical spectrum analysis and pattern recognition systems [74]. A typical Fourier transform lens operation is shown in Figure 19, where the optical field distributions in the input (x_0,y_0) plane on the left and the output (x_1,y_1) plane on the right are related through the two dimensional Fourier transform integrals given. The relationship holds for the case where each plane is a focal length away from the lens. Another significant processing feature evolved from the discovery of

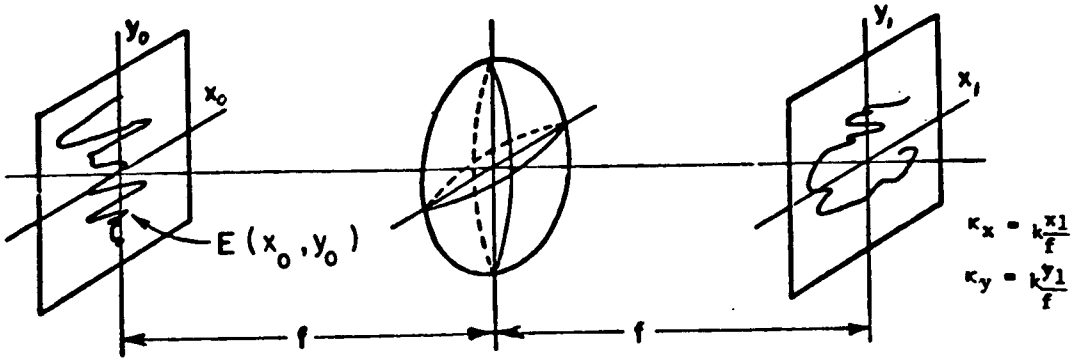

Note that if the input and output planes are focal planes, so that $d_1=d_0=f$ we have

$$E_1(x_1,y_1) = + \frac{jk}{2\pi} \frac{e^{j(k(n-1)\tau+2f)}}{f} \iint E_0(x_0,y_0) e^{\frac{+jk(x_0x_1+y_0y_1)}{f}} dx_0 dy_0 ,$$

the standard well known two-dimensional optical Fourier transform relationship:

$$E_1(\kappa_x+\kappa_y) = \frac{jk}{2\pi f} e^{-jk(2f+(n-1)\tau)} \iint_{-\infty}^{-\infty} E_0(x_0,y_0) e^{j(\kappa_x x_0+\kappa_y y_0)} dx_0 dy_0$$

Figure 19. Lens Fourier transform operation.

holography in the late 1940s, and the theory of wavefront reconstruction associated with that field [75].

Just as in the field of electronic computing, where analog computers preceded digital electronic computers, so it is in optical computing. Analog computing is restricted by dynamic range and accuracy constraints as well as the limited number of analogs.

This naturally led to investigating digital (numerical) optical computing concepts in the 1970s and 1980s. The fundamental advantages of optical digital computing include parallel processing of information

in a two dimensional array format, as opposed to serial (high speed) processing in digital electronic circuits, the ability to propagate optical signals in a small volume without being limited by electromagnetic interference, and general improvement of signal to noise ratio. The work presented in this report uses digital optical computing concepts in demonstrating the operation of a matrix-vector multiplier.

Digital optical computing research developed along several paths, ranging from design and construction of optical transducers and optical logic circuits to optical memories. In general, the proposed systems can be categorized into two groups. On one hand, optical systems were used to perform optical logic circuits (gates, flip flops, etc.) based on binary computing methods well established in digital electronics [15] On the other hand, an alternative to sequential binary logic based systems, where part of the parallelism offered by optics was lost, was sought. This required reverting to other types of arithmetic representations; one popular form, residue arithmetic, is used in the design described in this report. Several digital optical computer designs have been reported ranging from dedicated processors with specific applications [9,10,11], such as the work presented in this report for implementing an optical matrix vector multiplier [12], to the general all purpose optical computer designs [13,14].

Optical matrix multiplier designs date from the late 1960's or early 1970s up to the present date. In what follows, a brief discussion of the typical designs is presented, including systolic structures,

designs using intensity coding via masks and transparencies, and position coded schemes.

Optical matrix multiplier designs generally have the form shown in Figure 20. Inputs in an array, shown in a plane at the left, are imaged individually, by rows or columns, or in parallel via spherical, cylindrical, and elliptical lenses onto a 'processing' plane. In this plane the input information is 'operated' upon to generate the desired arithmetic manipulations to perform multiplication or addition. The results of this 'processing' are in turn imaged back via further anamorphic optics onto an output plane shown on the right where an output array represents the product vector or matrix.

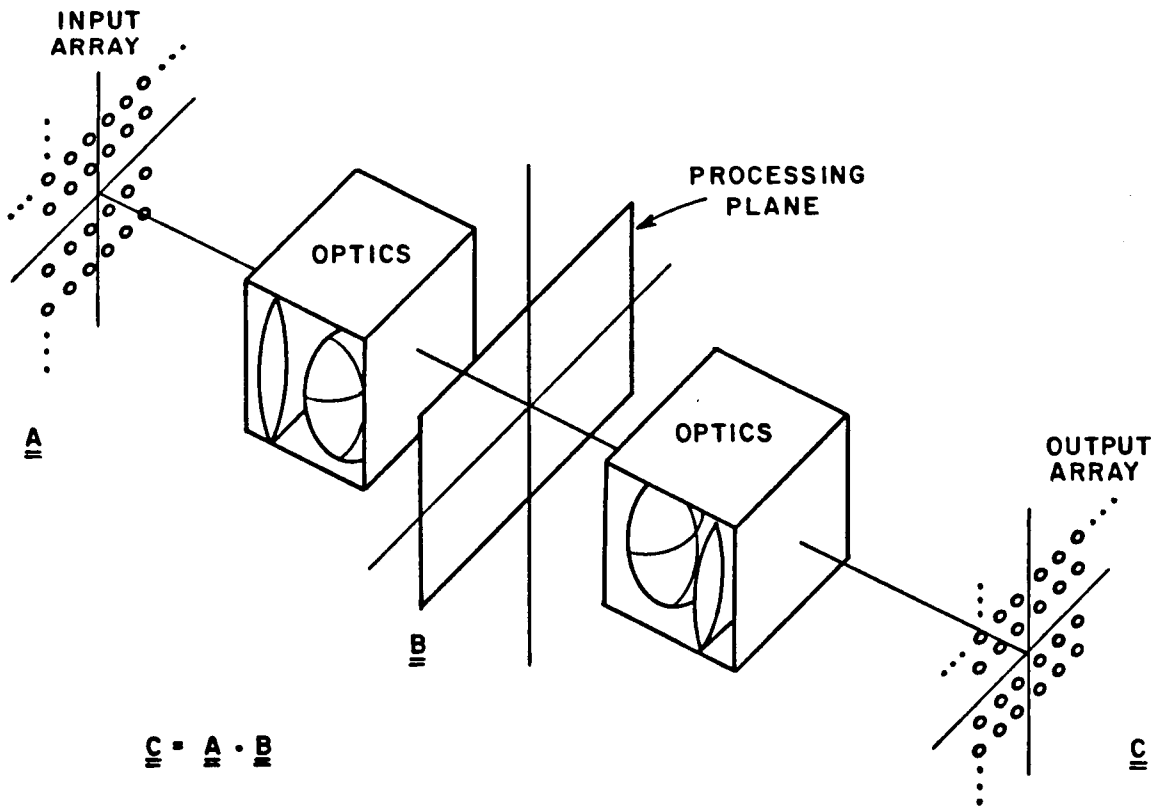

Figure 20. Typical optical matrix algebra processor configuration.

The early matrix multiplier designs involved the use of analog coherent optical correlation techniques based on the optical Fourier transform operation. The ground work was initially presented by Cutrona [5] in 1965, and later developed by Heinz et al. [30] in 1970. The basic idea was to represent the matrices by two-dimensional distributions whose correlation gave terms related to the products of the matrix elements. However, such techniques were inefficient in that energy in the form of irrelevant light outputs had to be sacrificed, especially as the matrix order increased. Interpretation of the output required the ability to distinguish between desired and undesired terms. The work reported by Heinz suggests methods for performing such isolation by transposing input arrays such that the desired outputs could be uniquely identified. Digital optical matrix-matrix multiplier designs promised more efficient systems.

One type of optical matrix algebra processor with both digital and analog designs is the systolic array processor. These operate in a similar manner to popular electronic systolic processors characterized by a rhythmic data and information flow through various registers. The basis for these processors is a variation of the theme presented by Tamura and Wyant in their 1976 paper [25], the theme of shifting the input and output matrix elements in their respective input and output array planes. The rhythmic data flow feature in systolic processor arrays is well suited to the repetitive nature of matrix multiplier operations. Several such designs have been reported using acousto-optic transducers [26] and RUBIC cube processors [27,28].

Various types of information coding techniques are used in digital optical matrix multiplier designs. Most designs rely on intensity or position coding of input and output. Other optical coding parameters include polarization, phase and wavelength, but designs using these properties are not as common.

Intensity coding of inputs and outputs, where the optical intensity represents the numerical value, was used in several designs; typical of such systems are the works reported by Tamura and Wyant [25] and Goodman et al. [31]. Tamura and Wyant, presented a method for the implementation of real time matrix multiplication. The inputs were intensity coded and the output could either be intensity or pulse position coded, depending on the location of the output plane. Goodman proposed an incoherent optical method for matrix-vector multiplication, a byproduct of a discrete Fourier transform system design. An input vector in the form of a linear LED array with controllable intensity, and a matrix in the form of a mask were used. Each LED illuminates a column of the mask using anamorphic optics. A cylindrical lenslet array for improved efficiency combined with a 'collecting' lens brings the total intensity of one column (i.e. summation) onto a photodetector. The desired output vector is then electronically decoded.

Position coding of inputs and outputs has been used for matrix vector multiplication [3,32,33] and for optical signal processing [34]. This type of coding involves representing the magnitude of a number by the position of an illuminated source in a linear or two dimensional array. This establishes a high signal to noise ratio in that a source

in a fixed position is either on or off. An example of such coding in an optical decimal to residue arithmetic converter [34] is shown in Figure 21. The numerical input value is represented by the column position in the input plane on the left, and the associated numerical output values are obtained in the columns of the output plane on the right. Input and output information is imaged using anamorphic optics.

What was needed at the point this work began was the construction and demonstration of an optical system showing the speed and high throughput capabilities of digital optical computing in a typical application. The application chosen is an optical matrix-vector multiplier where many parallel operations can be performed. The goal is to perform these operations in a minimum number of device cycles,

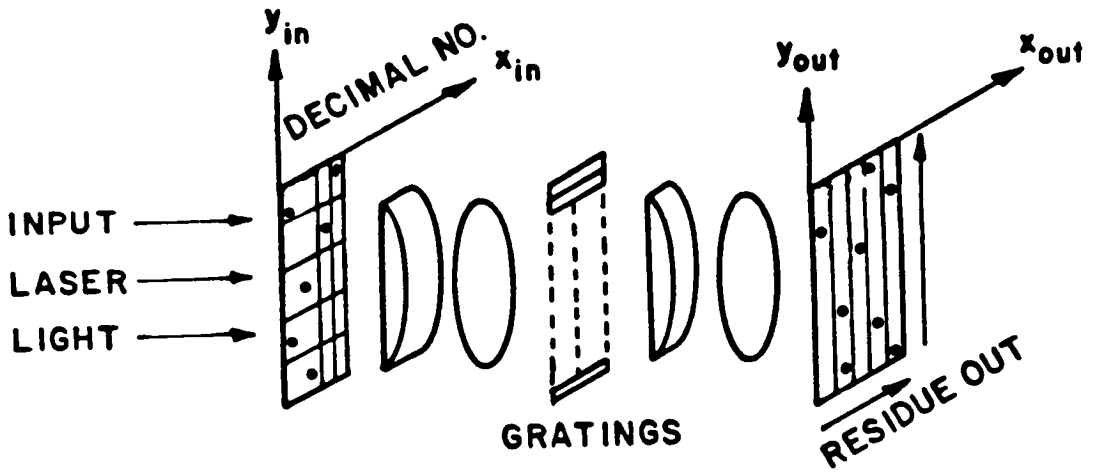

Figure 21. Typical position coded optical system.

minimizing the effect of typically slow optical transducers used in the design, but taking advantage of the high potential throughput in terms of optical resolution these devices possess. The following discussion of various design aspects is intended to provide background on the principles and devices used in this suggested design. These include position coding, holographic storage, residue arithmetic, and a Hughes liquid crystal light valve.

Design Aspects

In this section, background on the design aspects of a new optical matrix multiplier design are presented. These include position coding, holographic storage, the residue arithmetic representation, and the spatial light modulator used, a Hughes LCLV.

Position coding of inputs and outputs is used in this design to form optical look up tables. Position coding and table look up operations have been reported in the literature [3,32,33,34]. In this design, two forms of position coding are used. In one form, inputs and outputs are arranged in a two dimensional array with inputs vertically position coded and outputs horizontally position coded. The scheme for routing a light beam from input to output relies on two dimensional position coded light beam patterns. The second position coding form is used in generating these patterns from a holographic memory where the input position of a reconstruction beam is associated with an output pattern from the memory.

Simple holographic techniques are used to construct the holographic memory used in this design and to reconstruct the recorded images. A hologram is a recording of the interference between two coherent waves and the construction and reconstruction geometries of a simple hologram are shown in Figure 22. The hologram is made with a plane wave reference beam at the left and an object beam at the top left in Figure 22a. The object and reference beams are incident at different angles on the photographic emulsion shown at the right of Figure 22a. The object in this case is a transparency with a pattern of spots illuminated with a plane wave. Once the emulsion is processed and

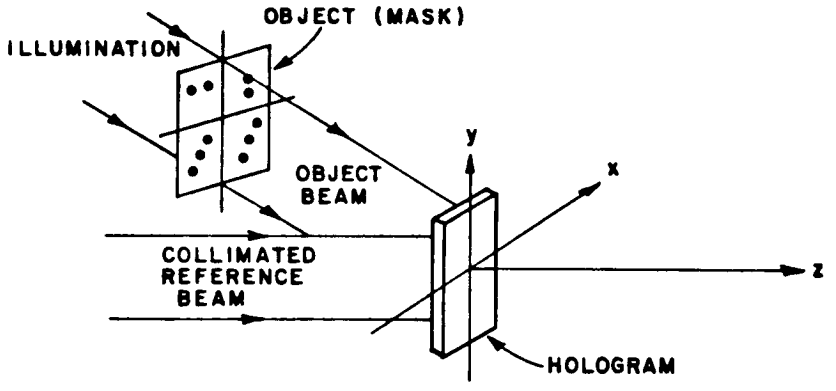

(a) HOLOGRAM CONSTRUCTION

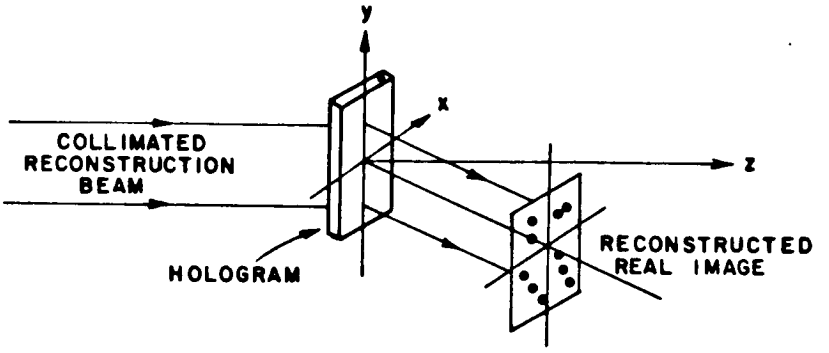

(b) HOLOGRAM RECONSTRUCTION

Figure 22. Hologram construction and reconstruction geometries.

repositioned in the original construction plane, then a plane wave reconstruction beam travelling in the same direction as the reference beam is used to reconstruct the original object as shown in Figure 22b. A real image of the object is obtained in a plane conjugate to the original object plane (on the opposite side of the emulsion) if the emulsion is rotated by 180° about the y axis, relative to its original orientation [65].

In this design, a set of angle multiplexed holograms will then be spatially multiplexed to form an optical storage unit. Angle multiplexing involves the use of given area of a photographic emulsion to record a set of exposures associated with different pairs of object and reference beams. The incident reference beam angle typically distinguishes a given pair of exposures from others. Spatial multiplexing involves the recording of many holograms in small areas on an emulsion, each spatially separated from other holograms.

Residue arithmetic is practical for parallel processing designs and will be used in the matrix vector multiplier implementation. In residue arithmetic a number is represented by a set of residues with respect to a set of moduli [2]. The residue of a number in a particular modulus is the remainder after dividing the number by the modulus. For example, consider the number seven and moduli two, three, and five. Seven has residue of one with respect to modulus two, (one modulo two), and similarly is represented by one modulo three and two modulo five. Thus, the number seven would be represented by the triplet (1,1,2) with respect to moduli 2, 3, and 5. This representation requires a limited set of numbers, those forming the equivalence partitions of the

C-2

residues, 0 to m-1 for each modulo m, and it has a range unique up to the product of the relatively prime moduli used.

The residues for the decimal numbers 0 through 30 modulo 2, 3, and 5 are given in Table 5. Using the table entries it is evident that arithmetic operations are performed in parallel in each modulos. The residues of 3, are (1,0,3) and the residues of 9 are (1,0,4). The sum of the residues is 0,0,2, (where 4+3 modulo 5 is 2), and the triplet (0,0,2) represents decimal number 12 as expected.

In order to implement the designs involving real time computing it is necessary to have a nonlinear optical transducer, typically in the form of a spatial light modulator (SLM). In this design the SLM is a relatively slow, high resolution device, the Hughes liquid crystal light valve (LCLV); it has been used in previous work in a range of optical computation applications [15,16,17,18]. The Hughes liquid crystal light valve (LCLV) is a two dimensional spatial light modulator whose basic operation is a function of the birefringent property of liquid crystal molecules.

The active area of the device is the central one square inch with a resolution of about 600 lines per inch. This provides an array of 600 x 600 simultaneously and independently accessible image elements, and has a switching time of about 1msec. The device requires 6 to 10 volts A.C. for operation [1].

A crossection of the layered structure of the Hughes Liquid Crystal Light Valve is shown in Figure 23. The three major components of the structure are the liquid crystal layer shown at the right of the figure,

Table 5

Residue Arithmetic Representation Of Decimal Numbers In Bases 2, 3, & 5

DECIMAL INTEGERS	RESIDUES		
	BASE 2	BASE 3	BASE 5
0	0	0	0
1	1	1	1
2	0	2	2
3	1	0	3
4	0	1	4
5	1	2	0
6	0	0	1
7	1	1	2
8	0	2	3
9	1	0	4
10	0	1	0
11	1	2	1
12	0	0	2
13	1	1	3
14	0	2	4
15	1	0	0
16	0	1	1
17	1	2	2
18	0	0	3
19	1	1	4
20	0	2	0
21	1	0	1
22	0	1	2
23	1	2	3
24	0	0	4
25	1	1	0
26	0	2	1
27	1	0	2
28	0	1	3
29	1	2	4
30	0	0	0

dielctric mirror in the center, and a CdS photosensitive semiconductor at the left. The AC voltage signal, applied to transparent electrodes forming the external layers of the sandwich, biases the field across the liquid crystal layer, typically to a level just below threshold. An incident write beam shown at the left strikes the photosensitive CdS film on the input side of the light valve. The intensity of this beam controls the total field produced across the liquid crystal layer. This in turn affects a change in the tip of the liquid crystal molecules at that location and hence provides control over their birefringence. A polarized read beam incident on the output side of the device at the

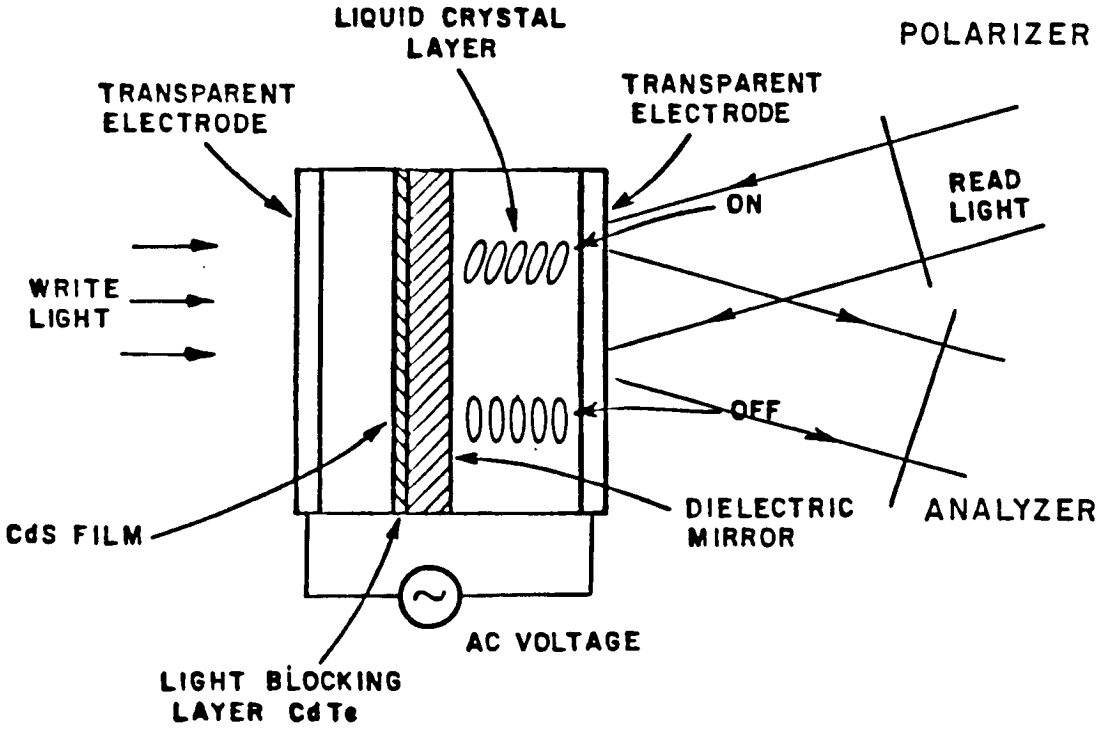

Figure 23. LCLV structure.

same coordinates as the write beam, shown at the right in Figure 23, is reflected by the dielectric mirror separating the semiconductor and liquid crystal layers. The polarization of the beam after traversing the liquid crystal layer twice is changed due to the birefringence of the molecules. Hence the intensity of the reflected beam after passing through an analyzer is controlled by the the intensity of the light incident on the LCLV input (write beam) side.

The write beam intensity level and AC voltage level can be adjusted to cause a predetermined amount of change in linear polarization states. In the suggested design, the intensity and voltage levels are chosen such that for no input write beam intensity the incident read beam polarization state is maintained and for maximum write beam intensity the read beam polarization is rotated by 90°.

Using this configuration, the light valve will be used to construct a birefringent gate providing a simple technique for implementing optical mapping units or interconnections between the position coded inputs and outputs described earlier, to build optical look up tables.

Appendix A Summary

A review of the field of numerical optical computing and specifically matrix multiplication, has been presented, complementing the background discussion given in Chapter I. The design aspects of the work presented in this report including position coding, holography, residue arithmetic and the Hughes LCLV have been introduced. These are essential to the matrix vector multiplier design for demonstrating a high-speed large-throughput system with position coded look up tables for interconnection schemes.

APPENDIX B

Mathematical Analysis of Polarization Decomposition at Non Normal Incidence in Liquid Crystals

An analysis of polarization decomposition in a liquid crystal cell for beams with non-normal incidence onto the cell is presented in this appendix. It will be shown that there is a preferred liquid crystal director orientation relative to the incidence plane and polarization, in which the birefringence of the liquid crystals is best exhibited. The results of this derivation are used in Chapters II and III.

Coordinate Transformations

Consider a homogeneous parallel liquid crystal alignment where the director orientation is initially parallel to the cell substrate. This is shown in Figure 24 with the director $\hat{n}$ initially in the z direction with no applied bias or field. This is also the direction of the optic axis of the liquid crystal. Let the liquid crystal molecule tip, induced by an applied voltage or input intensity, be in the xz plane with tip angle θ measured from the z axis.

Defining the x'y'z' coordinate system, shown in Figure 24(a), for the tipped molecules, then x'y'z' are expressed in terms of xyz as follows:

$$x' = (\cos\theta)\, x - (\sin\theta)\, z \tag{37}$$

$$y' = y \tag{38}$$

$$z' = (\sin\theta)\, x + (\cos\theta)\, z \tag{39}$$

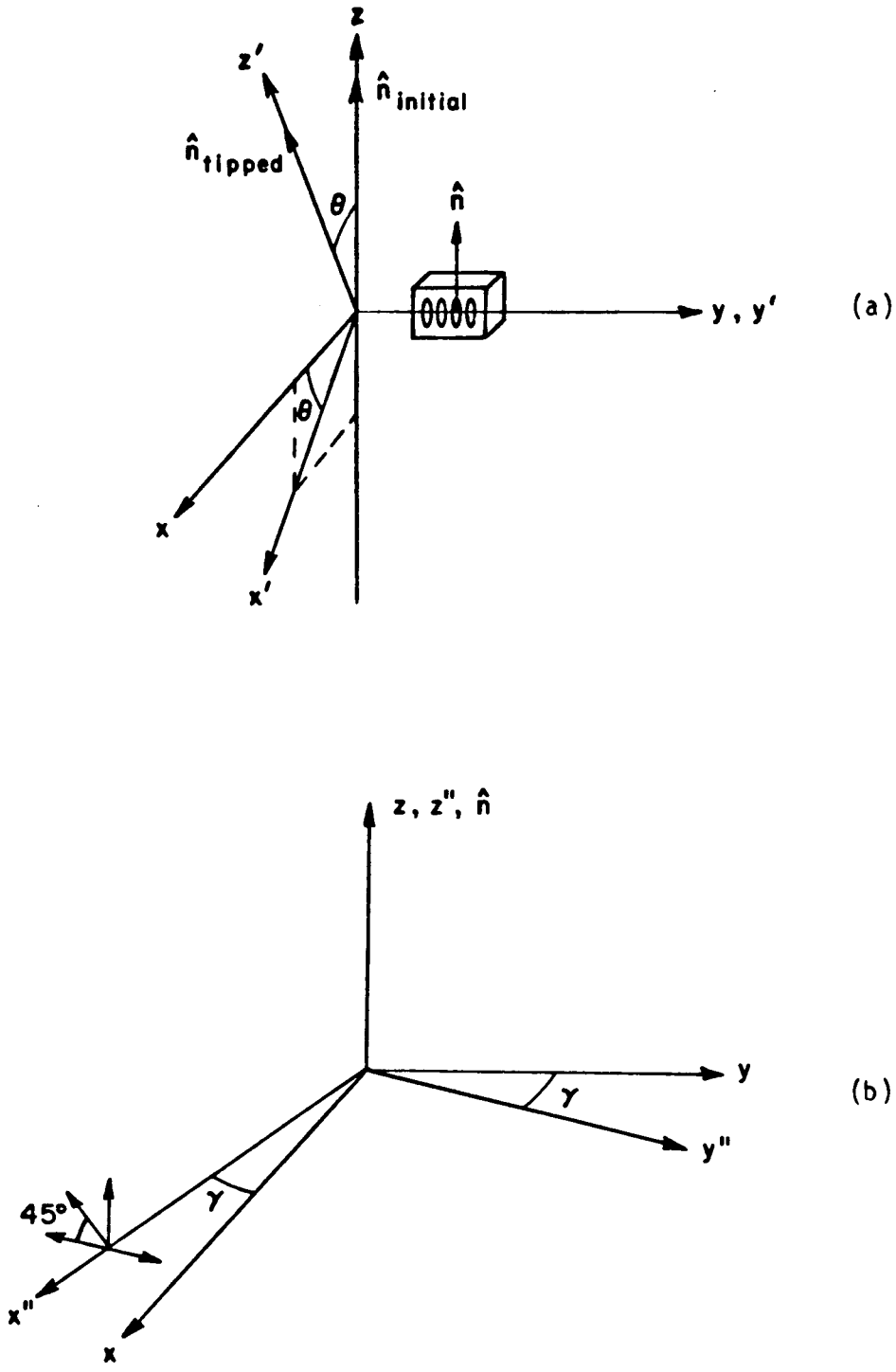

Figure 24. Coordinate systems.

Consider a beam incident on the cell in consideration at an angle γ from the normal, polarized at 45° to the y" and z" directions as shown in Figure 24(b). Another coordinate transformation relates coordinates x"y"z" to xyz as follows:

$$x = (\cos\gamma)\, x" + (\sin\gamma)\, y" \quad (40)$$
$$y = -(\sin\gamma)\, x" + (\cos\gamma)\, y" \quad (41)$$
$$z = z" \quad (42)$$

Combining Equations (37) through (42) gives x'y'z' in terms of x"y"z":

$$x' = \cos\gamma(\cos\theta)\, x" + \sin\gamma(\cos\theta)\, y" - (\sin\theta)\, z" \quad (43)$$
$$y' = -(\sin\gamma)\, x" + (\cos\gamma)\, y" \quad (44)$$
$$z' = \cos\gamma(\sin\theta)\, x" + \sin\gamma(\cos\theta) y" + (\cos\theta)\, z" \quad (45)$$

Polarization decomposition.

The decomposition of the input read beam polarization along the two allowed mutually orthogonal polarization directions will be analyzed using the coordinate transformations of Equations (43) to (45). The analysis involves the birefringent polarization ellipsoid of the anisotropic uniaxial liquid crystal molecules expressed in terms of an index ellipsoid [76].

The propagation of waves in anisotropic media is expressed in terms of the refractive index variation relative to the wave propagation direction, incidence angle, and polarization. The index variation is represented in an index ellipsoid [11,76], an ellipsoid of revolution for the uniaxial case, as shown in Figure 25, with refractive index n_e in the z direction, and n_o in the x,y plane. In this case, the optic axis is defined by the direction normal to the circular cross section of the ellipsoid, and for liquid crystals this direction is parallel to the

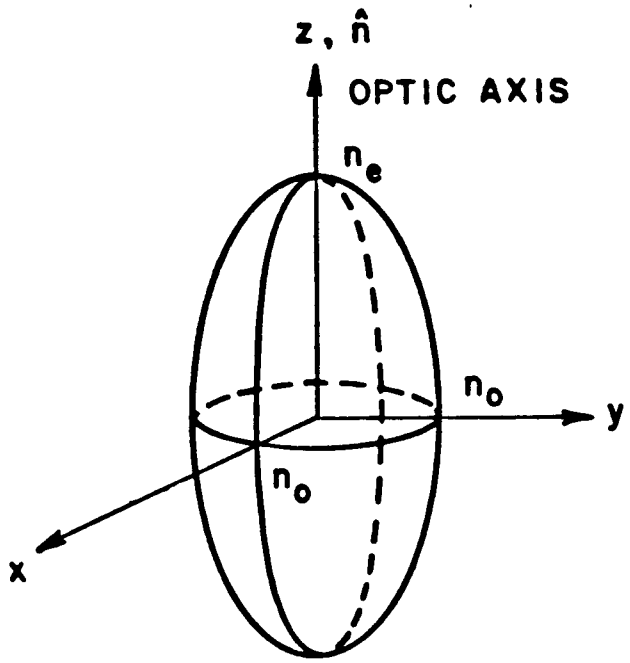

Figure 25. Index ellipsoid.

director. As the liquid crystal molecules rotate, the ellipsoid orientation and the optic axis direction also change.

The allowed polarization directions are in a plane passing through the center of the ellipsoid, perpendicular to the propagation direction. Generally this plane and the ellipsoid intersect to form a polarization ellipse where the allowed polarization directions are parallel to the axes of that ellipse. For the efficient operation of the liquid crystal cell in selecting or transmitting one of two orthogonal polarization components as a function of the tip angle θ it is desirable to have the input polarization decompose into two equal components along the allowed polarization directions. It will be shown that careful attention to liquid crystal orientation and incident beam propagation direction, are necessary for this to occur.

The ordinary (n_o) and extraordinary (n_e) refractive indices are used to define the index ellipsoid equation in the given coordinate system:

$$x^2/n_x^2 + y^2/n_y^2 + z^2/n_z^2 = 1 \qquad (46)$$

with $n_z = n_e$, and $n_x = n_y = n_o$.

Similarly, in the x',y',z' coordinate system the index ellipsoid is written as follows:

$$x'^2/n_x'^2 + y'^2/n_y'^2 + z'^2/n_z'^2 = 1 \qquad (47)$$

where $n_x' = n_y' = n_x = n_y = n_o$ and $n_z' = n_z = n_e$.

Substituting for x', y', and z' from Equations (43), (44), and (45) respectively, in Equation (47), gives the following relationship between the incident beam coordinates and the refractive indeces:

$$\frac{[\cos\gamma(\cos\theta)x''+\sin\gamma(\cos\theta)y''-(\sin\theta)z'']^2}{n_o^2} + \frac{[-(\sin\gamma)x''+(\cos\gamma)y'']^2}{n_o^2}$$

$$+ \frac{[\cos\gamma(\sin\theta)x''+\sin\gamma(\cos\theta)y''+(\cos\theta)z'']^2}{n_e^2} = 1 \qquad (48)$$

When Equation (48) is expanded and evaluated in the x" = 0 plane, (a plane perpendicular to the propagation direction), then the following expression is obtained:

$$y''^2[n_e^2(\sin^2\gamma\cos^2\theta + \cos^2\gamma) + n_o^2\sin^2\gamma\sin^2\theta]$$

$$+ 2y''z''[\sin\theta\cos\theta\sin\gamma(n_o^2-n_e^2)]$$

$$+ z''^2[n_e^2\sin^2\theta + n_o^2\cos^2\theta] = n_e^2 n_o^2 \qquad (49)$$

Now consider the incident light polarization. The input is plane polarized at 45° to the y" and z" directions and thus it is decomposed into equal y" and z" components. It is desired that these components be equal and also parallel to the allowed polarization directions of the

ellipse, independent of θ and γ. This occurs when the cross term in Equation (49) vanishes, i.e., when the coefficient of the y"z" term goes to zero as given in the following expression,

$$\sin\theta \cos\theta \sin\gamma (n_o^2 - n_e^2) = 0 \qquad (50)$$

so that Equation (49) can be put in the form:

$$ay''^2 + bz''^2 = n_e^2 n_o^2 \qquad (51)$$

There are several trivial solutions in which expression (50) holds: if $n_e = n_o$ (no birefringence, isotropic medium), if θ=0 or 90° (which means that the liquid crystal cell must be operated in only one of two possible states), or if γ=0 (which implies normal incidence).

Consider this last case, (γ=0), before two other general solutions are presented. At normal incidence x" = x', y"=y', and Equation (49) reduces to:

$$y''^2 [n_e^2] + z''^2 [n_e^2 \sin^2\theta + n_o^2 \cos^2\theta] = n_e^2 n_o^2 \qquad (52)$$

Let the ellipse intersect the y" axis at y_o" and the z" axis at z_o". This gives:

$$y_o''^2 [n_e^2] + z_o''^2 [n_e^2 \sin^2\theta + n_o^2 \cos^2\theta] = n_e^2 n_o^2 \qquad (53)$$

Evaluating y_o" when z_o" = 0 gives the effective refractive index $n_{eff}(x",y",z")$ in the y" direction; from Equation (53) this is seen to be:

$$y_o'' = n_{eff}(0,y_o'',0) = n_o$$

and y_o is independent of θ. Simlarly, for y"=0, the effective index is

$$z_o'' = n_{eff}(0,0,z_o'') = \frac{n_e n_o}{[n_e^2 \sin^2\theta + n_o^2 \cos^2\theta]^{1/2}} \qquad (54)$$

Checking the last expression, $n_{eff}(0,0,z_o")$ should be n_e at $\theta=0$, and n_o at $\theta = 90°$; this is easily verified.

Now consider the case where $\gamma \neq 0$. The expressions for the effective index or the ellipse principal axes are more complicated and are now functions of both θ and γ. The non-zero cross term in Equation (49) can be eliminated only by changing the physical orientation of the liquid crystal cell, the input polarization or both. Two approaches are presented here.

a. Relative rotation between polarization ellipse and input polarization plane.

In the first approach, a relative rotation by an angle ε is introduced between the polarization ellipse and the input polarization plane, such that the polarization ellipse axes and the directions of equal polarization decomposition are parallel, implying that the cross term in Equation (49) vanishes. This can be expressed in terms of a coordinate rotation about the x" direction where orthogonal directions y"z" are rotated into y''' z'''.

$$x" = x'''$$
$$y" = (\cos\varepsilon)\, y''' + (\sin\varepsilon)\, z''' \quad (55)$$
$$z" = -(\sin\varepsilon)\, y''' + (\cos\varepsilon)\, z''' \quad (56)$$

Equations (55) and (56) can be written in matrix form:

$$\begin{pmatrix} y" \\ z" \end{pmatrix} = \begin{pmatrix} \cos\varepsilon & \sin\varepsilon \\ -\sin\varepsilon & \cos\varepsilon \end{pmatrix} \begin{pmatrix} y''' \\ z''' \end{pmatrix} \quad (57)$$

Equation (49) also can be written in matrix form as follows:

$$\begin{pmatrix} y" \\ z" \end{pmatrix}^T \begin{pmatrix} A & B \\ B & C \end{pmatrix} \begin{pmatrix} y" \\ z" \end{pmatrix} = n_e^2 n_o^2 \quad (58)$$

where $A = n_e^2(\sin^2\gamma \cos^2\theta + \cos^2\gamma) + n_o^2 \sin^2\gamma \sin^2\theta]$

$$B = [\sin\theta \cos\theta \sin\gamma (n_o^2 - n_e^2)]$$

and $$C = [n_e^2 \sin^2\theta + n_o^2 \cos^2\theta].$$

Introducing the coordinate transformation of Equation (57) to Equation (58), then the conditions for diagonalizing the matrix in Equation (58) so that the y"z" term vanishes, can be derived. The following matrices are multiplied,

$$\begin{pmatrix} \cos\varepsilon\, y''' + \sin\varepsilon\, z''' \\ -\sin\varepsilon\, y''' + \cos\varepsilon\, z''' \end{pmatrix}^T \begin{pmatrix} A & B \\ C & D \end{pmatrix} \begin{pmatrix} \cos\varepsilon & \sin\varepsilon \\ -\sin\varepsilon & \cos\varepsilon \end{pmatrix} \begin{pmatrix} y''' \\ z''' \end{pmatrix} = n_e^2 n_o^2 \tag{59}$$

to give:

$$y'''^2 [A \cos^2\varepsilon - 2B \sin\varepsilon \cos\varepsilon + C \sin^2\varepsilon]$$
$$+ 2\, y'''z''' [B (\cos^2\varepsilon - \sin^2\varepsilon) + (A - C) \sin\varepsilon \cos\varepsilon]$$
$$+ z'''^2 [A \sin^2\varepsilon + 2B \sin\varepsilon \cos\varepsilon + C \cos^2\varepsilon] = n_e^2 n_o^2 \tag{60}$$

Setting the coefficient of the y'''z''' term to zero gives the condition on ε:

$$B (\cos^2\varepsilon - \sin^2\varepsilon) + (A - C) \sin\varepsilon \cos\varepsilon = 0$$

or

$$B (\cos^2\varepsilon - \sin^2\varepsilon) = (C - A) \sin\varepsilon \cos\varepsilon \tag{61}$$

Dividing both sides of Equation (61) by $\cos^2\varepsilon$ and using the trignometric identitity $1 - \tan^2\varepsilon = 2 \tan\varepsilon / \tan 2\varepsilon$ gives:

$$B (1 - \tan^2\varepsilon) = (C - A) \tan\varepsilon$$

or $$B (2\tan\varepsilon / \tan 2\varepsilon) = (C - A) \tan\varepsilon$$

hence $$\tan 2\varepsilon = 2B/(C - A) \tag{62}$$

Solving for ε gives:

$$\varepsilon = \tan^{-1}[2B/(C - A)] / 2 \tag{63}$$

Substituting for A, B, and C in Equation (63) gives:

$$\varepsilon = \frac{1}{2}\tan^{-1}\left[\frac{2\,[\sin\theta\cos\theta\sin\gamma\,(n_o^2-n_e^2)]}{n_e^2(\sin^2\theta - \sin^2\gamma\cos^2\theta - \cos^2\gamma) + n_o^2(\cos^2\theta - \sin^2\gamma\sin^2\theta)}\right] \tag{64}$$

It is clear that ε is a function of both θ and γ, implying a physical rotation of the liquid crystal cell or polarization plane every time θ or γ changes.

Using the condition given in Equation (62) and substituting for B from that equation in the y'''^2 and z'''^2 coefficents in Equation (60), and simplifying, results in the following expression:

$$y'''^2\,\frac{[A\cos^2\varepsilon - C\sin^2\varepsilon]}{\cos^2\varepsilon - \sin^2\varepsilon} + z'''^2\,\frac{[C\cos^2\varepsilon - A\sin^2\varepsilon]}{\cos^2\varepsilon - \sin^2\varepsilon} = n_e^2 n_o^2 \tag{65}$$

This last expression has the form:

$$\frac{y'''^2}{n_o'''^2} + \frac{z'''^2}{n_e'''^2} = 1$$

Solving for n_o''' and n_e''' gives:

$$\frac{1}{n_o'''^2} = \frac{[A\cos^2\varepsilon - C\sin^2\varepsilon]}{n_e^2 n_o^2(\cos^2\varepsilon - \sin^2\varepsilon)} \tag{66}$$

and

$$\frac{1}{n_e'''^2} = \frac{[C\cos^2\varepsilon - A\sin^2\varepsilon]}{n_e^2 n_o^2(\cos^2\varepsilon - \sin^2\varepsilon)} \tag{67}$$

Substituting for cos2ε from Equation (62) using the identities tan2ε = sin2ε/cos2ε, and sin2ε = $\sqrt{1-\cos^2 2\varepsilon}$, it can be shown that $n_o''' = n_o$, as desired. A similar substitution in Equation (67) gives the following expression for n_e''':

$$n_e'''^2 = n_e^2\, n_o^2 \,/\, [n_e^2 \sin^2\theta \cos^2\gamma + n_o^2\,(1-\sin^2\theta \cos^2\gamma)]$$

This should reduce to the expression for the effective refractive index, n_{eff}, in the normal incidence case where $\gamma = 0$, as in Equation (54). Indeed,

$$n_e'''^2\Big|_{\gamma=0} = n_{eff}^2 = n_e^2\, n_o^2 / (n_e^2 \sin^2\theta + n_o^2 \cos^2\theta)$$

The solution suggested in this subsection satisfies the conditions, but its implementation requires a physical rearrangement of components each time the LC molecule tip angle is changed or the incidence direction is changed.

There is one orientation in which the dependence on θ and γ does not require a physical rotation of components, suggesting a more practical solution. This orientation is discussed in the next subsection.

b. Orientation of LC cell and incidence plane.

In this second approach, the incidence plane and the liquid crystal rotation plane are coincident. This ensures that a beam polarized at 45° in a plane perpendicular to the propagation direction will be decomposed into one component that remains parallel to one of the principal axes of the polarization ellipse, and another component at an angle $\theta \pm \gamma$ away from the other ellipse principal axis direction.

The suggested orientation is shown in Figure 26, where the liquid crystal optical axis or director is initially in the y direction and the tip plane is the xy (or x'y', or x"y") plane.

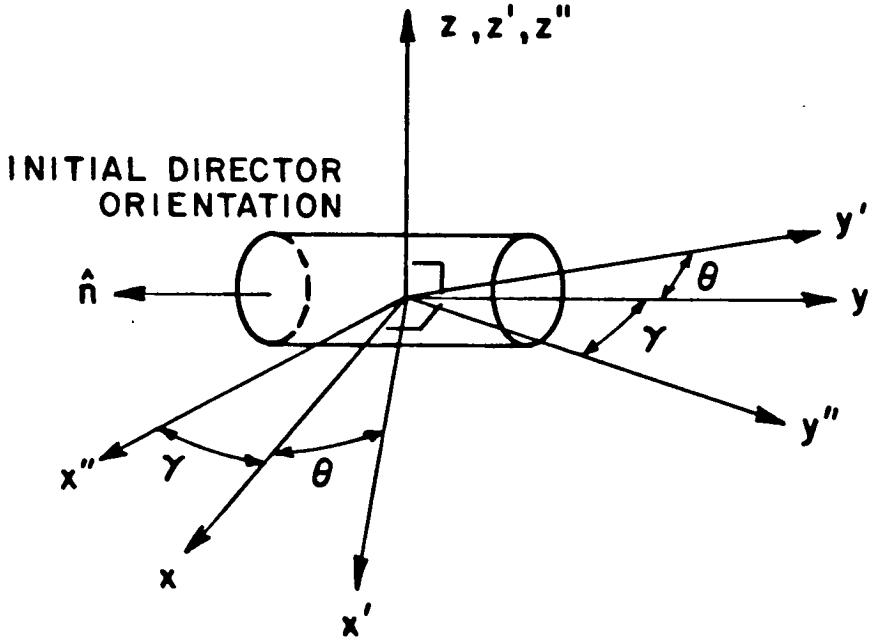

Figure 26. Liquid crystal orientation with rotation in incidence plane.

The coordinate transformations presented earlier take a simpler form. Equations (37) to (39) are replaced by the following:

$$x' = (\cos\theta)\, x + (\sin\theta)\, y \quad (68)$$
$$y' = -(\sin\theta)\, x + (\cos\theta)\, y \quad (69)$$
$$z' = z \quad (70)$$

and similarly Equations (40) to (42) are replaced by:

$$x = (\cos\gamma)\, x'' + (\sin\gamma)\, y'' \quad (71)$$
$$y = -(\sin\gamma)\, x'' + (\cos\gamma)\, y'' \quad (72)$$
$$z = z'' \quad (73)$$

and therefore x'y'z' are written in terms of x"y"z" as follows:

$$x' = \cos\gamma(\cos\theta)x''+\sin\gamma(\cos\theta)y''+\cos\gamma(\sin\theta)y''-\sin\gamma(\sin\theta)x'' \quad (74)$$
$$y' = -\cos\gamma(\sin\theta)x''-\sin\gamma(\sin\theta)y''-\sin\gamma(\cos\theta)x''+\cos\gamma(\cos\theta)y'' \quad (75)$$
$$z' = z'' = z \quad (76)$$

Applying these transformations in the ellipsoid equation by substituting into Equation (47) gives:

$$n_e^2[[(\cos\gamma\cos\theta-\sin\gamma\sin\theta)x"+(\sin\gamma\cos\theta+\cos\gamma\sin\theta)y"]^2 + z"^2]$$
$$+ \quad n_o^2\ [(-\cos\gamma\sin\theta-\sin\gamma\cos\theta)x"+(\cos\gamma\cos\theta-\sin\gamma\sin\theta)y"]^2 \quad = \quad n_e^2 n_o^2 \tag{77}$$

Combining terms and using trignometric identities gives:

$$n_e^2[[\cos(\gamma+\theta)x"+\sin(\gamma+\theta)y"]^2 + z"^2] + n_o^2[-\sin(\gamma+\theta)x"+(\cos(\gamma+\theta)y"]^2$$
$$= \quad n_o^2 n_e^2$$

After expanding and combining terms again the following expression is obtained:

$$(x")^2\ [n_e^2\ \cos^2(\gamma+\theta) + n_o^2\ \sin^2(\gamma+\theta)]$$
$$+ (y")^2\ [n_e^2\ \sin^2(\gamma+\theta) + n_o^2\ \cos^2(\gamma+\theta)] + n_e^2(z")^2$$
$$+ 2(x")(y")[(n_e^2-n_o^2)]\ \sin(\gamma+\theta)\cos(\gamma+\theta) = \quad n_o^2 n_e^2 \tag{78}$$

For x"=0 then Equation (78) reduces to:

$$(y")^2\ [n_e^2\ \sin^2(\gamma+\theta) + n_o^2\ \cos^2(\gamma+\theta)] + n_e^2(z")^2 = \quad n_o^2 n_e^2 \tag{79}$$

This expression can be rearranged to give:

$$\frac{(y")^2\ [n_e^2\ \sin^2(\gamma+\theta) + n_o^2\ \cos^2(\gamma+\theta)]}{n_o^2 n_e^2} + \frac{(z")^2}{n_o^2} = 1 \tag{80}$$

The intersections of the polarization ellipse with the ellipsoid can now be found. Solving for $z_o"$ at y"=0 gives $z_o"=n_o$ as expected, independent of θ or γ. Similarly, solving for $y_o"$ at z"=0 gives:

$$y_o" = n_{eff}(0,y_o",0) = \frac{n_e\ n_o}{[n_e^2\ \sin^2(\gamma+\theta) + n_o^2\ \cos^2(\gamma+\theta)]^{1/2}} \tag{81}$$

as desired.

Using the orientation shown in Figure 26, it is possible to have a continuous range of angles θ and γ and still have the equal polarization component directions and the prinipal axes of the ellipse parallel. The only requirements are that the incidence plane and the molecule rotation plane be the same and that the input polarization be at 45° in a plane normal to the incidence plane. These concepts are used in Chapters II and III.

APPENDIX C

Hologram Coupled Wave Theory

The derivation of the expressions for the incident reconstruction and the diffracted wave amplitudes, their coupling, and the form of the diffraction efficiency in the phase transmission hologram described in Chapter II, are presented in this Appendix. The discussion involves a solution of the wave equation and Kogelnik's coupled wave theory [46,47,50,77].

The hologram emulsion geometry, previously shown in Figure 8 is repeated here in Figure 27 for convenience. An inset has been added showing the vector diagram for the incident and reconstructed wave directions $\underline{\kappa}_i$, $\underline{\kappa}_d$ respectively and the resultant grating normal $\underline{\kappa}$. The

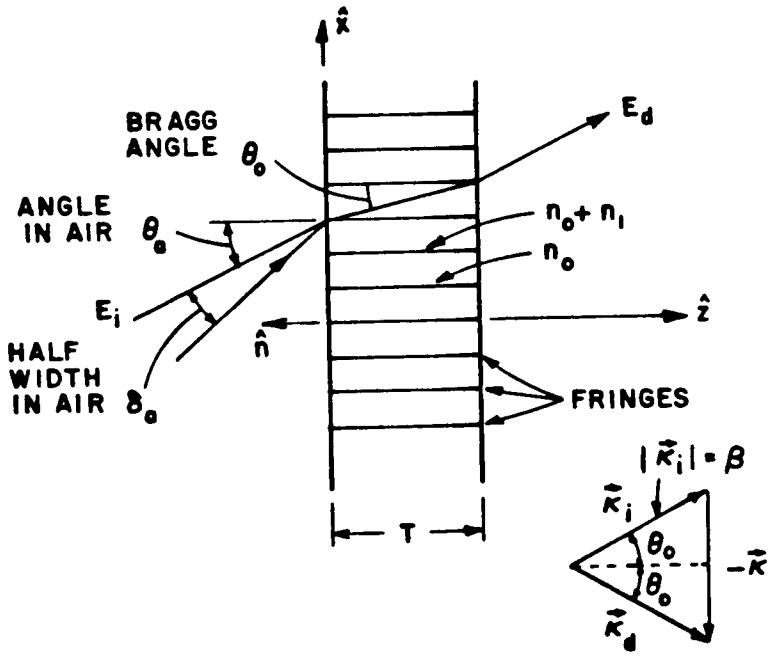

Figure 27. Hologram geometry.

incident reconstruction beam is indicated at the right using the notation $E_r = E_i$ and the diffracted wave shown at the left is denoted by $E_s = E_d$. Mathematically, the incident and diffracted plane waves are expressed as

$$E_i = E_r = R(z) \exp(-j\underline{\kappa}_i.\underline{r}) \tag{82}$$

$$E_d = E_s = S(z) \exp(-j\underline{\kappa}_d.\underline{r}) \tag{83}$$

where R(z) and S(z) are the complex field amplitudes desired.

Consider the propagation of a plane wave, denoted by E in general, in an emulsion with relative dielectric constant ε, and conductivity σ, frequency ω and let the free space permeability and dielectric constant be μ_o and ε_o respectively. It must satisfy the wave equation expressed as [50]:

$$\nabla^2 E + (k_o)^2 E = 0 \tag{84}$$

where $(k_o)^2 = (\omega^2/c^2)\varepsilon - j\omega\mu_o\sigma$ is the general form from which the propagation constant, k_o is obtained. Substituting $c = (\varepsilon_{oo}\mu_o)^{1/2}$, the wave equation is written in the following form:

$$\nabla^2 E + (\omega^2\mu_o\varepsilon_{oo}\varepsilon - j\omega\mu_o\sigma)E = 0 \tag{85}$$

For a holographic emulsion where the exposure forms a sinusoidal transmission grating due to the interference of two plane waves the dielectric constant ε and conductivity σ, are assumed to have a sinusoidal variation, each about a mean value ε_o and σ_o respectively. Thus

$$\varepsilon = \varepsilon_o + \varepsilon_1 \cos(\underline{\kappa}.\underline{r}) \tag{86}$$

$$\sigma = \sigma_o + \sigma_1 \cos(\underline{\kappa}.\underline{r}) \tag{87}$$

Substituting Equations (86) and (87) into the expression for k_o^2 gives:

$$k_o^2 = (\omega^2\mu_o\varepsilon_{oo}\varepsilon - j\omega\mu_o\sigma)$$

$$= \omega^2\mu_o\varepsilon_{oo}[\varepsilon_o + \varepsilon_1 \cos(\underline{\kappa}.\underline{r})] - j\omega\mu_o[\sigma_o + \sigma_1\cos(\underline{\kappa}.\underline{r})]$$

$$= \omega^2\mu_o\varepsilon_{oo}\varepsilon_o - j\omega\mu_o\sigma_o + (\omega^2\mu_o\varepsilon_{oo}\varepsilon_1 - j\omega\mu_o\sigma_1)\cos(\underline{\kappa}.\underline{r}) \quad (88)$$

Substituting k^2 for the expression $\omega^2\mu_o\varepsilon_{oo}$ and (88) in (84) gives:

$$\nabla^2 E + [k^2\varepsilon_o - j\omega\mu_o\sigma + (k^2\varepsilon_1 - j\omega\mu_o\sigma_1)\cos(\underline{\kappa}.\underline{r})]E = 0 \quad (89)$$

The propagation constant, the term in the brackets, is now rewritten as follows:

$$k_o^2 = k(\varepsilon_o)^{1/2}[k(\varepsilon_o)^{1/2} - \frac{2j\omega\mu_o\sigma_o}{2\,k(\varepsilon_o)^{1/2}} + 2[\frac{k\varepsilon_1}{2\,(\varepsilon_o)^{1/2}} - \frac{j\omega\mu_o\sigma_1}{2\,k(\varepsilon_o)^{1/2}}]\cos(\underline{\kappa}.\underline{r})] \quad (90)$$

Using the following substitutions:

$$\beta = k(\varepsilon_o)^{1/2} = 2\pi n_o/\lambda_a \quad (91)$$

$$\alpha = \omega\mu_o\sigma_o/2k(\varepsilon_o)^{1/2} \quad (92)$$

$$\chi = 0.5[k\varepsilon_1/2(\varepsilon_o)^{1/2} - j\omega\mu_o\sigma_1/2k(\varepsilon_o)^{1/2}] \quad (93)$$

$$= 0.5[k\varepsilon_1/2(\varepsilon_o)^{1/2} - j\alpha_1] \quad (94)$$

$$\alpha_1 = \omega\mu_o\sigma_1/2k(\varepsilon_o)^{1/2} \quad (95)$$

The propagation constant can be written as follows:

$$k_o^2 = \beta[\beta - 2j\alpha + 2\chi\,(\exp[j\underline{\kappa}.\underline{r}] + \exp[-j\underline{\kappa}.\underline{r}])]$$

$$= \beta^2 - 2j\alpha\beta + 2j\chi\beta\,(\exp[j\underline{\kappa}.\underline{r}] + \exp[-j\underline{\kappa}.\underline{r}]) \quad (96)$$

The coefficient χ is a complex coupling constant relating the incident and diffracted waves.

Recalling the plane wave forms of Equations (82) and (83), and that:

$$\underline{\kappa}_d = \underline{\kappa}_i - \underline{\kappa} \tag{97}$$

and making the substitution $E = E_i + E_d$ in Equation (C-8), as well as the form of the propagation constant given in Equation (96) gives:

$$\nabla^2[R(z)\exp(-j\underline{\kappa}_i.\underline{r}) + S(z)\exp(-j\underline{\kappa}_d.\underline{r})] + [\beta^2 - 2j\alpha\beta + 2j\chi\beta(\exp[j\underline{K}.\underline{r}] + \exp[-j\underline{K}.\underline{r}])][R(z)\exp(-j\underline{\kappa}_i.\underline{r}) + S(z)\exp(-j\underline{\kappa}_d.\underline{r})] = 0 \tag{98}$$

Equation (97) must be satisfied for arbitrary $\underline{\kappa}$ and the coefficients of the $\exp(-j\underline{\kappa}_i.\underline{r})$ and the $\exp(-j\underline{\kappa}_d.\underline{r})]$ terms must separately be zero. The other terms involving $\exp(-j[\underline{\kappa}+\underline{\kappa}_i].\underline{r})$ and $\exp(-j[\underline{\kappa}-\underline{\kappa}_d].\underline{r})$ are ignored as they represent waves that do not satisfy the Bragg condition. Noting that

$$\begin{aligned} \underline{\kappa}_i.\underline{r} &= \kappa_{ix}x + \kappa_{iz}z \\ \underline{\kappa}_d.\underline{r} &= \kappa_{dx}x + \kappa_{dz}z \\ \kappa_i^2 &= \kappa_{ix}^2 + \kappa_{iz}^2 \\ \kappa_d^2 &= \kappa_{dx}^2 + \kappa_{dz}^2 \end{aligned}$$

then combining the terms with $\exp(-j\underline{\kappa}_i.\underline{r})$ and $\exp(-j\underline{\kappa}_d.\underline{r})]$ coefficients gives the following two equations:

$$R'' - 2j\kappa_{iz}R' - \kappa_i^2 R + \beta^2 R - 2j\alpha\beta R + 2\chi\beta S = 0 \tag{99}$$

and

$$S'' - 2j\kappa_{dz}S' - \kappa_d^2 S + \beta^2 S - 2j\alpha\beta S + 2\chi\beta R = 0 \tag{100}$$

Equations (99) and (100) are a pair of coupled equations which can be stated in another form by considering the following assumptions and definitions.

The complex field amplitudes R(z) and S(z) are assumed to be slowly varying functions, thus the second order derivatives in Equations (99)

and (100) can be neglected. As defined in Figure 27, $|\underline{\kappa}_i| = \beta$, thus eliminating two terms in Equation (99).

A second assumption involves the $(\beta^2 - \kappa_d^2)S$ terms of (100). In the general case let the reconstruction beam incidence angle deviate by a small angle δ_o about the Bragg angle θ_o inside the medium such that $\theta = \theta_o + \delta_o$. The $(\beta^2 - \kappa_d^2)$ coefficient represents the resultant deviation in the vector diagram due to the incident beam deviation from the Bragg angle. Using a small angle approximation it can be shown that [50]:

$$(\beta^2 - \kappa_d^2) = 2\,\beta^2\,\delta_o \sin 2\theta_o \tag{101}$$

Let $\Gamma = \beta\,\delta_o \sin 2\theta_o$, then using the notation $(\beta^2 - \kappa_d^2) = 2\beta\Gamma$, $c_R = \kappa_{iz}/\beta$, and $c_S = \kappa_{dz}/\beta$, [49], and dividing the left and right hand sides of Equations (99) and (100) by $-2j\beta$, gives the following simplified forms:

$$c_R R' + \alpha R = -jxS \tag{102}$$

$$c_S S' + (\alpha + j\Gamma)S = -jxR \tag{103}$$

In this form, the coupling between the incident complex wave amplitude and the corresponding diffracted complex wave amplitude is evident with the coupling coefficient appearing in both of the above equations. The particular form in which the coupling occurs is a function of the type of recording medium, affecting the specific form of the coupling factor x and the phase factor Γ. To see these effects the expressions for the complex field amplitudes must be derived and then the parameters for the specific situation can be substituted.

This can be done by substituting Equation (102) in (103) to obtain the following second order differential equation:

$$R'' + (\alpha/c_R + \alpha/c_S + j\Gamma/c_S)R' + (1/c_Rc_S)(\alpha^2 + j\alpha\Gamma + \chi^2)R = 0 \quad (104)$$

Equation (104) has a solution of the form $R(z) = \exp(\gamma z)$ which results in the following characteristic quadratic equation for γ,

$$\gamma'' + (\alpha/c_R + \alpha/c_S + j\Gamma/c_S)\gamma' + (1/c_Rc_S)(\alpha^2 + j\alpha\Gamma + \chi^2)\gamma = 0 \quad (105)$$

and the roots:

$$\gamma_1 = ((\alpha/c_R+\alpha/c_S-j\Gamma/c_s) + [(\alpha/c_R-\alpha/c_S-j\Gamma/c_s)^2 - 4\chi^2/c_rc_s]^{1/2})/2$$

$$\gamma_2 = ((\alpha/c_R+\alpha/c_S-j\Gamma/c_s) - [(\alpha/c_R-\alpha/c_S-j\Gamma/c_s)^2 - 4\chi^2/c_rc_s]^{1/2})/2$$

The solution to Equation (104) has the general form:

$$R(z) = R_1\exp(\gamma_1 z) + R_2\exp(\gamma_2 z) \quad (106)$$

and from Equation (102), S(z) has the form:

$$S(z) = S_1\exp(\gamma_1 z) + S_2\exp(\gamma_2 z) \quad (107)$$

where R_1, R_2, S_1, and S_2 are obtained from the boundary conditions, and γ_1 and γ_2, differ for each type of recording medium.

Consider a solution of the coupled wave equations for a lossless phase transmission hologram of the type described in Chapter II. Assuming an emulsion of thickness T and a hologram emulsion located with its left edge at z=0 and its right edge at z=T, then consider an incident plane wave from the left, R(z), of unity (normalized) amplitude which produces a diffracted wave, S(z).

First the general form for the diffracted wave, S(z), is determined. This will be a function of the emulsion thickness, the characteristic equation roots, γ_1 and γ_2, and the coupling constant χ. The value of S(z) at z=T, i.e. S(T), is then determined for the special case. This value is then used to find the diffraction efficiency by using the expression $\eta = SS^*/RR^*$.

The boundary condition gives:

$$R(0) = 1 = R_1 + R_2$$

$$S(0) = 0 = S_1 + S_2$$

Using $S'(0) = \gamma_1 S_1 + \gamma_2 S_2$ from Equation (107) and the boundary conditions, in Equation (103) gives:

$$c_s(\gamma_1 S_1 + \gamma_2 S_2) = -j\chi$$

and solving for S_1 and S_2,

$$S_1 = -S_2 = -j\chi/[c_s(\gamma_1-\gamma_2)] \tag{108}$$

Substituting into Equation (107) and evaluating at z=T gives,

$$S(T) = j[\chi/(c_s(\gamma_1-\gamma_2))]\,[\exp(\gamma_1 T)-\exp(\gamma_2 T)] \tag{109}$$

Equation (109) is the general form to be used in determining the diffracted wave for all cases.

For the special case of a phase transmission hologram the emulsion is considered a lossless dielectric, and so $\alpha = \alpha_1 = 0$. The roots γ_1 and γ_2 of Equation (104) take on the following simplified forms:

$$\gamma_1 = (-j\Gamma/c_s + [(-j\Gamma/c_s)^2 - 4\chi^2/c_r c_s]^{1/2})/2$$

$$\gamma_2 = (-j\Gamma/c_s - [(-j\Gamma/c_s)^2 - 4\chi^2/c_r c_s]^{1/2})/2$$

Noting that $c_r = c_s = \cos\theta$ and using the parameters defined in Equations (5) an (6) in Chapter II and rewritten here,

$$\xi = \delta\beta T/\sin\theta_o = \Gamma T/2\cos\theta_o \tag{110}$$

$$\nu = \chi T/\cos\theta = \nu(T) \tag{111}$$

the roots γ_1 and γ_2 are rewritten as follows:

$$\gamma_1 = (1/T)[-j\xi + j(\xi^2+\nu^2)^{1/2}] \tag{112}$$

$$\gamma_2 = (1/T)[-j\xi - j(\xi^2+\nu^2)^{1/2}] \tag{113}$$

To evaluate S(T), substitute the following combinations in Equation (109):

$$\gamma_1 - \gamma_2 = (2j/T)(\xi^2+\nu^2)^{1/2}$$

$$\gamma_1 T = [-j\xi + j(\xi^2+\nu^2)^{1/2}]$$

and $$\gamma_2 T = [-j\xi - j(\xi^2+\nu^2)^{1/2}]$$

Therefore,

$$S(T(\xi,\nu)) = -j \exp(-j\xi) \frac{\sin[(\xi^2+\nu^2)^{1/2}]}{(1+\xi^2/\nu^2)^{1/2}} \tag{114}$$

Substituting in the expression for diffraction efficiency:

$$\eta = SS^*/RR^* = |S(T)|^2/|R(0)|^2 \tag{115}$$

gives:

$$\eta = |S(T(\xi,\nu))|^2 = \frac{\sin^2[(\xi^2+\nu^2)^{1/2}]}{(1+\xi^2/\nu^2)} = \nu^2 \frac{\sin^2[(\xi^2+\nu^2)^{1/2}]}{(\xi^2+\nu^2)} \tag{116}$$

This is the expression used in Equation (9) in Chapter II for the diffraction efficiency of a phase transmission hologram.

To better understand the physical coupling between the incident and the diffracted waves, the expression for the incident wave complex field amplitude will now be derived and a simple case is considered.

Substituting Equations (106) and (107) in Equation (102) gives:

$$(c_R\gamma_1 R_1 + \alpha R_1) \exp(\gamma_1 z) + (c_R\gamma_2 R_2 + \alpha R_2)\exp(\gamma_2 z)$$
$$= -j\chi S_1 \exp(\gamma_1 z) - j\chi S_2 \exp(\gamma_2 z) \tag{117}$$

Equating the $\exp(\gamma_1 z)$ and $\exp(\gamma_2 z)$ coefficients on both sides of Equation (117) and solving for R_1 and R_2 gives:

$$R_1 = -j\chi S_1/(c_R\gamma_1 + \alpha)$$

$$R_2 = -j\chi S_2/(c_R\gamma_2 + \alpha)$$

Substituting for S_1 and S_2 from Equation (C-27) gives:

$$R_1 = [-jx/(c_R\gamma_1 + \alpha)]\ [-jx/[c_s(\gamma_1-\gamma_2)]]$$

$$= -x^2/c_s(\gamma_1-\gamma_2)(c_R\gamma_1 + \alpha)$$

$$R_2 = [-jx/(c_R\gamma_2 + \alpha)]\ jx/[c_s(\gamma_1-\gamma_2)]$$

$$= x^2/c_s(\gamma_1-\gamma_2)(c_R\gamma_2 + \alpha)$$

Replacing R1 and R2 in Equation (106) gives the following expression for R(z):

$$R(z) = [x^2/c_s(\gamma_1-\gamma_2)][\exp(\gamma_2 z)/(c_R\gamma_2+\alpha)\ -\exp(\gamma_1 z)/(c_R\gamma_1+\alpha)] \tag{118}$$

Evaluating Equation (118) for a phase transmission hologram, (α=0) at z=T and at Bragg incidence, (δ=0, ξ=0), and substituting for $\gamma_1 T$, $\gamma_2 T$, and c_R and c_S as before, gives:

$$R(T) = [x^2T^2/\cos^2\theta]\ (\cos\nu)/\nu^2$$

but $\nu = xT/\cos\theta_o$ thus,

$$R(T(0,\nu)) = (\cos\nu)$$

and $$|R(T(0,\nu))|^2 = (\cos^2\nu) \tag{119}$$

Recalling the expression for S(T) from Equation (114) and evaluating at Bragg incidence gives:

$$|S(T(0,\nu))|^2 = (\sin^2\nu) \tag{120}$$

Equations (119) and (120) are plotted in Figure 28. Note that as ν increases from zero, the amplitude of the incident wave decreases while the amplitude of the diffracted wave increases until the point $\nu = \pi/2$ is reached. This shows the coupling of energy out of the incident wave and into the diffracted wave, with 100% conversion at $\nu=\pi/2$ for

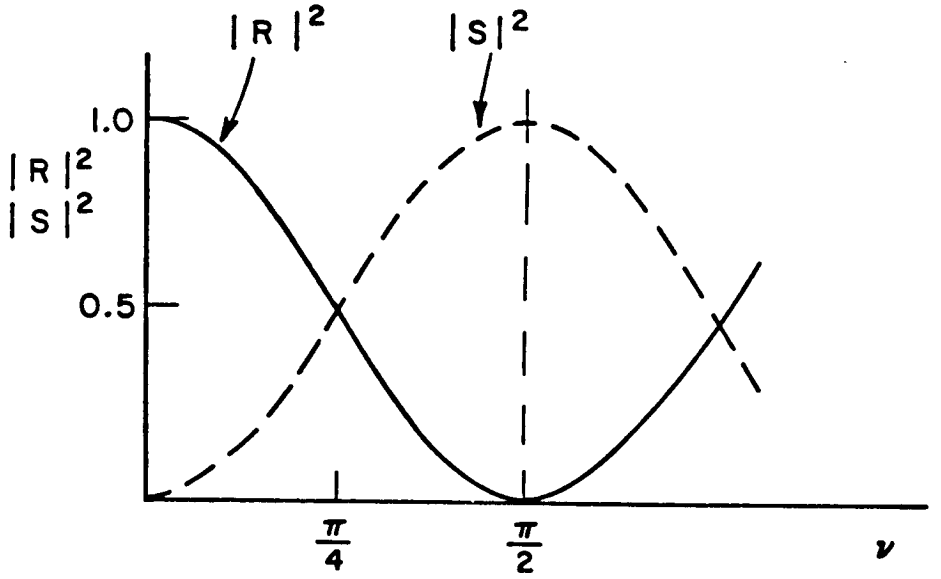

Figure 28. Coupling between incident and diffracted waves in a holographic emulsion.

Bragg incidence. The change in ν is interpreted in two ways. First consider the expression for ν:

$$\nu = \chi T/\cos\theta$$

where in the general case,

$$\chi = 0.5[k\varepsilon_1/2(\varepsilon_0)^{1/2} - j\alpha_1]$$

For a lossless phase transmission hologram $\alpha_1 = 0$, so,

$$\chi = [k\varepsilon_1/4(\varepsilon_0)^{1/2} \qquad (121)$$

Using Equation (86) for the spatial variation of the dielectric constant ε, and the definition of the refractive index $n^2 = \varepsilon$, then,

$$n^2 = \varepsilon = \varepsilon_0 + \varepsilon_1 \cos(\underline{\kappa}.\underline{r})$$

The refractive index can also be written in terms of an average medium index, n_0, and a variation about the average, n_1:

$$n^2 = \varepsilon_o + \varepsilon_1 \cos(\underline{\kappa}.\underline{r}) = (n_o + n_1 \cos(\underline{\kappa}.\underline{r}))^2$$

Assuming $n_1 << n_o$, then performing the square operation in the above expression gives $n_o = (\varepsilon_o)^{1/2}$, and $2n_o n_1 = \varepsilon_1$, so

$$n_1 = \varepsilon_1/2n_o = \varepsilon_1/2(\varepsilon_o)^{1/2} \qquad (122)$$

Substituting Equation (122) in (121) gives:

$$\chi = (kn_1/2)$$

or $$\chi = (\pi n_1/\lambda_a) \qquad (123)$$

Replacing χ in the expression for ν gives:

$$\nu = (\pi n_1/\lambda_a)T/\cos\theta$$

$$\nu = \pi n_1 T/\lambda_a \cos\theta \qquad (124)$$

From Equation (124), it is seen that ν can change by changing n_1 or T, assuming the wavelength is constant. This leads to the following interpretation of Figure 28. The refractive index variation, n_1, is a function of the exposure and for a given emulsion thickness T, it is desired that the exposure give n_1 such that $\nu=\pi/2$, or from Equation (124), that

$$n_1 = \lambda_a \cos\theta/2T$$

When this condition is met, there will be 100% coupling between the incident and reconstructed waves at Bragg incidence.

A second interpretation assumes that n_1 is determined by the exposure and now T is allowed to vary, i.e. the coupling is observed at different emulsion thicknesses. It is again seen that at the emulsion thickness determined from Equation (124) for $\nu=\pi/2$, namely $T=\lambda_a \cos\theta/2n_1$, then 100% coupling between incident and reconstructed waves occurs.

Appendix C Summary

The expressions for the incident reconstruction and the diffracted wave amplitudes were derived leading to the expression for diffraction efficiency in phase transmission hologram used in Chapter II. The coupling between the incident and diffracted waves inside the emulsion was also described in Figure 28.

APPENDIX D

Description of Matrix-Vector Multiplier Apparatus

The appartus for the optical matrix vector multiplier is described in this appendix. A list of all the components is presented and drawings of the individual groups of components shown in Figure 11 in Chapter III, based on photographs of the matrix-vector multiplier apparatus will be shown. An overall view of the system is presented first in Section 1, followed by a discussion of each group of components and its function in Sections 2 through 7.

1. Matrix-Vector Multiplier Apparatus: Overall Optical Configuration.

A general overall review of the system is presented in this section. The optical components for the matrix multiplier are shown in Figure 29 and a list of all the components is given in Table 6. The lenses and mirrors are numbered and are denoted by L# and M# respectively. The system also uses one light valve, LCLV, shown at the center, two laser sources, a microprocessor controlled CRT and a holographic memory. LASER 1, shown at the left, and the CRT, shown at the top center are used to implement the multiplication mapping unit. LASER 2, shown at the bottom, and the holographic storage unit, shown at the right, are used to implement the addition mapping units. The laser sources are used here only for demonstration purposes to simulate inputs generated from an array of sources, perhaps an array of optical fibers.

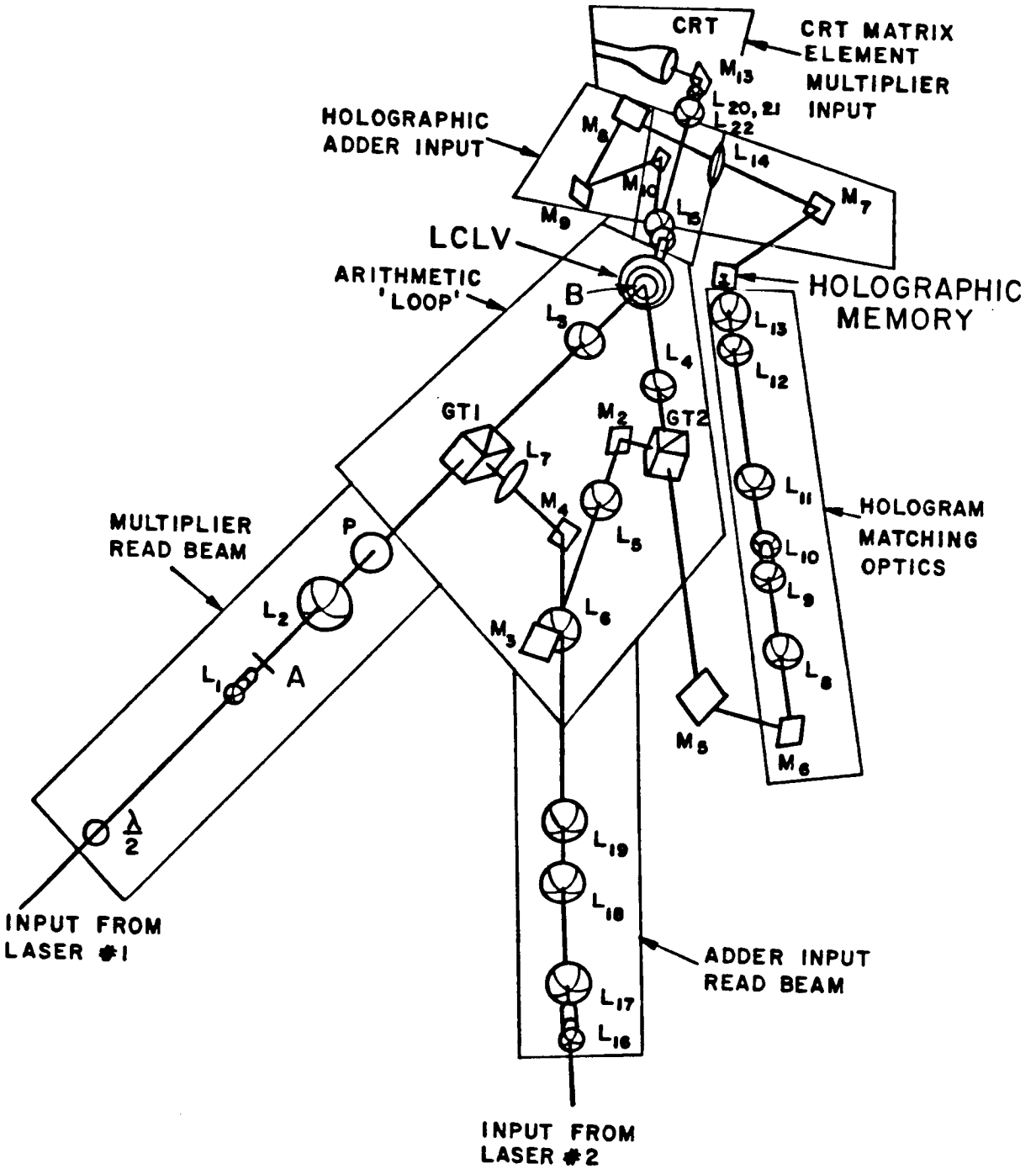

Figure 29. Optical matrix vector multiplier demonstration apparatus.

Table 6

Matrix Vector Multiplier Optical Components

Component	Description
laser 1	Argon ion laser, λ = 514.6 nm
laser 2	Argon ion laser, λ = 514.6 nm
light valve	Hughes Liquid Crystal Light Valve, homeotropic alignment, # H4050
CRT	Clinton CE656-M6P1
half wave plate	$\lambda/2$, for λ=514.6 nm
M1	Flat mirror for LASER 1 input
L1	10 X microscope objective
L2	40 mm ϕ, 125 mm focal length (fl)
GT1	Glan Thompson polarizing cube
L3	42 mm ϕ, 250 mm fl
L4	42 mm ϕ, 250 mm fl
GT2.	Glan Thompson polarizing cube
M2	Flat dielectric coated mirror
L5	42 mm ϕ, 250 mm fl
L6	42 mm ϕ, 250 mm fl, field lens
M3	Flat dielectric coated mirror
M4	Flat dielectric coated mirror
L7	42 mm ϕ, 250 mm fl
M5	Flat mirror
M6	Flat mirror
L8,	40 mm ϕ, 125 mm fl
L9,	42 mm ϕ, 250 mm fl, field lens
L10.	10 X microscope objective
L11	40 mm ϕ, 150 mm fl
L12	49 mm ϕ, 550 mm fl
L13	62 mm ϕ, 100 mm fl
holographic memory	Kodak 649F, bleached emulsion
M7	mirror
L14	51 mm ϕ, 240 mm fl
M8	Flat mirror
M9	Flat mirror
M10	Flat mirror
L15	60mm ϕ, 127 mm fl, compound lens
M11	Flat mirror for LASER 2 input
M12	Flat mirror for LASER 2 input
L16	10 X microscope objective
L17	40 mm ϕ, 110 mm fl, field lens
L18	42 mm ϕ, 250 mm fl
M13	Flat mirror for CRT input
L19	42 mm ϕ, 250 mm fl
L20	47 mm ϕ, 56 mm fl, compound lens
L21	40 mm ϕ, 170 mm fl, field lens
L22	50 mm ϕ, 121 mm fl, compound lens

There are six main groups of components each with a specific task. The groups will be identified first before giving the detailed features and operations performed by each in the following sections. The components in each group are listed below.

* Multiplication input read beam components:

  LASER 1 and M1, not shown, $\lambda/2$ plate, L1, and L2 provide a collimated horizontally polarized input read beam for the multiplier mapping unit.

* Loop components:

  GT1, L3, LCLV, L4, GT2, M2, L5, L6, M3, M4, L7, form a set identified as the loop used to shift the input beam sideways as it reflects successively off different light valve spots. This set of components constitutes the 'polarizing mirror' of Figures 3 and 4.

* Hologram addressing components:

  M5, M6, L8, L9, L10, L11, L12, and L13 are the components providing the position coded input to the holographic memory to give a reconstruction beam matching the reference beam.

* Holographic memory output imaging components:

  M7, L14, M8, M9, M10, and L15 are used to image the patterns generated from the holographic memory onto the LCLV write side.

* Adder input read beam components:

  LASER 2, M11 and M12, not shown, L16, L17, L18, and L19, are used to provide a vertically polarized input beam for the adder mapping unit focussed in the plane of M3, past the edge of the mirror, and directed towards mirror M4 and lens L7.

* CRT Imaging components:

  CRT, M13, L20, L21, L22, L15, are used to image the CRT generated patterns for multiplication on the write beam side of the LCLV.

2. Multiplication Input Read Beam Component Description

The components providing a polarized input read beam for the multiplier mapping unit, are shown in Figure 30. They are: LASER 1, λ/2 plate, M1, L1, and L2. The remaining components in the figure, GT1, L3, L4 and the light valve are shown for convenience. The object is to provide a collimated, horizontally polarized beam into GT1. Subsequently the beam is focused on the light valve output face.

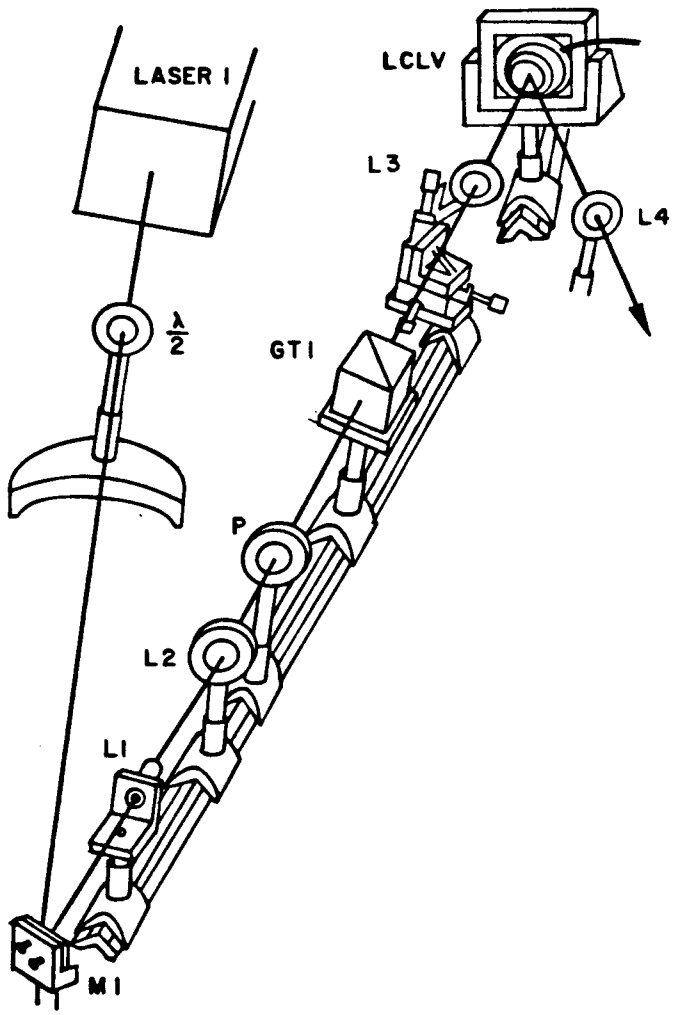

Figure 30. Drawing of multiplier input read beam optics.

Lenses L1 and L2 provide the desired collimated input. Lens L2 is placed a focal length away from focussed spot produced by the 10X microscope objective L1. The Glan Thompson polarizing beamsplitter cube, GT1, reflects a vertical polarization and transmits a horizontal polarization when placed in collimated space, so a half wave plate placed immediately following the laser rotates the laser's vertical polarization by 90° to give a horizontally polarized input to GT1. The beam is focussed onto the light valve by lens L3. As shown in Figure 30, the read beam is at non normal incidence, in fact its optical axis is at an angle of approximately 15° to the light valve normal.

3. Loop Component Description

The loop components are shown in Figure 31. The same set of loop components is used in implementing both the multiplication and addition look up tables. The LCLV is shown at the top right and prism GT1 at the left, and prism GT2 in the center. The remaining loop components include L3, L4, M2, L5, L6, M3, M4, and L7. The purpose of the loop components is to take a spot focused by lens L3 onto the light valve plane and image it onto an adjacent spot in that plane. This is done in two stages. First the spot is imaged onto auxiliary mirror M3 using lenses L4 and L5, and then that spot is imaged back onto the light vavle using lenses L7 and L3. The image position on the light valve is controlled by tilting mirror M3. This causes the beam directed towards the light valve to shift sideways as it reflects successively off different light valve spots.

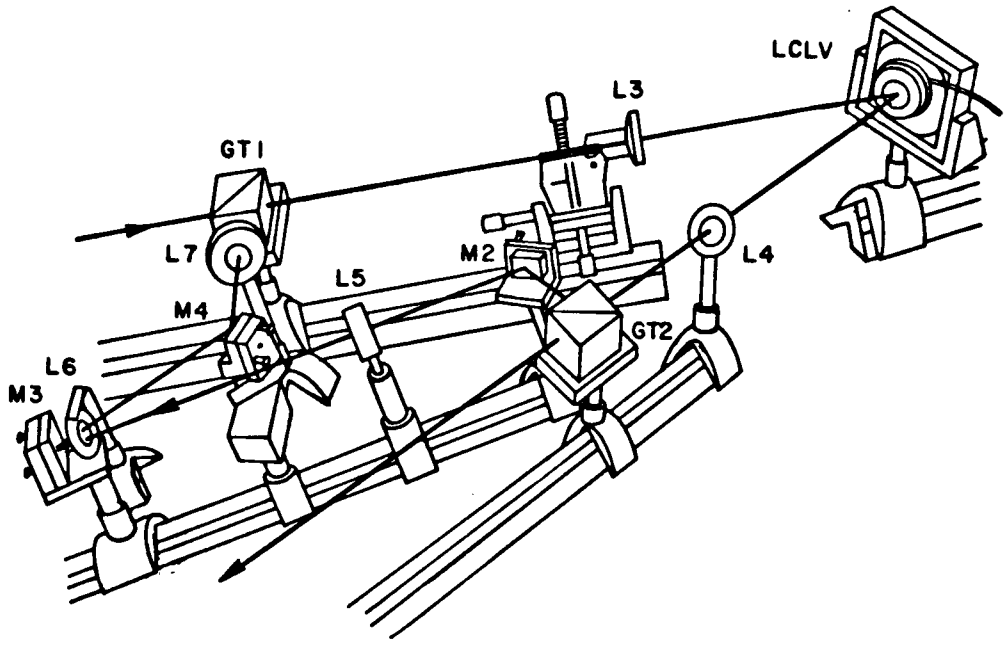

Figure 31. Drawing of loop components.

The two polarizing cubes provide a means of input to (GT1) and output from (GT2) the system by controlling polarization; they must operate in collimated space which is provided between the pair of lenses used to image from light valve to auxiliary mirror (between L4 and L5) and back (between L7 and L3). Lenses L3 and L4 are each a focal length away from the light valve and lenses L5 and L7 are each a focal length away from mirror M3. The light valve operating conditions are set so that if the write beam intensity is high the read beam polarization is changed by 90° and if the write beam intensity is low the read beam polarization is unchanged. In this way the 'polarizing mirror' of Figures 3 and 4 is realized.

The polarization of the light beams in the loop are significant. To remain inside the loop, reflected by both polarizing cubes, the light must be vertically polarized. Otherwise it exits the loop after being transmitted by GT2. Consider the case where the beam reflected off the light valve has a vertical polarization. In this case the light beam is to be redirected onto the light valve. The beam is reflected off GT2 and imaged onto mirror M3. A field lens L6 in front of mirror M3 ensures that all the light remains within the effective aperture of the system. The light reflected off mirrors M3 and M4 is collimated by lens L7 and since it is still vertically polarized it is reflected by prism GT1 back onto the light valve, focused by lens L3 again. Mirror M3 is tilted in such a way that the reflected beam travelling back toward the light valve is focused at a shifted position with respect to the point it was initially reflected from. With the aid mirrors M2 and M4, the shift can be arranged to be in any orientation. The particular shift direction chosen in this case is the Diagonal Shift Orientation discussed in Chapter III, providing reflections along a 45° line with respect to the horizontal.

Now assuming the beam polarization is unchanged after the second bounce, it will be reflected again by both prisms and mirror M3 back to the light valve. The beam remains in this loop, each time shifted in the same direction as the first shift, until its polarization is changed by a write beam positioned opposite one of the reflections off the LCLV. In that case it is transmitted by prism GT2 and exits the loop components.

4. Hologram Addressing Component Description.

The hologram addressing components are shown in Figure 32. The holographic memory composed of a Kodak 649F photographic plate is shown at the top right. The remaining components after GT2 used in matching the loop output to the desired hologram reconstruction beam input include M5, M6, L8, L9, L10, L11, L12, and L13. These components provide the position coded input to the holographic memory.

For the case where the beam reflected off the light valve is horizontally polarized, it passes prism GT2 and is directed by mirrors M5 and M6 to L8. Lens L8 effectively images the light valve plane. This images the possible position coded array of multiplier output spots representing the beams that reflect off the light valve, in the focal plane of the microscope objective lens, L10. Lens L9 is a field lens in

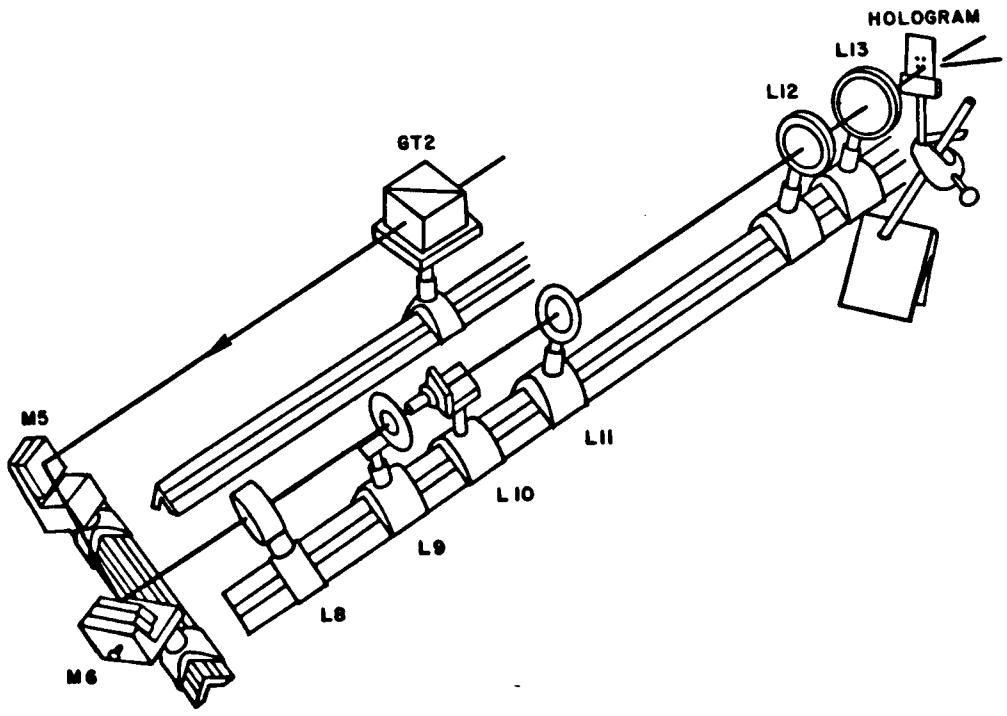

Figure 32. Drawing of hologram addressing components.

the light valve image plane in front of the microscope objective. Lenses L11 and L13 form a telescope to give the desired angular magnification for the beams from the microscope objective, to match the angular range of beams used in constructing the hologram. This gives a position coded array of 'sources' addressing the holographic memory as desired.

5. Holographic Memory Output Imaging Components

The components used to image the pattern reconstructed from the holographic memory onto the LCLV write side are: M7, L14, M8, M9, M10, and L15. They are arranged as shown in Figure 33.

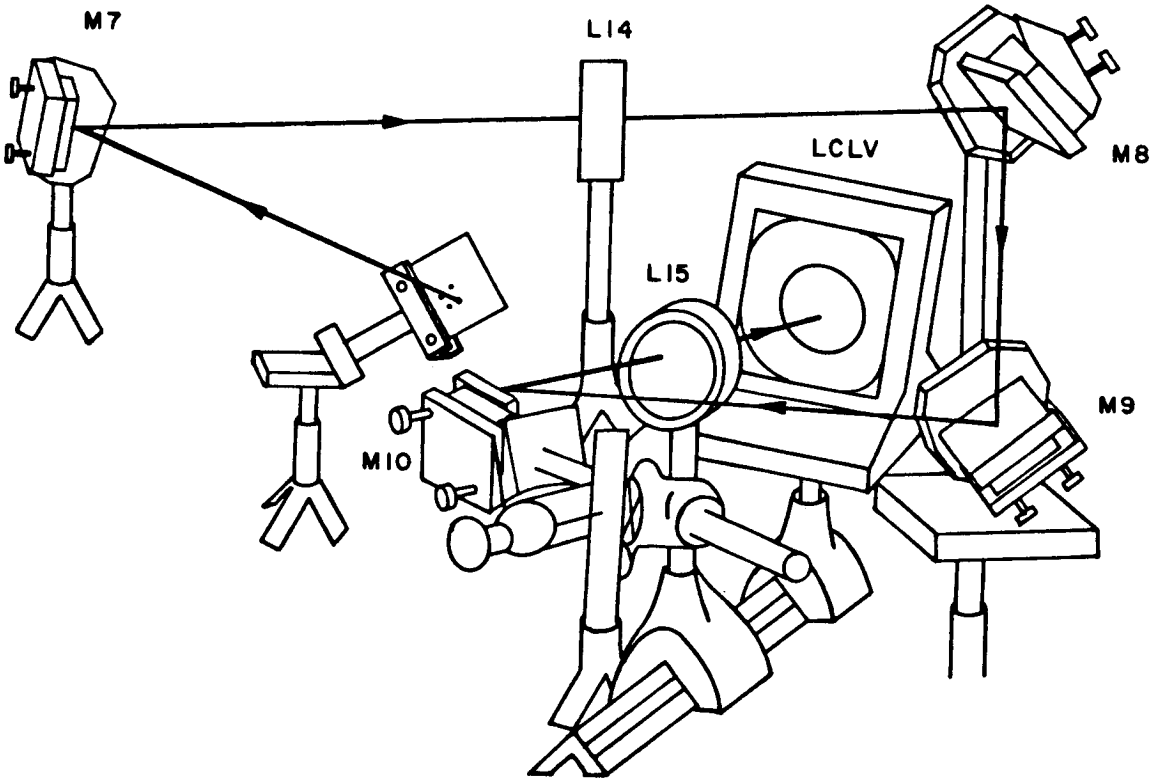

Figure 33. Drawing of holographic memory output imaging components.

Depending on which of the light valve bounces addresses the hologram a different pattern is reconstructed. The patterns are imaged one at a time using lenses L14, L15, and mirrors M7, M8, M9, and M10 onto the light valve write beam side shown in the center of Figure 33, adjacent to the area on which the CRT generated patterns are imaged. Due to the special orientation of beams and light valve in this design, the holographic memory output imaging components are arranged in a plane at 45° to a plane parallel to the optical bench containing most of the other components. This is shown in Figure 33. The hologram generated patterns can now be used to implement an addition mapping unit.

6. Addition Look up Table Input Read Beam

The adder input read beam components include LASER 2, M11, M12, L16, L17, L18, and L19, providing the vertically polarized input beam for the adder look up table and are shown in Figure 34. Other components, M3, M4, L6, L7 and GT1, are shown for convenience.

The laser source, LASER 2, is shown at the bottom, and mirror M3 toward the center. The generated read beam is oriented by mirrors M11 and M12 and focussed by microscope objective lens L16, in the focal plane of L18. Lens L17 is a field lens in that plane. Then L19 focusses the collimated beam from L18 in the plane of mirror M3 just past the edge of that mirror, a plane conjugate to the light valve plane. The vertically polarized beam is therefore in the focal plane of lens L7 and mirrors M11 and M12 ensure that the beam is directed towards the aperture of L7 via M4, proceeding collimated to prism GT1. It is directed toward the area where the addition mapping unit write beam

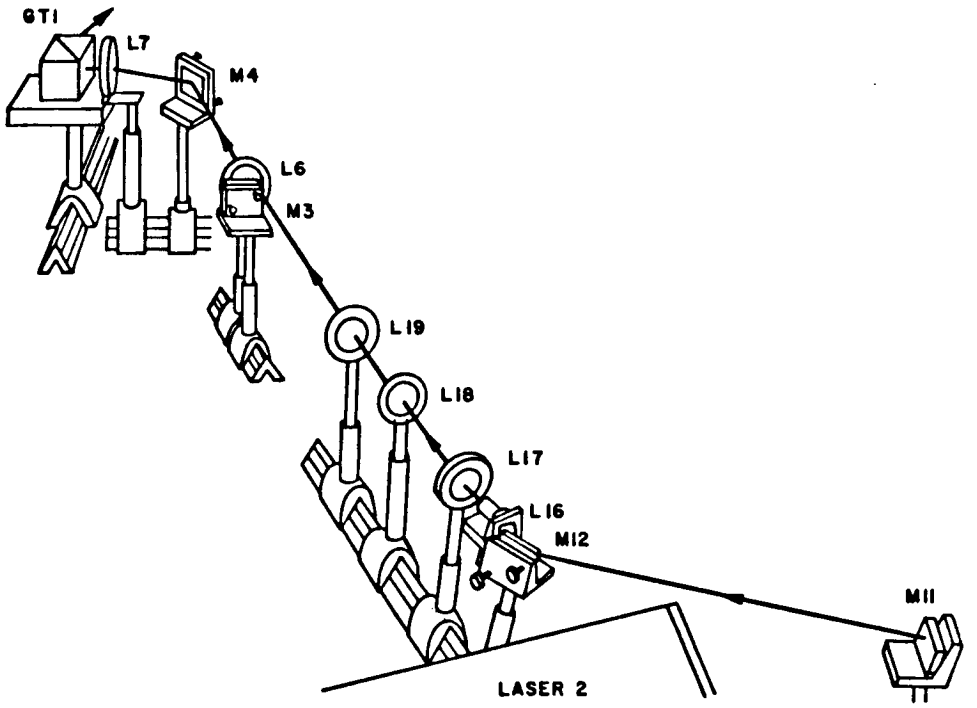

Figure 34. Drawing of addition mapping unit input read beam components.

pattern is imaged. Depending on which row of a hologram generated pattern the read beam is shifted along, the reflected beam is either horizontally or vertically polarized and is treated in the same manner as the multiplication mapping unit read beam.

7. CRT Imaging Components

Finally, the components used in imaging the CRT generated patterns onto the light valve write beam are identified. These are M13, L20, L21, L22, and L15 used to provide the multiplication mapping unit patterns. These are shown in Figure 35 with the CRT at the right and the LCLV at the left. Mirror M13 and lens L20 are used to image the CRT

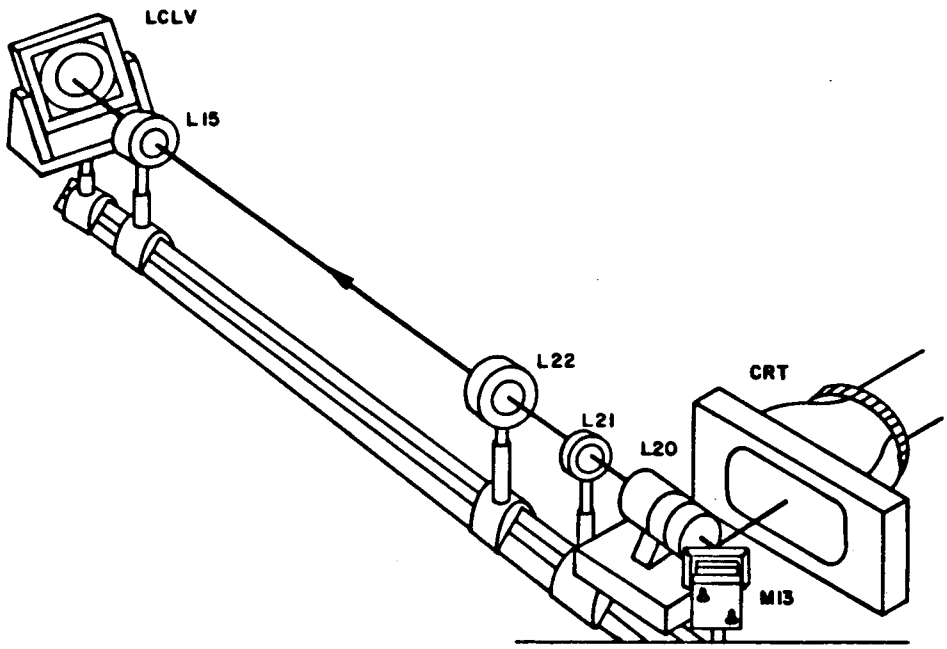

Figure 35. Drawing of CRT imaging components.

plane in the focal plane of lens L22. Lens L21 is a field lens in that plane. The collimated beam past L22 is focussed by lens L15 to image the CRT patterns with a magnification factor of 0.5, matching the spacing of the shifted read beams. The CRT output intensity is adjusted to the level necessary to drive the light valve.

Appendix D Summary

The appartus for the optical matrix vector multiplier was described in this appendix showing drawings of the individual groups of components shown in Chapter III. An overall view of the system was first presented followed by a discussion of each individual group of components and its function.

APPENDIX E

Operational Modification Affecting Resolution

The optical matrix-vector multiplier presented in this work was designed so that the maximum light valve resolution could be used in the implementation and demonstration, as discussed in Chapter III. Power requirements set by the limited efficiency of the particular hologram constructed and used in the demonstration necessitated modifying the design as described in this appendix, restricting the system resolution.

The components used in the design were intended to allow using the light valve at its resolution limit. The lenses in the loop of Figure 11 were chosen to give focussed spots consistent with that limit. The CdS resolution does not limit the read beam spot size for this particular apparatus but does affect the spacing between multiple reflections off the light valve. Initially the design called for focussing the read beam to its smallest size as it passed through the liquid crystal layer, on the order of $f\lambda/D$, which turns out to be about 6.4μm for lens L3 with a beam diameter of 1 cm. (This is smaller than the light valve write beam resolution limit of 42μm.) However, to obtain the needed power to generate a pattern from the hologram that would have enough intensity to drive the light valve, it was necessary to increase the initial input laser power. The liquid crystals could not handle the power density at the focussed design spot size.

In the actual demonstration a slightly larger spot size was used so that desired power needed to overcome the hologram efficiency limits would be available without affecting the liquid crystal operation. The best results were obtained when lens L3 was translated along the direction of propagation so that the read beam was slightly defocussed as it propagated through the liquid crystal layer. This is because of the power density and polarization properties of the system.

Initially the incident beam intensity was measured using a Jodon 450B silicon cell detector with a reading of 2.48 mW, for the beam with a theoretical 6.4 μm spot size radius. This gives a power density of approximately 20,000 mW/mm^2 in the focussed spot whereas the recommended maximum power density [78] is on the order of 10 mW/mm^2. (Researchers at Hughes have not reported any observed effects for operating the light valve at power densities above the stated maximum rating.) In fact this is one of the system energy limits discussed in Chapter II. A set of rings were observed in the reflected beam past the analyzer prism GT2. These rings signify a radial phase change in the converging or diverging beam such that nonplanar phase fronts are traversing the liquid crystal layer, suggesting a nonuniform polarization in the radial direction due to thermal effects in the liquid crystal layer. With a translated lens L3 giving a .35mm spot size radius, a power density of about 6 mW/mm^2 is obtained and the rings were no longer observed. Researchers working in opto-opto modulation in nematic liquid crystals [79], also have reported observing ring patterns in the output beams due to thermal effects when operating at high power densities.

In summary, the design system resolution was modified by using a slightly larger spot size in the matrix-vector multiplier demonstration apparatus discussed in Chapter III. This is due to power requirements set by the efficiency limits of the particular hologram constructed which forced using more power at the input than could be handled by the light valve at the designed resolution. Using more efficient holograms would allow the use of the designed resolution limits.

Appendix F

Hologram Construction Apparatus and Exposure Procedure

The hologram construction apparatus and exposure procedure are described in more detail in this appendix, complementing the material presented in Chapter III. A set of patterns reconstructed from the recorded hologram will be shown.

Hologram Construction Apparatus

A list of all the components used for the hologram construction shown originally in Figure 14 and repeated for convenience in Figure 36, is given in Table 7. A laser source is directed by two mirrors M1 and

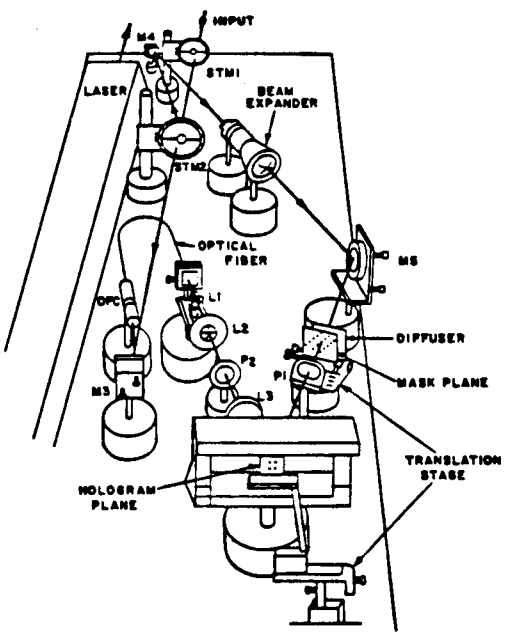

Figure 36. Hologram exposure apparatus.

Table 7

Hologram Construction Apparatus

Component	Description
Laser	45mW helium neon laser source
shutter	
M1	Mirrors M1 and M2 for beam height
M2	and direction alignment.
STM 1	variable beamsplitter, attenuator
STM 2	variable beamsplitter, semi-transparent mirror for beam intensity ratio control
Reference beam components	
M3	directs reference beam into optical fiber
optical fiber coupler (OFC)	See Appendix G
optical fiber	Single mode 4 μm core, 125 μm cladding
Positioner	NRC output end optical fiber positioner, for angle multiplexing
L1	10x microscope objective
L2	42 mm ϕ, 250 mm fl
L3	62 mm ϕ, 100 mm fl
P1	polarizer
Object beam components	
M4	directs object beam into beam expander
beam expander	expands laser beam to 1" diameter
P2	polarizer
M5	direct object beam onto mask plane
masks	produce patterns for objects
translation stage	positions masks in object beam
diffuser	provides even illumination onto hologram
aperture	
photographic plate	positioned by a translation stage in hologram plane for exposure.
translation stage	positions hologram plate for spatial multiplexing

M2 and two semi transparent mirrors, STM1 and STM2, to provide the object and reference beam sources. STM 1 is used basically as an attenuator to control the exposure intensity, as described later. STM2 is used to control the object and reference beam ratio; the transmitted portion gives the reference beam and the reflected portion gives the object beam.

The object and reference beam components are listed separately in Table 7. For the reference beam the optical fiber is used for the angle multiplexing of the reference beam. The output end of the fiber is positioned in the focal plane of microscope objective lens, L1, generating a collimated reference beam propagating in a different direction for every fiber position. Lenses L2 and L3 are separated by the sum of their focal lengths and act as a telescope providing the angular magnification needed for the different reference beam directions such that the angular separation between reference beams satisfies the angular selectivity of the holographic emulsion derived in Chapter II. The object beam is provided by a beam expander illuminating a mask plane. The masks are arranged side by side on a screen and shifted sideways using a translation stage to provide different mask patterns for each of the different reference beam directions. A diffuser placed in front of the mask plane allows uniform illumination of the recording aperture in the hologram plane. The holographic plate is mounted on a translation stage to allow moving the plate for each set of multiple exposure holograms. In the experiment performed, four recording areas were exposed two with five superimposed exposures in one row, and two with 4 superimposed exposures in another row.

The recorded patterns were for the addition operations modulo 4 and 5. The masks for modulo 5 have the same shape as the mapping unit patterns shown in Figure 2b. A similar set of masks for modulo 4 were used in that case.

Exposure Procedure

The exposure procedure for producing a set of four multiplexed holograms, of the type described in Chapter III is presented in this appendix. A detailed 27 step procedure is given for producing four multi-exposure holograms arranged in a square. Two of the four multiple exposure holograms have four superimposed (angle multiplexed) exposures while the other two have five superimposed exposures.

The 27 step procedure follows:

1. Arrange all optical components as shown in Figure 36 for convenience, except for the photographic plate and lenses. Verify that the path lengths for object and reference beams are equivalent taking into account the length of the optical fiber.

2. Turn on laser beam and align beam axis parallel to optical table at the desired height.

3. Align mirrors in the object and reference beam paths to establish axes and have both beams intersect in the hologram plane. The axes should be oriented at angles of about 30° on opposite sides of the hologram normal. Bypass the optical fiber at this stage replacing it with a mirror so that the light is directed toward the hologram plane.

4. Insert lenses maintaining beam axis directions.

5. Replace the mirror in the reference beam path with the optical fiber, the input coupler and the output positioner. Using mirror M3 direct the light into the optical fiber coupler (OFC). Adjust and align the fiber coupler for maximum output from the fiber using a detector at the output end.

6. Position the output end of the fiber so that the beam emerges parallel to the established axis, i.e., centered in the microscope objective immediately following the fiber. The reference beam should now be filling the exposure area aperture in the hologram plane. Again verify that the object and reference beam path lengths are equivalvent, including the fiber length. Slight adjustments can be made by moving the OFC closer or further away from mirror M3.

7. Align beam expander in object beam to give a collimated output.

8. Position the mask screen using the translation stage. Observe pattern imaged onto the hologram plane and adjust it such that it is centered on the exposure aperture in that plane.

9. Adjust object and reference beam polarizers such that the same polarization is incident on the hologram plane.

10. Adjust STM 1 so that about 50% of the intensity is transmitted to allow for increases in intensity at a later stage.

11. Check that all patterns formed by masks mounted on the translation stage can be positioned in the center of the object beam; mark the position for each pattern such that it can be set again in the dark. Similarly change the position of the fiber output end to check that all the generated reference beams overlap in the aperture plane. Adjustment of the position of lens L3 may be necessary.

12. Set the optical fiber and mask screen to the positions to be used for the first exposure.

13. Turn off room lights.

14. Measure object and reference beam intensities. Adjust the variable beam splitter to ensure that the reference to object beam ratio is in the 2:1 to 3:1 range. If the reference beam intensity is too weak due to the polarizer, rotating the fiber may change polarization allowing a stronger intensity. The total intensity for both beams should be adjusted so that exposure times can remain short, on the order of 0.5 seconds. If the total intensity is too weak adjust STM 1.

15. As a check before starting the exposures, position each of the patterns in the object beam, and the optical fiber in the associated reference beam position. Adjust STM 1 for each set to give the appropriate increase in intensity over the first exposure. Verify that the object to reference beam ratio is maintained throughout.

16. Reposition the masks and fiber to their positions for the first exposure.

17. Determine the exposure time and set the shutter. The same exposure time is used throughout; increasing the exposure level is done by increasing the total intensity by adjusting STM1.

18. Remove the photographic plate from storage and position it using a translation stage to perform the first set of exposures.

19. Expose the emulsion.

20. Change the pattern and fiber position to those used for the next exposure.

21. Set STM 1 to give the desired increase in intensity.
22. Set the shutter.
23. Expose the emulsion.
24. Repeat steps 20 - 23 until all exposures have been made.
25. Move the photographic emulsion to its new position for the next set of superimposed exposures.
26. Repeat steps 20-25 until all spatially multiplexed holograms are recorded.
27. Process the emulsion in the appropriate chemicals.

In the experiment performed the set of four exposed areas, two with four superimposed exposures and two with five superimposed exposures, were recorded using the above procedure. Kodak 649F-AH, 2"x2" plates were used. The intensities of the reference and object beams for the different exposures are listed in Table 8. The exposure time in each case was 0.5 sec. The values used closely match those determined from Equation (27) in Chapter II for 10% conversion per exposure.

The chemical processing steps and times are listed below [69]:

1. Developer, D-19; 5 minutes.
2. Stop bath; 30 seconds.
3. Fixer, Rapid Fixer; 5 minutes.
4. Wash, distilled water; 10 minutes.
5. Bleach, 5% Cupric Bromide solution; 7 minutes after clearing.
6. Rinse, Distilled water: 30 seconds.
7. Clearing bath, mixture of two solutions; one part of a potassium permanganate solution (5g in 1 liter of distilled water), to ten parts of a potassium bromide solution (10 cm^3 sulfuric acid, 110gms KBr, in 1 liter distilled water); until clear.
8. Wash, distilled water; ten minutes.
9. Dry at room temperature.

Table 8

Exposure Table

	Intensity			Ratio	
Exposure # n	Reference beam	Object beam	Total	I_r/I_o	I_n/I_1
1	.0960	.0357	.1350	2.69	1.0
2	.1053	.0395	.1490	2.66	1.1
3	.1210	.0455	.1700	2.66	1.25
4	.1287	.0510	.1850	2.52	1.37
5	.1395	.0539	.1972	2.59	1.46

It is assumed that bleaching the hologram provides a complete change of absorption variation into a refractive index variation. However, some variation in thickness invariably introduces noise into the system due to scattering. In order to minimize the scattering the emulsion was put in a mineral oil gate before using the hologram in the experimental apparatus for the matrix vector multiplier. Mineral oil has a refractive index of approximately 1.48 close to the emulsion refractive index of 1.5. A cover glass placed on top of the mineral oil film was held securely by two metal spring clamps.

The eighteen exposures for the constructed holographic memory were recorded using the procedure outlined above and processed using the processing steps listed. The photograms of the patterns reconstructed from the recorded holograms are shown in Figure 37.

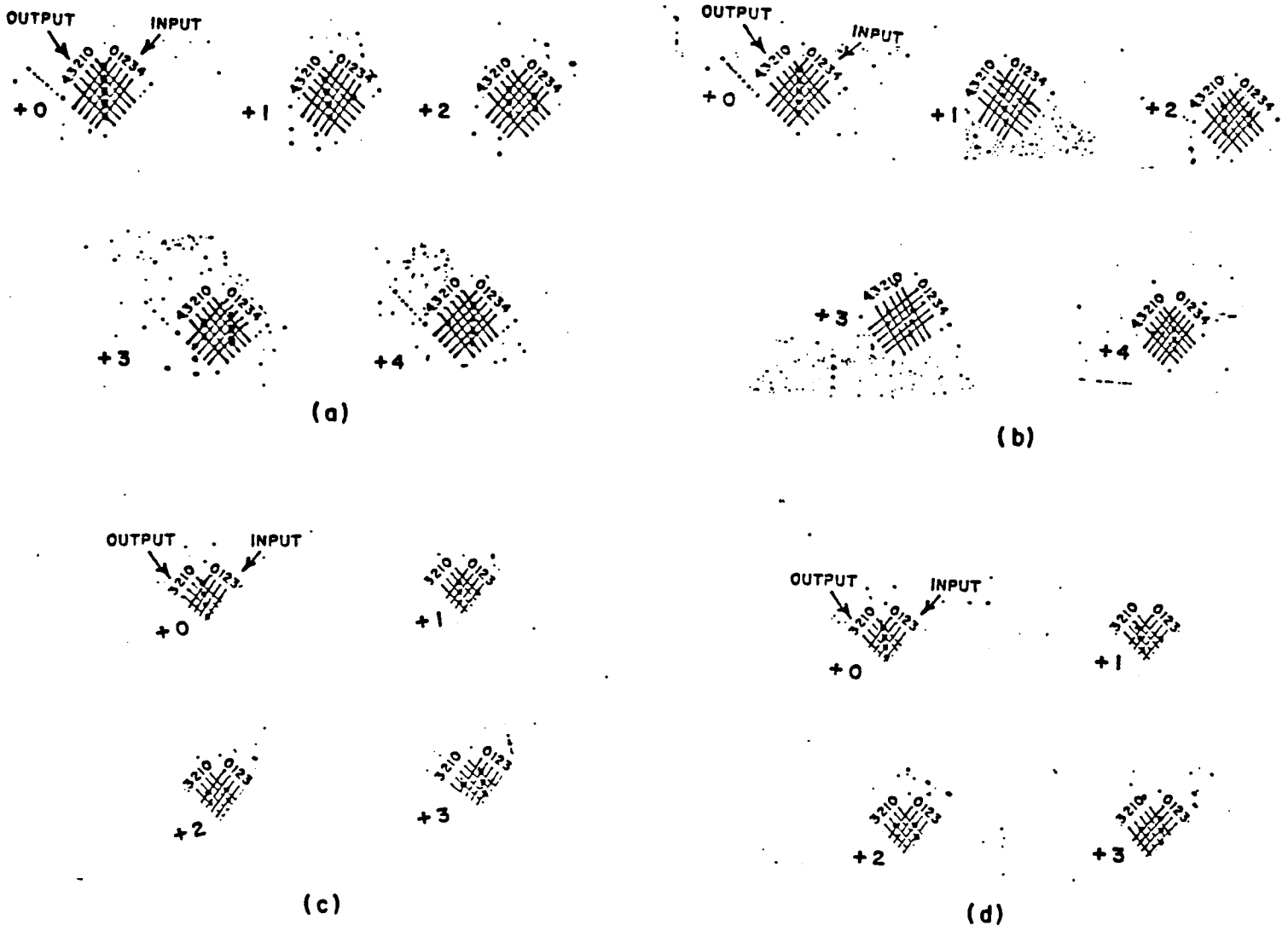

Figure 37. Hologram Generated Patterns.

It is noted again that the generated patterns are rotated by 45° to accomodate the light valve Diagonal Shift Orientation used in the design. The position coded input source array used to reconstruct the different patterns was oriented at a 45° angle to the horizontal and consequently, the reconstructed patterns are too.

Appendix Summary

The hologram construction apparatus and exposure procedure were described in this appendix. Photograms of four sets of patterns reconstructed from the recorded hologram were shown. One of these sets, with five reconstructed modulo five addition patterns was used in the optical matrix vector multiplication demonstration apparatus described in Chapter III.

APPENDIX G

Description of Optical Fiber Coupler

A description of the optical fiber coupler used to couple light into a single mode optical fiber is presented in this appendix. This fiber is used to provide the reference beam in the hologram construction apparatus described in Chapter III and Appendix F.

A lens is typically used to couple light efficiently into a single mode optical fiber. A lens with the appropriate matching numerical aperture and the fiber must be aligned such that the fiber core is located in the focal plane of the lens. A single mode fiber has a core of approximately 4μm diameter into which the light must couple, and a 125μm cladding. The alignment is usually accomplished by using a positioner with multi-axis control; however this positioner is expensive and takes up valuable bench space.

A simpler positioner was designed and constructed to accomplish the alignment needed. This type of positioner was initially used to align fibers in an array of inputs for an optical temporal integrator. One of these devices was used to couple light into the fiber used in the hologram construction apparatus.

A diagram of the cylindrically shaped positioner is shown Figure 38. There are two main sections to the unit, one to hold and position the fiber shown at the left in Figure 38, and another to hold and

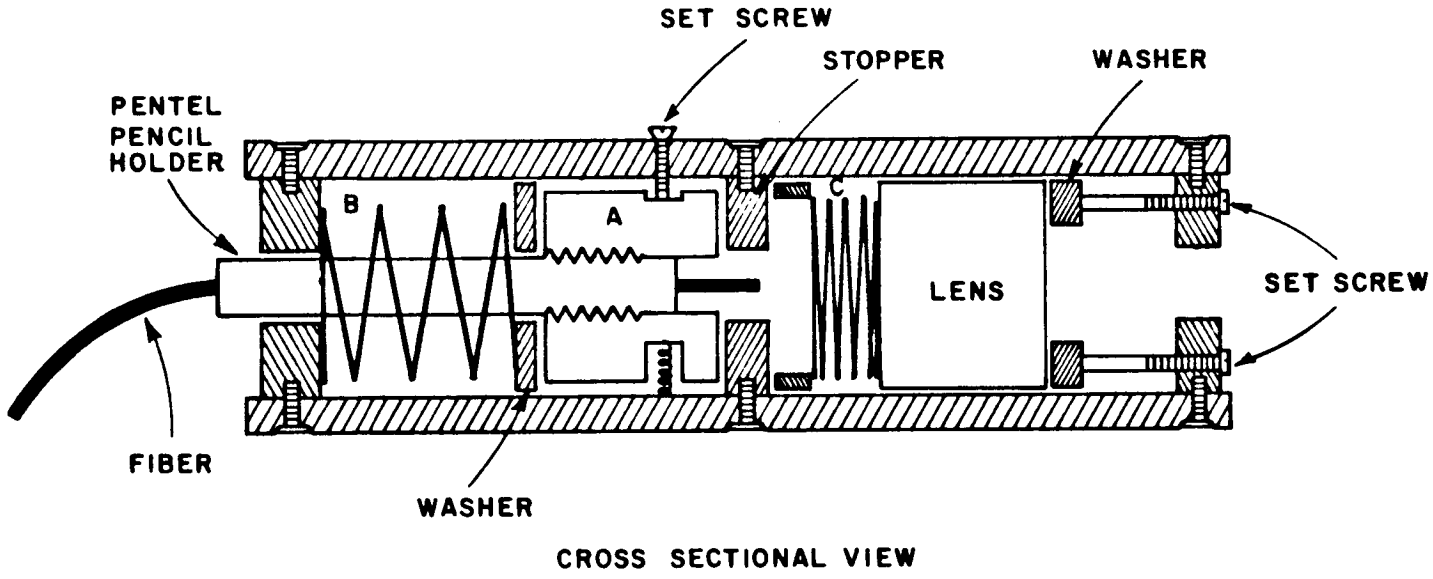

Figure 38. Optical fiber coupler.

position the lens shown at the right. Both these sections are inserted into a hollow tube. The fiber used was purchased from Lightwave Technologies and the lens was a 10X student microscope objective.

The fiber is placed in the shaft of a Pentel pencil holder (.3 mm lead size) with the holder end tightly holding the fiber tip. This end of the shaft is threaded and is inserted into a unit with matching thread (A in Figure 38). This unit is spring loaded such that a pair of set screws one of which is shown at the top can be used to control the x and y position of the fiber end. The threaded unit is held in place in the z direction by a washer and spring (B in Figure 38).

The lens is inserted into the other end of the cylindrical tube. The microscope objective lens optics is used intact after the outer metallic lens holder is discarded. A spring (C in Figure 38), is located between the lens and a stopper inside the tube so that two set screws and a washer on the far right of the tube can control the z position of the lens.

With the x and y axis control at the fiber end and the z control at the lens end of the tube, it is possible to couple light travelling through the lens into the fiber. A window located near the fiber tip position along the tube allows initial alignment of the components.

In summary, a simple tube shaped optical fiber holder has been described where a fiber mounted in a Pentel pencil holder is inserted in one end of the tube and a 10X microscope objective is inserted into the other end. The fiber and lens are positioned to couple light into the core of the single mode fiber.

APPENDIX H

TIME RESPONSE

The response time of the system from the time an input read beam for the multiplier loop is turned on, until the adder output appears, is documented in this appendix. This is essentially one light valve response time (plus the negligible light propagation delay in the system).

A detector placed in the adder ouptut array position was used to measure the response time. The detector output was displayed on an oscilloscope and the trace is shown in Figure 39. The response time is seen to be on the order of one second.

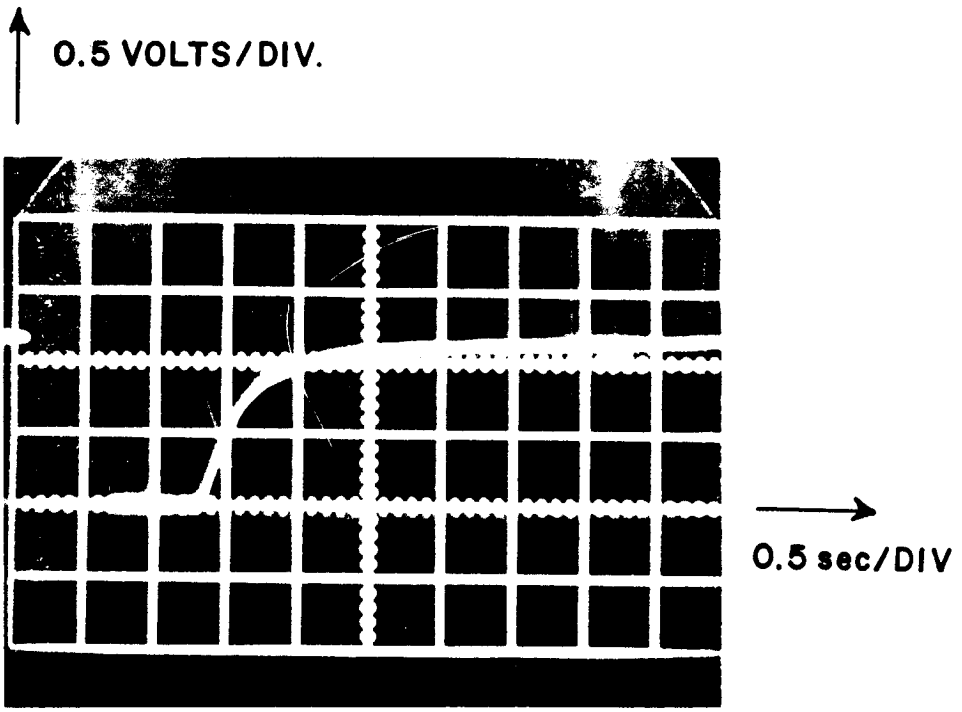

Figure 39. Response time.

LIST OF REFERENCES

1. Grinberg, J., A. Jacobson, W. Bleha, L. Miller, L. Fraas, D. Boswell and G. Myer, "A New Real-Time Non-Coherent to Coherent Light Image Converter, The Hybrid Field Effect Liquid Crystal Light Valve", Opt. Eng. 14, p. 217, 1975.

2. Szabo, N.S., and R.I. Tanaka, Residue Arithmetic and its Applications to Computer Technology, McGraw-Hill, New York, 1967.

3. Guest, C.C., and T.K. Gaylord, "Truth-table Look-up Optical Processing Utilizing Binary and Residue Arithmetic," Appl. Opt. Vol. 19, 1201, 1980.

4. Goodman, J.W., Operations Achievable with Coherent Optical Information Processing Systems, Proc. IEEE, Vol. 65, p. 29, 1977.

5. Cutrona L.J., Optical and Electro-Optical Information Processing, J.T. Tippett et.al. editors, pg. 96-98, MIT Press, Cambridge, Mass., 1965.

6. Preston, K. Jr., Coherent Optical Computers, McGraw-Hill, New York, 1972.

7. Lohmann, A.W. "What Classical Optics Can Do for the Digital Optical Computer," Appl. Opt., Vol 25, p. 1543, 1986.

8. Hausler, G., "Optical Software Survey," Optica Acta, Vol. 24, p. 965, 1977.

9. Athale, R.A., and S.H. Lee, "Development of an Optical Parallel Logic Device and a Half-Adder Circuit for Digital Optical Processing," Opt. Eng., Vol. 18, p. 513, 1979.

10. Jenkins B. K., A.A. Sawchuk, T.C. Strand, R. Forchheimer and B.H. Soffer, "Sequential Optical Logic Implementation," Appl. Opt., Vol. 23, p. 3455, 1984.

11. Yen, C.Y., and S.A. Collins Jr., "Operation of a Numerical Optical Data Processor", Proceedings of 1980 International Optical Computing Conference, SPIE Vol. 232, 1980.

12. Habiby,S.F. and S.A. Collins, Jr., "Design of an Optical Residue Arithmetic Matrix-vector Multiplier Using Holographic Lookup Table," Proceedings of the Topical Meeting on Optical Computing, Lake Tahoe, Nevada, March 18-20, 1985.

13. Huang, A., "Design for an Optical General Purpose Digital Computer," Proceedings of the Society of Photo-optical Instrumentation Engineers, Vol. 232, p. 119, 1980.

14. Bell, T.R., editor, 'Optical Computing: a Field in Flux,' IEEE Spectrum, Vol. 23, p. 34, 1986.

15. Fatehi, M.T., K.C. Wasmundt, and S.A. Collins Jr. "Optical Logic Gates using Liquid Crystal Light Valve: Implementation and Application Example," Appl. Opt., Vol. 20, p. 2250, 1981.

16. Athale, R.A., and S.H. Lee, "Bistability and Thresholding by a New Photoconductor-twisted Nematic Liquid Crystal Device with Optical Feedback," Appl. Opt., Vol. 20, p. 1424, 1981.

17. Jenkins B. K., A.A. Sawchuk, T.C. Strand, R. Forchheimer, and B.H. Soffer, "Architectural Implications of a Digital Optical Processor," Appl. Opt. Vol. 23, p. 3465, 1984.

18. Chandran, V., T.F. Krile, and J.F. Walkup, "Optical Techniques for Real-time Binary Multiplication," Appl. Opt., Vol. 25, p. 2272, 1986.

19. Fisher, A.D., "A Review of Spatial Light Modulators," Tech. Digest OSA 1985 Optical Computing Meeting, TuC1-1, (Optical Society of America, Washington D.C.), 1985.

20. Warde, C, A.M. Weiss, A.D. Fisher, and J.I. Thackara, "Optical Information Processing Characteristics of the Microchannel Spatial Light Modulator," Appl. Opt, Vol. 20, p. 2066, 1981.

21. Pape, D.R., "Optically Addressed Membrane Spatial Light Modulator," Opt. Eng., Vol. 24, p. 107, 1986.

22. Peyghambarian, N., and H.M. Gibbs, Opt. Eng., Vol. 24, p. 68, 1985.

23. Gibbs, H.M., Optical Bistability: Controlling Light with Light, Academic Press Inc., New York, 1985.

24. Smith, S.D., "Optical Bistability, Photonic Logic, and Optical Computation," Appl. Opt., Vol. 25, p. 1550, 1986.

25. Tamura, P.N. and J.C. Wyant, "Matrix Multiplication Using Coherent Optical Techniques," Proc. SPIE Vol. 83, p. 97, 1976.

26. Casasent, D., J. Jackson, and C. Newman, 'Frequency-Multiplexed and Pipelined Iterative Optical Systolic Array Processors,' Appl. Opt. Vol. 22, p. 115, 1983.

27. Bocker, R.P., H.J. Caulfield, and K. Bromley, "Rapid Unbiased Bipolar Incoherent Calculator Cube," Applied Optics, Vol. 22, p. 804, 1983.

28. Bocker, R.P., "Optical Digital RUBIC Cube Processor," Optical Engineering, Vol. 23, p. 26 , 1984.

29. Habiby, S.F., and S.A. Collins, "Holographic Multiple Exposure Look-up Table for Optical Computing," Topical Meeting on Holography Technical Digest 86:5, (Optical Society of America, Washington, D.C. 1986) p. 124.

30. Heinz, R.A., J.O. Artman, S.H. Lee, "Matrix Multiplication by Optical Methods," Appl. Opt., Vol. 9, p. 2161, 1970.

31. Goodman, J. W., A.R. Dias, and L.M. Woody, "Fully Parallel, High-speed Incoherent Optical Method for Performing Discrete Fourier Transforms," Opt. Lett., Vol. 2, p. 1, 1978.

32. Guest, C.C., and T.K. Gaylord, "Two Proposed Holographic Numerical Optical Processors," Proc. SPIE, Vol. 185, p. 42, 1979.

33. Huang, A., "The Implementation of a Residue Arithmetic Unit via Optical and Other Physical Phenomena," International Optical Computing Conference, Digest of Papers, Washington, D.C., IEEE Catalog No. 75CH0941-5C, p. 14, 1975.

34. Psaltis, D., and D. Casasent, "Optical Residue Arithhmetic: a Correlation Approach," Appl. Opt., Vol. 18, p. 163, 1979.

35. Gardner, H.L., "The Residue Number System," IEEE Trans. Elec. Comp. EC-8, P. 140, 1959,

36. Huang, A., Y. Tsunoda, J.W. Goodman, and S. Ishihara, "Optical Computing using Residue Arithmetic," Appl. Opt., Vol. 18, p. 149, 1979.

37. Huang, A., and J.P. Goodman, "Number Theoretic Processors, Optical and Electronic," Proceedings of the Symposium on Optical Processing Systems, Huntsville, Alabama, May 22-23, SPIE Vol. 185, p.28, 1979.

38. Taylor, F.J., "Residue Arithmetic: A Tutorial with Examples," Computer, Vol. 17, p. 50, 1984.

39. Tai, A., I. Cindrich, J.R. Fienup, and C.C. Aleksoff, "Optical Residue Arithmetic Computer with Programmable Computation Modules," Appl. Opt., Vol. 18, p. 2812, 1979.

40. Horrigan, F.A., and W.W. Stoner, "Residue-based Optical Processor," Optical Information Systems Processing Conference, Proc. SPIE, Vol. 185, p. 19, 1980.

41. Collins, S.A., Jr., "Numerical Optical Data Processor," Proceedings of the Symposium of Effective Utilization of Optics in Radar Systems, Huntsville, Alabama, SPIE Vol. 128, p. 313, Sept. 1977.

42. Knight, G.R., "Holographic Associative Memory and Processor," Appl. Opt. Vol. 14, p. 1088, 1975.

43. Guest, C.C., M.M. Mirsalehi, T.K. Gaylord, "EXCLUSIVE OR Processing (Binary Image Subtraction) Using Thick Fourier Holograms," Appl. Opt., Vol. 23, p. 19, 1984.

44. Caulfield, H.J., (Editor), Handbook of Optical Holography, Academic Press, New York, 1979.

45. Vander Lugt, A., "Design Relationships for Holographic Memories," Appl. Opt., Vol. 12, p. 1675, 1973.

46. Kogelnik, H., "Reconstrucing Response and Efficiency of Hologram Gratings," Proceedings of the Symposium of Modern Optics, p. 605-617, Polytechnic Press, New York, 1967.

47. Kogelnik, H., "Coupled Wave Theory for Thick Hologram Gratings," Bell System Technical Journal, Vol. 48, p. 2909, 1969.

48. Upatnieks, J. and C. Leonard, "Efficiency and Image Contrast of Dielectric Holograms," J. Opt. Soc. Am., Vol. 60, p. 297, 1970.

49. Solymar, L., and D.J. Cooke, Volume Holography and Volume Gratings, Academic Press, London, 1981.

50. Collier, R.J., C.B. Burckhardt, and L.H. Lin, Optical Holography, Academic Press, New York, 1971.

51. Lieth, E.N., A. Kozma, J. Upatnieks, J. Marks, and N. Massey, "Holographic Data Storage in Three Dimensional Media," Appl. Opt., Vol. 5, p. 1303, 1966.

52. Freisem A.A. and J.L. Walker, "Thick Absorption Recording Media in Holography," Appl. Opt., Vol. 9, p. 201, 1970.

53. Friesem, A.A., A. Kozma and G.F. Adams, "Recording Parameters of Spatially Modulated Coherent Wavefronts," Appl. Opt., Vol. 6, p. 851 1967.

54. Caulfield, H.J., S. Lu, and J.L. Harris, "Biasing for Single Exposure and Multiple Exposure Holography," J. Opt. Soc. Am., Vol. 58, p. 1003, 1968.

55. Fatehi, M.T., A Study of a Holographic Analog Associative Memory with Application to Pattern Recognition, Ph.D. Dissertation, Ohio State University, 1975.

56. Nishida, N., and M. Sakaguchi, "Improvement of Nonuniformity of the Reconstructed Beam Intensity from a Multiple Exposure Hologram," Appl. Opt., Vol. 10, p. 439, 1971.

57. Lin L.H., and C.V. LoBianco, "Experimental Techniques in Making Multicolor White Light Reconstructed Holograms," Appl. Opt., Vol. 6, p. 1255, 1967.

58. Johnson, K.M., H.L. Hesselink and J.W. Goodman, "Multiexposure Holographic Display of C.T. Medical Data," Proc. SPIE, Vol. 367, p. 149, 1982.

59. Johnson, K.M., H.L. Hesselink and J.W. Goodman, "Holographic Reciprocity Law Failure," Appl. Opt., Vol. 23, p. 218, 1984.

60. Williamson, T.L., Scattering Theory of Holographic Diffraction, PhD Dissertation, Ohio State University, 1975.

61. R.A. Athale, "Optical Matrix Algebraic Processors: A Survey," Proceedings of the IEEE, Tenth Optical Computing Conference, IEEE Catalog No. CH1880-4/83, p.24, 1983.

62. Habiby, S.F., "A Design Study of a Numerical Optical Temporal Integrator Using Residue Arithmetic," Masters Thesis, The Ohio State University, Columbus, Ohio, 1982.

63. Collins, S.A., Jr., and S.F. Habiby, patent, 'Improved Optical Matrix Vector Multiplication Apparatus,' submitted April 1986.

64. Caulfield, H.J., "Wavefront Multiplexing by Holography," Appl. Opt., Vol. 9, p. 1218, 1970.

65. Lieth, E.N., and J. Upatnieks, "Wavefront Reconstruction with Diffused Illumination and Three-Dimensional Objects," J. Opt. Soc. Am., Vol. 54, p. 1295, 1964.

66. James, T.H. and G.C. Higgins, Fundamentals of Photographic Theory, Chapter 3, Morgan and Morgan, third edition, 1968.

67. Hamilton, J.F., and F. Urbach, in The Theory of the Photographic Process, 3rd ed., C.E.K. Mees and T.H. James, editors, The Macmillan Co., New York, 1966.

68. Collins, S.A. Jr., S.F. Habiby, and A.F. Zwilling "Numerical Optical Computing at The Ohio State University," AGARD Conference Proceedings No. 362, Digital Optical Circuits Technology p. 18-1, 1984.

69. Lehmann, M., J.P. Lauer, and J.W. Goodman, "High Efficiencies, Low Noise, and Suppression of Photochromic Effects in Bleached Silver Halide Holography." Appl. Opt., Vol. 9, p.1948, 1970.

70. Super AR dielectric anti-reflection coatings for λ = .514μm, made by Satis America, Cleveland, Ohio, 1986.

71. Quantrad Corporation 100-PV-BNC detector data sheet.

72. CVI Corporation, Polarizing Beam Splitter Cubes data sheet.

73. Maiman, T.H., "Stimulated Optical Radiation in Ruby Masers," Nature, Vol. 187, p. 493, 1960.

74. Cutrona, L.J., E.N. Leith, L.J. Porcello, and W.E. Vivian, "On the Application of Coherent Optical Processing Techniques to Synthetic-Aperture Radar," Proc. IEEE, Vol. 54, p. 1026, 1966.

75 Gabor, D., Proc. Roy. Soc. (London), A, Vol. 197, p. 454, 1949.

76. Zernike, F. and J.E. Midwinter, Applied Nonlinear Optics, John Wiley and Sons, New York, 1973.

77. Gaylord, T.K., and M.G. Moharam, "Analysis and Applications of Optical Diffraction by Gratings," Proc. IEEE, Vol. 73, p. 894, 1985.

78. Hughes Aircraft Company, Hughes Liquid Crystal Light Valve Data Sheet, private communication.

79. Martin-Pereda, J.A., and F.J. Lopez, "Opto-optical Modulation in N-(p-methoxybenzylidene)-p-butylaniline," Opt. Lett, Vol. 7, p. 590, 1982.